

LINEAR VISCOELASTIC CHARACTERISTICS OF
MICHIGAN ASPHALT MIXTURES AND THE EFFECT
OF SAMPLE SIZE ON MATERIAL PROPERTIES

By

Anas Jamrah

A THESIS

Submitted to
Michigan State University
in partial fulfilment of the requirements
for the degree of

Civil Engineering - Master of Science

2013

ABSTRACT

LINEAR VISCOELASTIC CHARACTERISTICS OF MICHIGAN ASPHALT MIXTURES AND THE EFFECT OF SAMPLE SIZE ON MATERIAL PROPERTIES

By

Anas Jamrah

The Mechanistic-Empirical Pavement Design Guide (M-E PDG) is becoming the state-of-the-practice in both newly constructed and rehabilitated pavement designs. A number of different material inputs are required by the M-E PDG, and accurate measurement of these inputs is crucial for the accuracy of the distress predictions. The main objective of the research study presented in this thesis was to investigate linear viscoelastic characteristics of asphalt mixtures and binders commonly used in Michigan. This is important for implementation of the M-E PDG in Michigan and for accurate prediction of flexible pavement distresses. The second objective was to develop analytical models in efforts to provide improved $|E^*|$ predictions of asphalt mixtures used in the State of Michigan. For this, the Modified Witczak model was locally calibrated. In addition, an Artificial Neural Network (ANN) model was developed and trained for Michigan asphalt mixtures. Another objective of this study was to investigate the Representative Volume Element (RVE) requirement for complex (dynamic) modulus ($|E^*|$) of asphalt mixtures. Small thin mixture beam (TBM) specimens (0.5"x0.25"x4.5") were tested using the Bending Beam Rheometer (BBR) testing machine to obtain the Creep Compliance ($D(t)$). This study showed that there is a trend in $D(t)$ values obtained from the BBR, but on the other hand; the factor between $|E^*|$ -based and TBM-based $D(t)$ values was not consistent and ranged between 1.5 and 4 factors.

TO MY FAMILY...

ACKNOWLEDGEMENTS

First and foremost, I would like to thank my advisor, Dr. M. Emin Kutay for his support, guidance, and patience throughout my graduate studies. Dr. Kutay has always provided me with the guidance and support that I needed. I consider myself very lucky to have had him as my advisor.

I would also like to thank the other committee members of my advisory committee, Dr. Neeraj Buch and Dr. Karim Chatti. Their knowledge and support has been very important throughout this study. Special thanks are due to Dr. Syed Haider, and Dr. Gilbert Baladi for all the research guidance and support.

I would also like to thank the Michigan Department of Transportation (MDOT) for their financial support of this study. In addition, the efforts of and the comments made by the MDOT research advisory panel members are sincerely appreciated.

TABLE OF CONTENTS

LIST OF TABLES	vii
LIST OF FIGURES	viii
1. INTRODUCTION.....	1
1.1 Objectives.....	2
1.2 Outline.....	3
2. LITERATURE REVIEW.....	5
2.1 Introduction and background on $ E^* $ test	5
2.2 Complex modulus (E^*).....	6
2.3 Development of $ E^* $ master curve	8
2.4 Relevance of $ E^* $ to M-E PDG	12
2.4.1 Introduction	12
2.4.2 $ E^* $ as a design input in M-E PDG	15
2.5 Dynamic modulus $ E^* $ prediction models	18
2.5.1 Original Witczak model (Andrei et al. 1999) – OW (NCHRP 1-37A)	19
2.5.2 Modified Witczak model (Bari 2005) – MW (NCHRP 1-40D)	20
2.5.3 Hirsch model (Christensen et al. 2003) – HM	21
2.5.4 Law of mixtures parallel model (Al-Khateeb Model)	23
2.5.5 Summary of inputs for $ E^* $ prediction models	23
2.6 Sample geometry and Representative Volume Element (RVE) for $ E^* $	24
3. RESEARCH METHODOLOGY.....	28
3.1 Introduction	28
3.2 Materials used	28
3.2.1 Asphalt mixtures	28
3.2.2 Asphalt binders	29
3.3 Laboratory testing of materials collected	29
3.3.1 Details of laboratory $ E^* $ tests	29
3.3.2 Details of laboratory $ G^* $ tests	30
3.4 Investigation of the Representative Volume Element (RVE) requirement for dynamic modulus $ E^* $ of asphalt mixtures using Thin Beam Mixtures (TBMs)	32
4. LABORATORY TESTING: RESULTS & DISCUSSION	35
4.1 Complex modulus $ E^* $ testing of asphalt mixtures	35
4.1.1 Summary of $ E^* $ values based on MDOT mix designation for each region	39
4.1.2 Comparison of variation in $ E^* $ master curves based on MDOT mix designation..	39
4.1.3 Comparison of variation in $ E^* $ master curve for HMA and WMA asphalt mixtures	43
4.2 Dynamic shear modulus $ G^* $ testing of asphalt binders	45
4.2.1 Comparison of variation in $ G^* $ master curves based on binder PG grade	46

5. E^* PREDICTION MODELS: RESULTS AND DISCUSSION	50
5.2 <i>Evaluation and calibration of the Modified Witczak's equation for Michigan asphalt mixtures</i>	50
5.3 <i>Validation of the calibrated Modified Witczak E^* predictive model for MDOT asphalt mixtures</i>	55
5.4 <i>Evaluation of the ANNACAP software for predicting E^* of MDOT mixtures</i>	57
5.5 <i>Development and validation of a new ANN-based E^* predictive model trained for Michigan asphalt mixtures</i>	58
5.5.1 <i>Structure of the ANN</i>	59
5.5.2 <i>Training the ANN</i>	61
6. INVESTIGATION OF SAMPLE GEOMETRY & RVE REQUIREMENT FOR E^* USING THIN BEAM MIXTURES (TBMs)	66
6.1 <i>Materials Used</i>	66
6.2 <i>Bending Beam Rheometer (BBR) testing on Thin Beam Mixtures (TBMs)</i>	67
6.3 <i>Results and Discussion</i>	69
7. CONCLUSIONS & RECOMMENDATIONS	75
APPENDICES	77
APPENDIX A: <i>VOLUMETRIC PROPERTIES AND AGGREGATE GRADATION OF THE TESTED ASPHALT MIXTURES.</i>	78
APPENDIX B: <i>A LIST OF ASPHALT MIXTURE SAMPLES TESTED IN THIS STUDY ALONG WITH THE CORRESPONDING AIR VOID LEVEL OF EACH SAMPLE</i>	85
APPENDIX C: <i>E^* MASTER CURVES OF THE TESTED ASPHALT MIXTURES GROUPED BASED ON THE MDOT MIX DESIGNATION</i>	93
APPENDIX D: <i>G^* MASTER CURVES GROUPED BASED ON THE PG GRADE</i>	102
REFERENCES	108

LIST OF TABLES

Table 2.1: A and VTS values reported in Birgisson et al. (2005).	14
Table 2.2: Parameters used in different $ E^* $ predictive models.	23
Table 4.1: HMAs tested for $ E^* $ master curve.....	34
Table 4.2: HMAs tested for $ E^* $ master curve (GGSP and LVSP Mixtures).....	36
Table 4.3: HMAs tested for $ E^* $ master curve (SUPERPAVE) – Mixtures that do not follow MDOT specifications but are permitted to be used.....	37
Table 4.4: HMAs tested for $ E^* $ master curve (GGSP and LVSP Mixtures) - Mixtures that do not follow MDOT specifications but are permitted to be used.	37
Table 4.5: Summary of $ E^* $ values for different asphalt mixture types in NGBSU Regions	40
Table 4.6: Summary of $ E^* $ values for different asphalt mixture types in the Metro Region.....	41
Table 4.7: Summary of $ E^* $ values for different asphalt mixture types in Superior Region.....	42
Table 4.8: List of binder PGs tested in this study.....	46
Table 5.1: Comparison between coefficients used in the original and optimized models.	55
Table 6.1: List of TBMs tested along with their volumetric properties and NMAS.....	68
Table A.1: Volumetric properties and aggregate gradation of the tested asphalt mixtures.....	79
Table B.1: List of HMAs tested and their air voids.....	86

LIST OF FIGURES

Figure 2.1: Illustration of cyclic loading of an asphalt specimen and corresponding strain response (for interpretation of the references to color in this and all other figures, the reader is referred to the electronic version of this thesis).7

Figure 2.2: Unshifted (original) $|E^*|$ data at different temperatures versus frequency.10

Figure 2.3: Illustration of shifted $|E^*|$ data at different temperatures versus reduced frequency to obtain the master curve.10

Figure 2.4: Shift factor ($a(T)$) coefficients at different temperatures for an asphalt mixture. (a) $|E^*|$ master curve. (b) Shift factor polynomial curve.11

Figure 2.5: Illustration of two typical $|E^*|$ mastercurves and expected fatigue and rutting performance trends for these $|E^*|$ master curves.17

Figure 3.1: Asphalt Mixture Performance Tester (AMPT)29

Figure 3.2: Illustration of the Dynamic Shear Rheometer (DSR) testing machine30

Figure 3.3: Illustration of stress-strain relationship of asphalt binders when they are subjected to cyclic shear load31

Figure 3.4: Illustration of Thin Beam Mixture sample preparation and testing.33

Figure 4.1: Dynamic Modulus master curves of all tested asphalt mixture specimens. The plot in log-log scale is to show the differences in low frequency/high temperature, and the plot in linear-log scale is to show the differences in high frequency/low temperature.38

Figure 4.2: $|E^*|$ master curves of four 3E3 mixtures, 3 of which (26* mixes) are from same region. NGBSU = North, Grand, Bay, Southwest and University Regions.43

Figure 4.3: WMA versus HMA $ E^* $ master curves for (3E30) MDOT mixture.....	44
Figure 4.4: WMA versus HMA $ E^* $ master curves for (LVSP) MDOT mixture.....	44
Figure 4.5: Aggregate gradation of WMA and HMA mixtures ((LVSP) MDOT mixture).....	45
Figure 4.6: $ G^* $ Master curves of seven different PG64-28 binders. NGBSU = North, Grand, Bay, Southwest and University Regions.....	47
Figure 4.7: Illustration of the effect of variation in $ G^* $ and δ on Longitudinal cracking predictions in the M-E PDG software.	48
Figure 4.8: Illustration of the effect of variation in $ G^* $ and δ on alligator cracking predictions in the M-E PDG software.	48
Figure 4.9: Illustration of the effect of variation in $ G^* $ and δ on IRI predictions in the M-E PDG software.	49
Figure 4.10: Illustration of the effect of variation in $ G^* $ and δ on rutting predictions in the M-E PDG software.	49
Figure 5.1: The modified Witczak's equation developed as part of the NCHRP 1-40D. The plot shows the predicted versus measured values before calibration for MDOT mixtures. $S_e/S_y = 0.5084$, $R^2 = 0.7881$ (linear-linear plot), and $S_e/S_y = 0.446$, $R^2 = 0.8369$ (log-log plot).	53
Figure 5.2: The modified Witczak's equation developed as part of the NCHRP 1-40D. The plot shows the predicted versus measured values after calibration for MDOT mixtures. $S_e/S_y = 0.3029$, $R^2 = 0.9248$ (linear-linear plot), and $S_e/S_y = 0.2053$, $R^2 = 0.965$ (log-log plot).	54
Figure 5.3: The modified Witczak's equation developed as part of the NCHRP 1-40D. The plot shows the predicted versus measured values for MDOT mixtures using the calibrated coefficients. $S_e/S_y = 0.3749$, $R^2 = 0.885$ (log-log plot).	56

Figure 5.4: Predicted versus measured values for MDOT mixtures using the ANNACAP software: (a) Linear-Linear plot, (b) Log-Log plot.	57
Figure 5.5: Structure of the ANN model.	60
Figure 5.6: Error versus the epochs in the ANN model developed in this study	63
Figure 5.7: Predicted versus measured $ E^* $ values for Training, Validation and Testing datasets as well as all the data (for mixtures used during development of the model).	64
Figure 5.8: Predicted versus measured values for MDOT mixtures using the MSU-ANN model for mixtures not used during development of the model	65
Figure 6.1: 3-point testing concept on asphalt mixtures.....	67
Figure 6.2: Comparison between $ E^* $ -based $D(t)$ values and TBM-based $D(t)$ values for 25.0mm NMAS.....	71
Figure 6.3: Comparison between $ E^* $ -based $D(t)$ values and TBM-based $D(t)$ values for 19.0mm NMAS.....	71
Figure 6.4: Comparison between $ E^* $ -based $D(t)$ values and TBM-based $D(t)$ values for 12.5mm NMAS.....	72
Figure 6.5: Comparison between $ E^* $ -based $D(t)$ values and TBM-based $D(t)$ values for 9.5mm NMAS.....	72
Figure 6.6: Comparison between $ E^* $ -based $D(t)$ values and TBM-based $D(t)$ values for all mixtures and NMASs.....	73
Figure C.1: Dynamic modulus $ E^* $ master curves for 3E30 mixes.....	94
Figure C.2: Dynamic modulus $ E^* $ master curves for 3E3 mixes.....	94

Figure C.3: Dynamic modulus $ E^* $ master curves for 3E10 mixes.....	95
Figure C.4: Dynamic modulus $ E^* $ master curves for 4E30 mixes.....	95
Figure C.5: Dynamic modulus $ E^* $ master curves for 4E3 mixes.....	96
Figure C.6: Dynamic modulus $ E^* $ master curves for 4E10 mixes.....	96
Figure C.7: Dynamic modulus $ E^* $ master curves for 4E1 mixes.....	97
Figure C.8: Dynamic modulus $ E^* $ master curves for 5E10 mixes.....	97
Figure C.9: Dynamic modulus $ E^* $ master curves for 5E03 mixes.....	98
Figure C.10: Dynamic modulus $ E^* $ master curves for 5E3 mixes.....	98
Figure C.11: Dynamic modulus $ E^* $ master curves for 5E1 mixes.....	99
Figure C.12: Dynamic modulus $ E^* $ master curves for 2E3 mixes.....	99
Figure C.13: Dynamic modulus $ E^* $ master curves for 5E30 mixes.....	100
Figure C.14: Dynamic modulus $ E^* $ master curves for ASCRL mixes.....	100
Figure C.15: Dynamic modulus $ E^* $ master curves for GGSP mixes.....	101
Figure C.16: Dynamic modulus $ E^* $ master curves for LVSP mixes.....	101
Figure D.1: $ G^* $ master curves of different PG70-28P binders. NGBSU = North, Grand, Bay, Southwest and University Regions.....	103

Figure D.2: $|G^*|$ master curves of different PG64-28 binders. NGBSU = North, Grand, Bay, Southwest and University Regions..... 103

Figure D.3: $|G^*|$ master curve of a PG70-28 binder. NGBSU = North, Grand, Bay, Southwest and University Regions..... 104

Figure D.4: $|G^*|$ master curves of different PG64-34P binders. NGBSU = North, Grand, Bay, Southwest and University Regions..... 104

Figure D.5: $|G^*|$ master curves of different PG64-22 binders. NGBSU = North, Grand, Bay, Southwest and University Regions..... 105

Figure D.6: $|G^*|$ master curves of different PG70-22P binders..... 105

Figure D.7: $|G^*|$ master curves of different PG58-22 binders. NGBSU = North, Grand, Bay, Southwest and University Regions..... 106

Figure D.8: $|G^*|$ master curves of different PG58-28 binders. NGBSU = North, Grand, Bay, Southwest and University Regions..... 106

Figure D.9: $|G^*|$ master curves of different PG58-22 binders. NGBSU = North, Grand, Bay, Southwest and University Regions. 107

Figure D.10: $|G^*|$ master curves of different PG58-34 binders..... 107

INTRODUCTION

Complex (Dynamic) Modulus $|E^*|$ is a unique viscoelastic material property that defines the stress-strain relationship of asphalt mixtures when they are loaded in a cyclic mode. The $|E^*|$ is also used as a measure of stiffness and to compute the primary response (i.e., response to low, non-damaging stress) of asphalt pavements at different temperatures and loading rates. In addition, $|E^*|$ is directly related to the expected pavement performance (i.e., rutting and fatigue cracking) in the field. The Mechanistic-Empirical Pavement Design Guide (M-E PDG) pavement design software developed under the NCHRP Project 1-37A is becoming the state-of-the-practice in both newly constructed and rehabilitated pavement designs. The M-E PDG utilizes semi-mechanistic and semi-empirical models to predict the distresses such as fatigue cracking, rutting and thermal cracking in asphalt pavements. The design software determines the modulus of asphalt materials at different temperatures and loading rates from a “master curve” generated to combine the effects of frequency and temperature on $|E^*|$. Once $|E^*|$ values are measured at different temperatures (T) and loading frequencies (f), the $|E^*|$ master curve is obtained using the time-temperature superposition (TTS) principle (Kim 2009). Laboratory test data at different temperatures and loading frequencies are shifted with respect to time to form a good sigmoid fit to the $|E^*|$ data. This constructed master curve describes the time (and frequency) dependency of the material. The amount of shifting for each test data at each temperature describes the temperature dependency of the material (NCHRP 9-19 2005). Development of $|E^*|$ master curve is very useful because once the sigmoid coefficients, shift factor coefficients, and reference temperature are known, $|E^*|$ at any temperature (T) and frequency (f) can be computed.

A number of different material inputs are required by the M-E PDG, and accurate measurement of these inputs is crucial for the accuracy of the distress predictions. Many State Departments of Transportation (DOTs) (including the Michigan Department of Transportation (MDOT)) do not have a testing program to measure certain key inputs required by the M-E PDG. In flexible (asphalt) pavement design, the most important and hard-to-obtain material inputs for the Level 1 analysis are: (i) complex (dynamic) modulus ($|E^*|$) master curve of asphalt mixture, (ii) complex (dynamic) shear modulus ($|G^*|$) master curve of asphalt binder, (iii) Indirect Tensile (IDT) Strength and creep compliance ($D(t)$) of the asphalt mixture. The $|G^*|$ master curve, which defines the linear viscoelastic property of an asphalt binder, is required by both Level 1 and Level 2 analyses of the M-E PDG. In Level 1 analysis, $|G^*|$ is primarily used in asphalt aging models, whereas in Level 2, it is used in both aging models and in predicting the $|E^*|$ master curve of the asphalt mixture using Witczak's predictive equation. It is noted that Witczak's equation predicts the $|E^*|$ of the mixture from the binder $|G^*|$ as well as mixture volumetrics such as the aggregate gradation, binder content etc. Level 3 analysis in M-E PDG does not require testing of $|E^*|$ and $|G^*|$ and uses typical values based on the binder performance grade (PG). However, in all levels (Levels 1, 2 and 3), thermal cracking prediction model requires the Indirect Tensile Strength (IDT) as well as the Creep Compliance ($D(t)$) values.

1.1 Objectives

The main objective of the research study presented in this thesis was to investigate linear viscoelastic characteristics of typical asphalt mixtures and asphalt binders used in Michigan. This

is important for implementation of the M-E PDG in Michigan and for accurate prediction of flexible pavement distresses.

The second objective was to develop analytical models that can better predict the dynamic modulus $|E^*|$ of asphalt mixtures commonly used in the State of Michigan. For this, the Modified Witczak model was locally calibrated. In addition; an Artificial Neural Network (ANN) model was developed and trained in an effort to develop a more improved $|E^*|$ predictive model. An ANN-based model was developed using the data generated as part of this study using similar inputs and volumetric properties required in the Modified Witczak model.

Another objective of this study was to investigate the Representative Volume Element (RVE) requirement for dynamic modulus $|E^*|$ of asphalt mixtures. Small thin mixture beam (TBM) specimens (0.5"x0.2"x4.5") were tested using the Bending Beam Rheometer (BBR) testing machine to obtain the Creep Compliance (D(t)). Using the basic theory of viscoelasticity, $|E^*|$ laboratory measurements on regular size specimens were converted to D(t) values and compared with the values measured using the BBR machine on the TBMs. Once the RVE requirement is investigated and verified, this will serve as a foundation for a study of the effect of aging on the material properties, and on pavement performance.

1.2 Outline

This thesis is organized as follows: Chapter 2 presents a literature review on the dynamic modulus ($|E^*|$) test background and development of the $|E^*|$ master curve. Also, a discussion on the relevance of this material characteristic to the M-E PDG software and how it effects the distress predictions is shown. Chapter 2 also discusses different $|E^*|$ predictive models and the

effect of sample geometry on the $|E^*|$ test and the Representative Volume Element (RVE) requirement for the $|E^*|$ test. Chapter 3 is the methodology used in this study and shows all of the materials used in the analysis. Chapters 4 and 5 present the results and discussion part on the laboratory testing and $|E^*|$ predictive models, respectively. Chapter 6 shows a study on the RVE requirement for asphalt mixtures and addresses the feasibility of using the Bending Beam Rheometer (BBR) test on thin asphalt mixture beams to obtain fundamental engineering material properties.

2. LITERATURE REVIEW

2.1 Introduction and background on $|E^*|$ test

The complex modulus testing for asphalt mixtures is a relatively old concept. Papazian (1962) was one of the first to use the triaxial cyclic complex modulus test in an effort to describe viscoelastic characterization of asphalt mixtures. A sinusoidal stress was applied to a cylindrical specimen at a given frequency, and the resulting sinusoidal strain response at the same frequency was measured (Clyne et al. 2003). He concluded that viscoelastic concepts could be applied to asphalt pavement design and performance. About fifty years later, we are still using the same concept to better understand the performance of pavement materials.

The most comprehensive research effort towards the complex modulus as a material property started in mid-90s as part of the NCHRP Project 9-19 “Superpave Support and Performance Models Management” and NCHRP Project 9-29 “Simple Performance Tester for Superpave Mix Design” (NCHRP 9-19 2005, and NCHRP 9-29 2002). This research effort was directed towards proposing new guidelines for the proper test specimen geometry and size. Specimen preparation, testing procedure, loading pattern, and empirical models were also addressed in the mentioned projects. After running numerous complex modulus tests, the research panel recommended using 100mm diameter cored specimens from 150mm diameter gyratory compacted specimens, with a saw cut final height of 150mm. In addition, fully lubricated end plates were found useful to minimize end restraint on specimens. The research projects also concluded that the $|E^*|$ test provides necessary input for structural analysis and is

tied to the M-E PDG design tool, and is a rational way to establish guidelines, and performance criteria (NCHRP Project 9-29).

2.2 Complex modulus (E^*)

The complex modulus E^* defines the stress-strain relationship of asphalt mixtures when they are loaded in a cyclic mode. Figure 2.1 shows a typical response of a cylindrical asphalt specimen when subjected to a haversine loading. As shown, the measured strain also has a haversine shape, with a delay in the peak as compared to the peak of the stress. This time delay is used to calculate the phase angle of the material. For perfectly elastic materials, the phase angle is zero; for perfectly viscous materials (e.g., fluids), the phase angle is 90 degrees. It should be noted that the behavior seen in Figure 2.1 is linear viscoelastic and only observed if the loading level does not result in strain levels larger than 100-120 microstrain. At higher load levels, plastic deformation occurs at high temperatures (40-70°C) and microcracking initiates at intermediate (10-30°C) temperatures.

The understanding of linear viscoelasticity concepts is vital for comprehension of the complex modulus test (Clyne et al. 2003). Based on the fundamental concepts of linear viscoelasticity, the one dimensional case of sinusoidal loading can be represented by the following equation (Ferry 1980):

$$\sigma = \sigma_0 \cdot e^{i\omega t} \quad [2.1]$$

where σ_0 is the stress amplitude and ω is the angular frequency related to the frequency f by the following equation:

$$\omega = 2\pi f \quad [2.2]$$

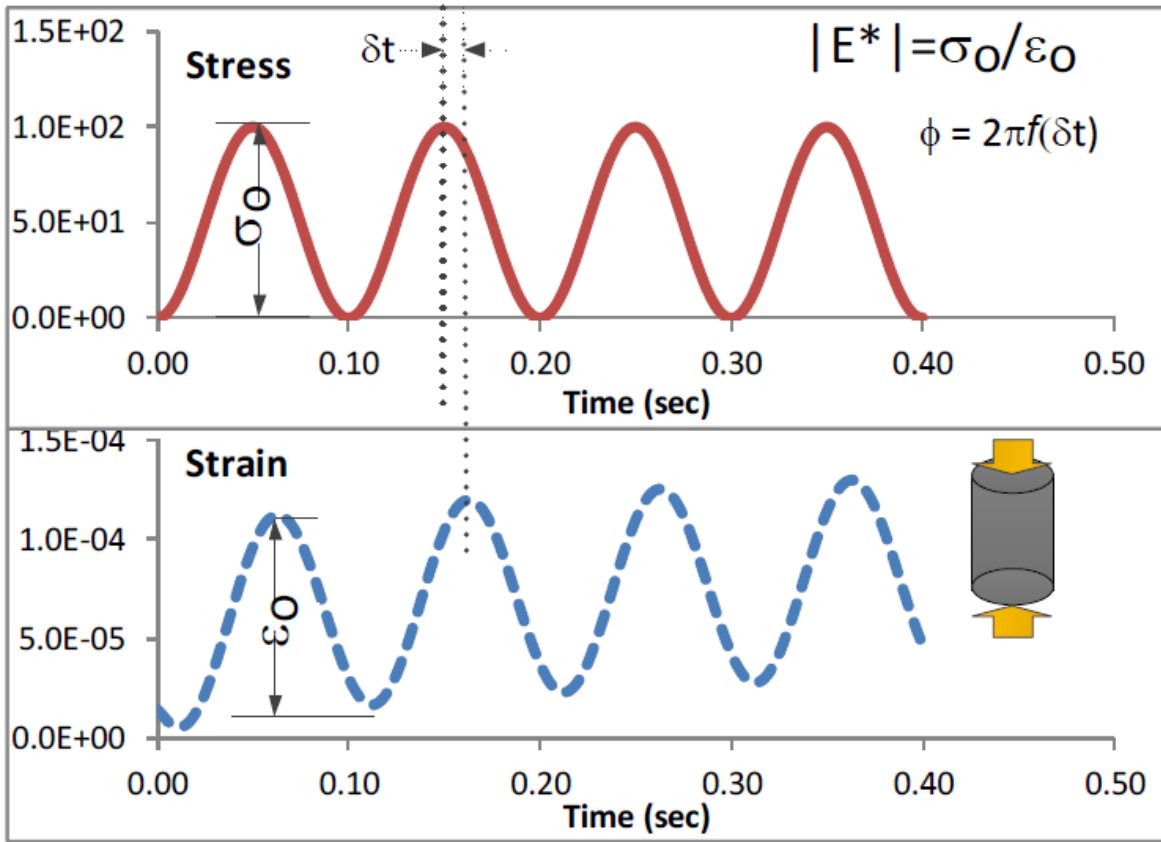


Figure 2.1: Illustration of cyclic loading of an asphalt specimen and corresponding strain response (for interpretation of the references to color in this and all other figures, the reader is referred to the electronic version of this thesis).

The resulting steady state strain is expressed by the following equation:

$$\varepsilon = \varepsilon_0 \cdot e^{(i\omega t - \delta)} \quad [2.3]$$

where ε_0 is the strain amplitude, and δ is the phase angle of the material caused by the time delay between applied stress and resulting strain shown in Figure 2.1. Complex modulus (E^*) is defined as:

$$E^* = E' + iE'' \quad [2.4]$$

where (E'') is the loss modulus, and (E') is the storage modulus. The loss modulus describes the viscous component and the storage modulus describes the elastic component expressed as (Birgisson et al., 2004):

$$E'' = |E^*|. \sin\delta \quad [2.5]$$

$$E' = |E^*|. \cos\delta \quad [2.6]$$

The phase angle of the material (δ) can be expressed as:

$$\delta = \tan^{-1} \left(\frac{E''}{E'} \right) \quad [2.7]$$

The dynamic modulus is the absolute value of the complex modulus defined as (Yoder & Witczak, 1975):

$$|E^*| = \frac{\sigma_{peak}}{\varepsilon_{peak}} \quad [2.8]$$

where σ_{peak} and ε_{peak} are the peak stress and strain, respectively.

1.2 Development of $|E^*|$ master curve

Asphalt mixtures have different $|E^*|$ values at different temperatures and loading frequencies. The $|E^*|$ increases with increasing frequency, decreases with increasing temperature. In order to be able to combine the effects of frequency and temperature on $|E^*|$, a master curve is generated. Once $|E^*|$ values are measured at different temperatures (T) and loading frequencies (f), the $|E^*|$ master curve is obtained using the time-temperature superposition (TTS) principle (Kim 2009). Figure 2.2 shows a graph of $|E^*|$ values at different temperatures and frequencies

that is generated from raw $|E^*|$ data. Based on the TTS principle, a single $|E^*|$ master curve can be obtained by shifting the $|E^*|$ data obtained at different temperatures horizontally as shown in Figure 2.3. Once shifted, the parameter in x-axis is called reduced frequency (f_R), which is defined as follows:

$$f_R = f \cdot a_T(T) \quad [2.9]$$

where f is the frequency of the load and $a_T(T)$ is the shift factor coefficient for a given temperature T . As shown in Figure 2.4, the shift factor coefficient ($a_T(T)$), i.e., the amount of horizontal shift for each temperature is different. During shifting process, the shift factors at each temperature are varied until a good sigmoid fit to the $|E^*|$ data of all temperatures is obtained. Typically the following sigmoid function is used:

$$\log(|E^*|) = b_1 + \frac{b_2}{1 + \exp(-b_3 - b_4 \cdot \log(f_R))} \quad [2.10]$$

where b_1 , b_2 , b_3 , and b_4 are the sigmoid coefficients, and f_R is the reduced frequency.

After the shifting is completed and the shift factor coefficients ($a_T(T)$) are determined, they are plotted against each temperature (T) as shown in Figure 2.4b. Then a second order polynomial is fitted to the data (also shown in Figure 2.4b) to obtain the polynomial coefficients a_1 and a_2 in the following equation:

$$a_T(T) = 10^{a_1(T^2 - T_{ref}^2) + a_2(T - T_{ref})} \quad [2.11]$$

where $a_T(T)$ is the shift factor coefficient, a_1 , and a_2 are the polynomial fit constants, and T_{ref} is the reference temperature.

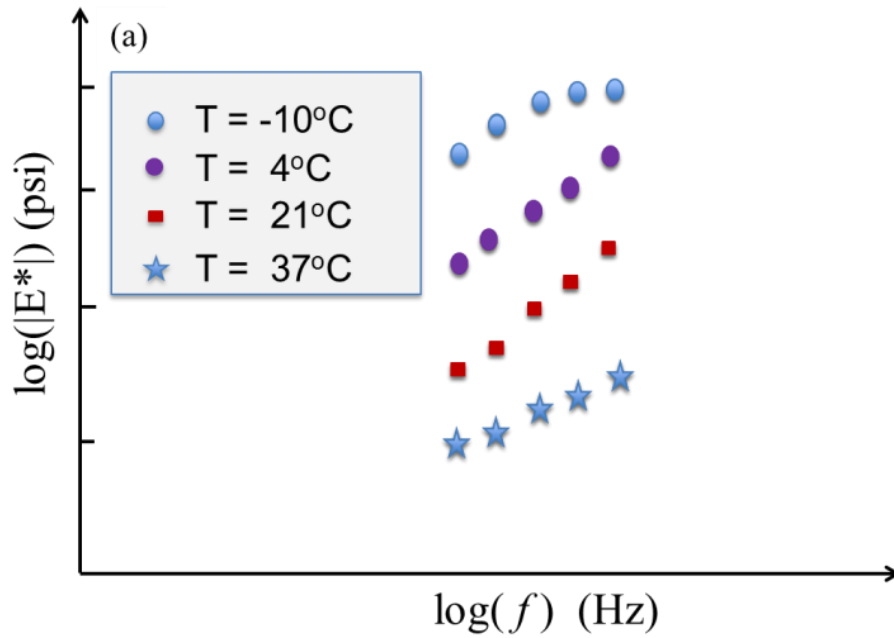


Figure 2.2: Unshifted (original) $|E^*|$ data at different temperatures versus frequency.

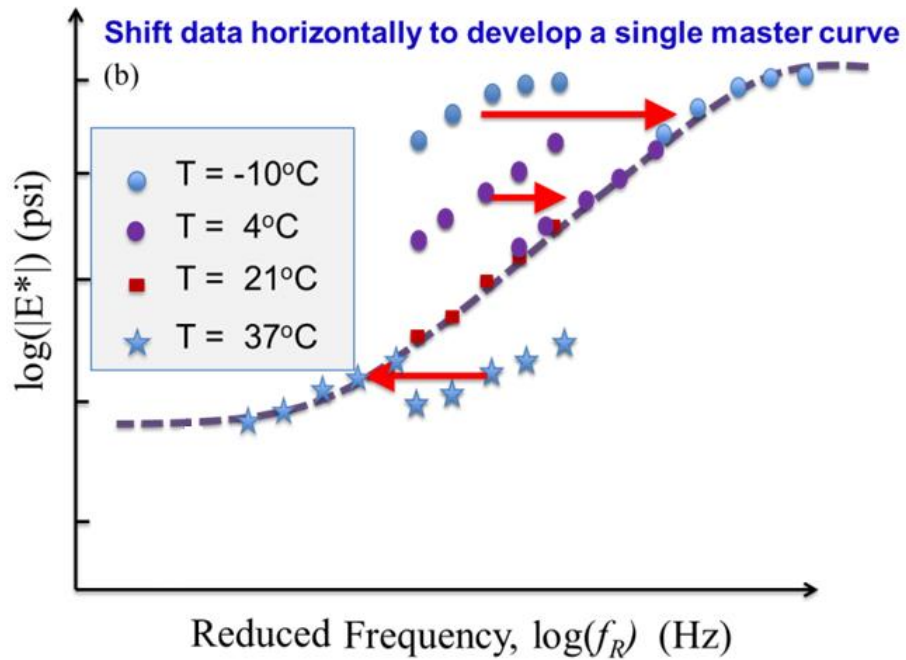


Figure 2.3: Illustration of shifted $|E^*|$ data at different temperatures versus reduced frequency to obtain the master curve.

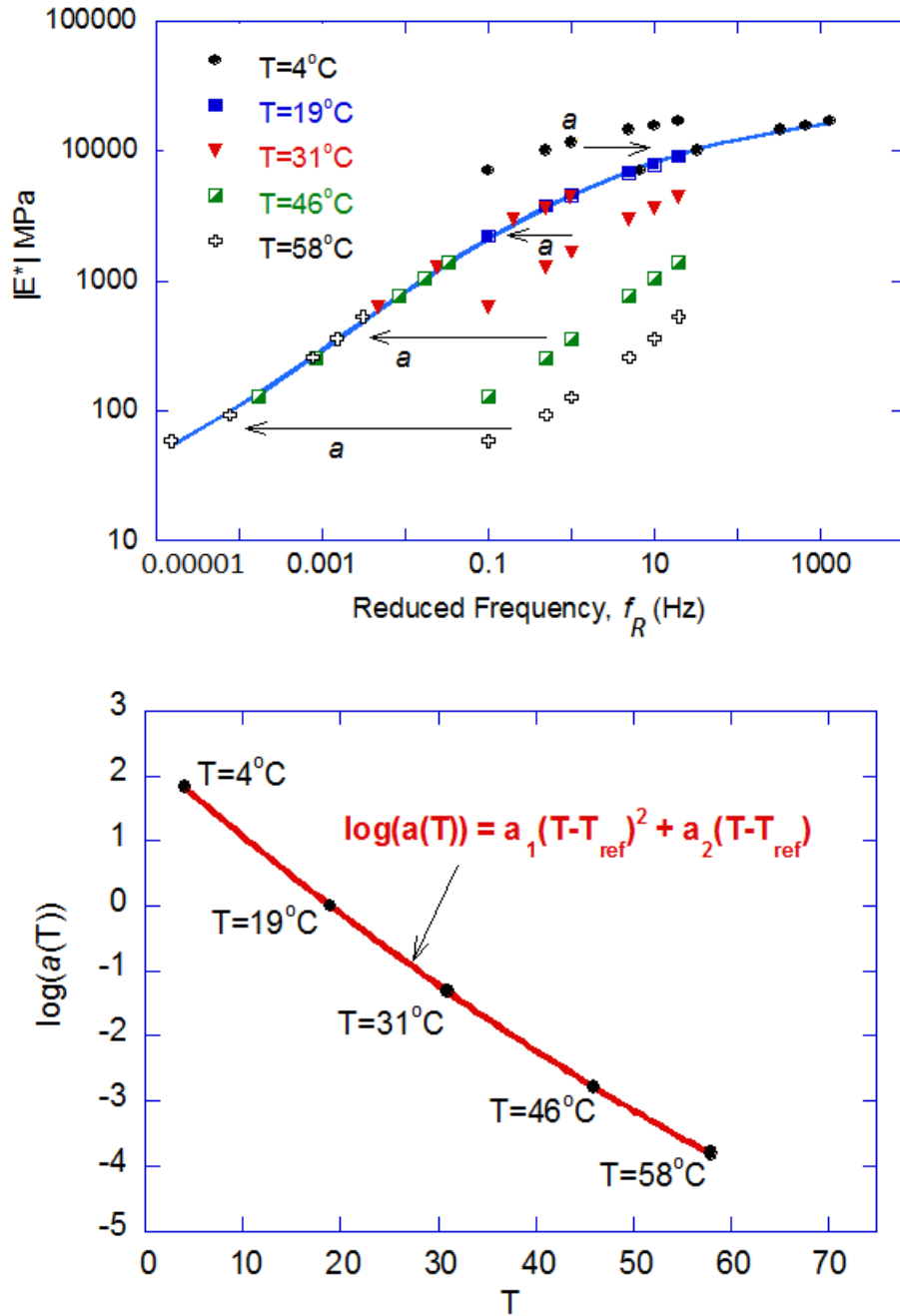


Figure 2.4: Shift factor ($a(T)$) coefficients at different temperatures for an asphalt mixture. (a) $|E^*|$ master curve. (b) Shift factor polynomial curve.

Development of $|E^*|$ master curve is very useful because once b_1 , b_2 , b_3 , b_4 , a_1 , a_2 and T_{ref} are known, $|E^*|$ at any temperature (T) and frequency (f) can be computed.

2.4 Relevance of $|E^*|$ to M-E PDG

2.4.1 Introduction

After inception of M-E PDG, several States conducted asphalt mixture characterization studies in support of M-E PDG (Flintsch et al. 2008, Mohammad 2010, Clyne et al. 2003, Flintsch et al. 2005, Birgisson et al. 2005). The key objective of these studies was to obtain the fundamental material characteristics of asphalt mixtures that are required by the M-E PDG software.

In support of M-E PDG implementation in Virginia, Flintsch et al. (2008) conducted $|E^*|$ tests on 11 different asphalt mixture types. The research team concluded that $|E^*|$ of the mixtures common in VA is sensitive to the constituent properties of asphalt mixture (aggregate type, asphalt content, percentage of recycled asphalt pavement, etc.). They also found that M-E PDG's level 2 $|E^*|$ prediction equation reasonably estimated the measured dynamic modulus; however, it did not capture some of the differences between the mixes as found in the measured data. They used the Original Witzcak's (OW) equation (which is based on the viscosity of asphalt binder) to predict $|E^*|$ and compared it to their measurements. The authors did not measure viscosity values at different temperatures; instead, they used empirical equations to calculate the viscosity at different temperatures.

Mohammad et al. (2007) conducted $|E^*|$ tests on 13 different asphalt mixture types common to Louisiana. The research team evaluated the Witzcak and Hirsch models and found that predictions of the dynamic modulus $|E^*|$ values were reasonable. They indicated that the Witzcak model accuracy increases for higher Nominal Maximum Aggregate Size (NMAS),

whereas the Hirsch model accuracy increases for lower NMAAS. They did not specify how they determined the viscosity or $|G^*|/\delta$ values for binder for use in Witczak's or Hirsch models.

Clyne et al. (2003) performed $|E^*|$ tests on four different asphalt mixtures commonly used in Minnesota from the MnROAD site. $|E^*|$ and phase angle vs. frequency mastercurves generated from the test data were compared to results obtained from Witczak's predictive equations. The modulus values calculated using the Original Witczak (OW) predictive equation provided a reasonable prediction of the dynamic modulus for only two of the four mixtures evaluated. It was stated that the 2000 predictive equation should be used with caution. However, smooth master curves for phase angle could not be obtained, and use of the same shift factors as for the complex modulus master curves did not result in smooth master curves for the phase angle. The authors also indicated that sample preparation techniques affect the results of dynamic modulus testing. The recommended procedure (NCHRP 9-29) of coring and cutting test specimens led to a lower modulus than that of specimens compacted directly to size for the mixture investigated. The authors indicated that the potential reason for this is that the cored specimens likely had rather uniform air voids throughout the specimen. The compacted specimens probably contained density gradients axially and radially throughout the specimens.

Birgisson et al. (2005) focused on the evaluation of the dynamic modulus predictive equation used in the M-E PDG for mixtures typical to Florida. The research program consisted of dynamic modulus testing of 28 different mixtures. The results showed that the predictive equation used appeared (on the average) to work well for Florida mixtures. However; they recommended a multiplier to account for the uniqueness of local mixtures. The results of the

study also identified optimal viscosity-temperature relationships that result in the closest correspondence between measured and predicted dynamic modulus values. The authors developed regression relationships that can be used to correct the predicted modulus values on the average (Table 2.1). It was found that the dynamic modulus predictions using input viscosities obtained from the Dynamic Shear Rheometer (DSR) test results were lower than the measured values. Hence, consistent with the recommendations by Witzcak et al. (2002), if the user wants to underestimate the dynamic modulus slightly, it was recommended that viscosity-temperature regression coefficient (A and VTS) values used to generate input viscosities for the predictive equation be obtained from the DSR test. The study also indicated that the viscosity-temperature regression coefficients (A and VTS) should be obtained from the Brookfield rotational viscometer test or alternatively the mix/ laydown conditions proposed by Witzcak and Fonseca (1996). The results also showed that dynamic modulus predictions at higher temperatures are generally closer to measured values than modulus predictions at lower temperatures.

Table 2.1: A and VTS values reported in Birgisson et al. (2005).

Regression Constants	From Brookfield Rotational Viscometer Test Results	From Dynamic Shear Rheometer Test Results	From Mix/Laydown Conditions suggested by Witzcak and Fonseca
A	-3.4655	-3.0165	-3.56455
VTS	10.407	9.0824	10.6768

2.4.2 $|E^*|$ as a design input in M-E PDG

The $|E^*|$ is one of the main parameters used in the bottom-up, top-down fatigue cracking and the rutting model for the mechanistic-empirical design procedure. Laboratory measured $|E^*|$ data are needed to develop master curves and shift factors based on Equation 2.8 and Equation 2.9 for the Level 1 analysis in the M-E PDG. The Modified Witczak predictive equation developed as part of the NCHRP Project 1-40D is used to predict $|E^*|$ using binder test data for Level 2 analysis. Level 3 analysis uses the Superpave binder Performance Grade (e.g., PG 64-22) to predict $|E^*|$ based on A-VTS relationship using the Original Witczak predictive equation developed as part of the NCHRP Project 1-37A.

Summary of procedure used by the M-E PDG for fatigue cracking and rutting predictions

The M-E PDG divides the pavement structure into sublayers and divides the analysis period (i.e., the performance prediction period) into one month intervals, then for each period:

- 1) The Enhanced Integrated Climatic Model (EICM) predicts the temperature variation with depth for each sublayer.
- 2) An equivalent frequency is chosen based on the traffic speed, type of road facility (interstate, urban street etc.) and depth of each sublayer.
- 3) From the temperature and frequency (steps 1 and 2 above), an $|E^*|$ is selected/computed and used as elastic modulus $E = |E^*|$ in a layered elastic pavement model called JULEA.

- 4) In the bottom-up fatigue cracking model, JULEA predicts the tensile strain at the base of the asphalt and uses it in the MS-1 model to predict the number of cycles to failure (N_f) for the given analysis period. Then this N_f is used in Miner's damage accumulation law to predict the damage caused by the bottom-up fatigue cracking.
- 5) In the top-down fatigue cracking model, JULEA predicts the tensile strain at the edge of the tire and uses it in another MS-1 type empirical model to predict the number of cycles to failure (N_f) for the given analysis period. Then this N_f is used in Miner's damage accumulation law to predict the damage because of top-down fatigue cracking.
- 6) In the rutting model, the resilient strain of the material is predicted by JULEA and used in the empirical rutting model, along with the temperature and number of load repetitions.

The detailed description of JULEA, MS-1, Miner's law and rutting models mentioned above can be found in the M-E PDG documentation (Appendices GG, II, and RR).

Effect of $|E^*|$ master curve on fatigue and rutting predictions in M-E PDG

Figure 2.5 illustrates two conceptual $|E^*|$ master curves labeled as Mix-A and Mix-B. In an $|E^*|$ master curve graph, the left side of the graph corresponds to high temperature and low frequency, whereas the right side of the graph corresponds to low temperature and high frequency, as illustrated in Figure 2.5. Typically, better fatigue resistance is expected if the $|E^*|$ curve is relatively low on the right side of the curve. Conversely, better rutting resistance is expected if the $|E^*|$ curve is relatively high in the left side of the curve. In Figure 2.5, Mix-A is typically expected to perform better in both rutting and fatigue resistance as compared to Mix-B. The middle of the $|E^*|$ master curve, for most mixtures, corresponds to 21°C (~70°F) at 0.1 Hz.

Therefore, relatively low temperatures (right side of the vertical dashed line in the middle of the curves in Figure 2.5) corresponds to temperatures less than 70°F, the left side is the temperatures higher than 70°F. It should be noted that this mid point (i.e., median temperature) can be slightly different for different mixtures.

It should be noted that very soft mixes may not necessarily lead to better fatigue resistance. The fatigue resistance, in addition to the $|E^*|$, is also related to the tensile strain at the base of the pavement structure being analyzed. Therefore, excessively soft asphalt mixtures may lead to excessive tensile strain at the base of the asphalt layer, which can cancel out the beneficial effect of low $|E^*|$ (see MS-1 model in the MEPDG documentation).

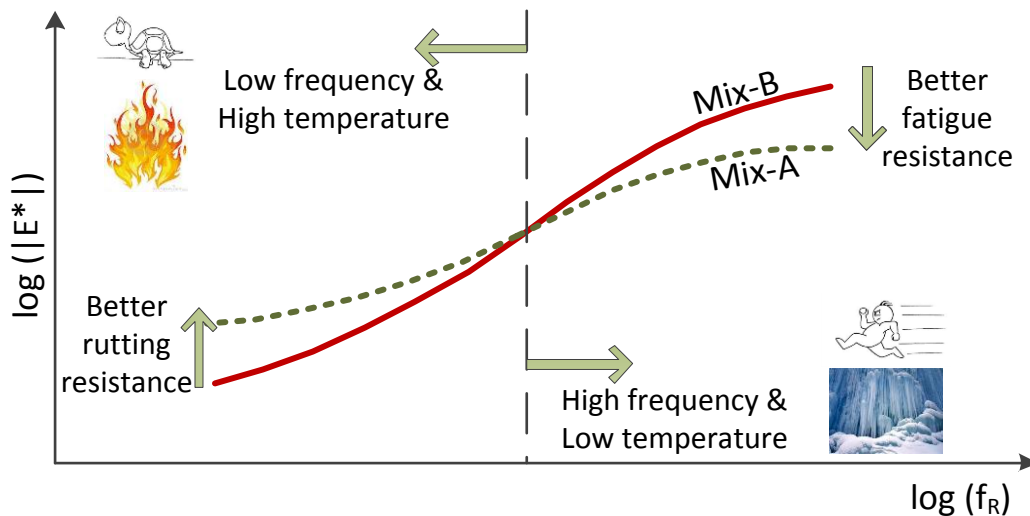


Figure 2.5: Illustration of two typical $|E^*|$ mastercurves and expected fatigue and rutting performance trends for these $|E^*|$ master curves.

2.5 Dynamic modulus $|E^*|$ prediction models

The dynamic modulus test is a tedious experiment and relatively expensive to perform and may take several days to develop a master curve for a unique asphalt mixture (Birgisson et al. 2005). In addition, costly equipment and trained personnel are needed for sample preparation, testing, and data analyses (Azari et al. 2007). Given the significance of $|E^*|$ as a design parameter in the M-E PDG software, and to overcome the difficulties of laboratory testing; several researchers developed relationships between the characteristics of asphalt mixture constituents (e.g., mix design parameters and binder characteristics) and $|E^*|$ master curve (Bonnaure et al. 1977, Andrei et al. 1999, Bari 2005, Christensen et al. 2003, Al-Khateeb et al. 2006).

2.5.1 Original Witczak model (Andrei et al. 1999) – OW (NCHRP 1-37A)

Andrei et al. (1999) developed a revised version of the original Witczak $|E^*|$ predictive equation based on data from 205 mixtures with 2,750 data points. The predictive model is given in the following equation:

$$\begin{aligned} \log_{10}|E^*| = & \\ & -1.249937 + 0.02923p_{200} - 0.001767(p_{200})^2 - 0.002841p_4 \\ & - 0.05809V_a - 0.082208 \frac{V_{beff}}{V_{beff} + V_a} \\ & + \frac{3.871977 - 0.0021p_4 + 0.003958p_{\frac{3}{8}} - 0.000017 \left(p_{\frac{3}{8}}\right)^2 + 0.00547p_{\frac{3}{8}}}{1 + \exp(-0.603313 - 0.313351\log f - 0.393532\log \eta)} \end{aligned} \quad [2.12]$$

where:

$$|E^*| = \text{Asphalt mix modulus, psi (x10}^5\text{)}.$$

- p_{200} = Percentage of aggregate passing #200 sieve.
- p_4 = Cumulative percentage of aggregate retained in #4 sieve.
- $p_{3/8}$ = Cumulative percentage of aggregate retained in 3/8-inch (9.56-mm) sieve.
- $p_{3/4}$ = Cumulative percentage of aggregate retained in 3/4-inch (19.01-mm) sieve.
- V_a = Percentage of air voids (by volume of mix).
- V_{beff} = Percentage of effective asphalt content (by volume of mix).
- f = Loading frequency (hertz).
- η = Binder viscosity at temperature of interest ($\times 10^6$ poise).

The preceding equation is based on nonlinear regression analysis using the generalized gradient optimization approach in Microsoft Excel Solver (Kim et al. 2011). This model is currently one of two options for levels 2 and 3 analyses in the M-E PDG software (NCHRP 1-37A, 2004). The M-E PDG software converts all level 2 and level 3 inputs into A-VTS values to develop the $|E^*|$ master curve (Kim et al. 2011).

One of the limitations of the Witczak equation is that it relies on other models to convert the $|G^*|$ to binder viscosity. Also, extrapolation beyond the calibration database is restricted since the predictive equation is based on regression analysis (Bari 2005). In addition, the need to improve sensitivity of the model to mixture volumetrics was noted by Dongre et al. (2005).

2.5.2 Modified Witczak model (Bari 2005) – MW (NCHRP 1-40D)

In order to include binder $|G^*|$ and phase angle (δ) in the predictive model, Witczak reformulated the model as follows:

$$\begin{aligned}
\log_{10}|E^*| = & \\
& -0.349 + 0.754(|G^*|_b^{-0.0052})(6.65 - 0.032p_{200} + 0.0027(p_{200})^2 + 0.011p_4 \\
& \quad + 0.006p_{\frac{3}{8}} - 0.00014\left(p_{\frac{3}{8}}\right)^2 - 0.08V_a - 1.06\frac{V_{beff}}{V_{beff}+V_a} + \\
& \frac{2.558 - 0.032V_a + 0.713\frac{V_{beff}}{V_{beff}+V_a} + 0.0124p_{\frac{3}{8}} - 0.0001\left(p_{\frac{3}{8}}\right)^2 - 0.0098p_{3/4}}{1 + \exp(-0.7814 - 0.5785\log |G^*|_b + 0.8834\log\delta_b)}
\end{aligned}
\tag{2.13}$$

where:

$|G^*|_b$ = Dynamic shear modulus of asphalt binder (pounds per square inch).

δ_b = Binder phase angle associated with $|G^*|_b$ (degrees).

Because some of the mixtures in their database did not contain $|G^*|_b$ data, Bari and Witczak (2007) used the Cox-Mertz rule, using correction factors for the non-Newtonian behaviors (see equations 2.14–2.16), was used to calculate $|G^*|_b$ from A-VTS values:

$$|G^*|_b = 0.0051f_s\eta_{f_s,T}(\sin\delta_b)^{7.1542-0.4929f_s+0.0211f_s^2}
\tag{2.14}$$

$$\begin{aligned}
\delta_b = & 90 + (-7.3146 - 2.6162 * VTS') * \log(f_s * \eta_{f_s,T}) \\
& + (0.1124 + 0.2029 * VTS') * \log(f_s * \eta_{f_s,T})^2
\end{aligned}
\tag{2.15}$$

$$\begin{aligned}
\log\log\eta_{f_s,T} = & \\
& 0.9699f_s^{-0.0527} * A + 0.9668f_s^{-0.0575} * VTS\log T_R
\end{aligned}
\tag{2.16}$$

where:

f_s = Dynamic shear frequency.

δ_b = Binder phase angle predicted from equation 2.14 (degrees).

$\eta_{f_s, T}$ = Viscosity of asphalt binder at a particular loading frequency (f_s) and temperature (T) determined from equation 2.15 (centipoise).

T_R = Temperature in Rankine

2.5.3 Hirsch model (Christensen et al. 2003) – HM

A limited number of data points (206) was used to determine the calibration coefficients in the Hirsch model, compared to 2750 and 7400 data points for the Original Witczak model and Modified Witczak model, respectively (Kim et al. 2011). Christensen et al. (2003) examined four different models based on the law of mixtures parallel model and incorporated the binder modulus, Voids in the Mineral Aggregate (VMA), and Voids Filled with Asphalt (VFA) because it provides accurate results in the simplest form (Christensen et al. 2003). The proposed $|E^*|$ prediction model is in the following equations:

$$|E^*|_m = P_c \left[4,200,000 \left(1 - \frac{VMA}{100} \right) + 3 |G^*|_b \left(\frac{VFA * VMA}{10,000} \right) \right] + \frac{(1 - P_c)}{\left(\frac{1 - VMA/100}{4,200,000} + \frac{VMA}{3 |G^*|_b (VFA)} \right)} \quad [2.17]$$

$$\emptyset = -21(\log P_c)^2 - 55 \log P_c \quad [2.18]$$

$$P_c = \frac{(20 + 3|G^*|_b(VFA)/(VMA))^{0.58}}{650 + (3|G^*|_b(VFA)/(VMA))^{0.58}} \quad [2.19]$$

where:

$|E^*|_m$ = Dynamic modulus of asphalt mixture (psi).

P_c = Aggregate contact volume.

ϕ = Phase angle of asphalt mixture.

An important strength of this model is the empirical phase angle equation (Equation 2.18), which is used for the interconversion of $|E^*|$ to the relaxation modulus ($E(t)$), or creep compliance ($D(t)$). On the other hand; the model lacks strong dependency on volumetric properties of the asphalt mixture, especially at low air void levels and VFA conditions (Kim et al. 2011).

2.5.4 Law of mixtures parallel model (Al-Khateeb Model)

Similar to the Hirsch model, this formulation is based on law of mixtures for composite materials. Al-Khateeb et al. (2006) later simplified the Hirsch model and introduced the following revised formulation:

$$|E^*|_m = 3 \left(\frac{100-VMA}{100} \right) \left[\frac{(90+10,000(|G^*|_b/VMA))^{0.66}}{1,100+(900(|G^*|_b/VMA))^{0.66}} \right] |G^*|_b \quad [2.20]$$

where $|G^*|_b$ = dynamic shear modulus of asphalt binder at the glassy state (assumed to be 145,000 psi (999,050 kPa)).

This model addresses one of the primary limitations of the Hirsch model by improving the ability to accurately predict $|E^*|$ of asphalt mixtures at low frequencies and high temperatures. On the other hand, weaknesses of this model include lack of verification and the fact that the authors developed this model based on $|E^*|$ tests at higher strain amplitudes (200 microstrain) than recommended (75-150 microstrain) (Kim et al. 2011).

2.5.5 Summary of inputs for $|E^*|$ prediction models

Table 2.2 shows a summary of the required inputs for the previously mentioned predictive equations.

Table 2.2: Parameters used in different $|E^*|$ predictive models.

Parameter	Description	Used in $ E^* $ Predictive Model?			
		OW	MW	H	A
VMA	Voids in mineral aggregate (%)			✓	✓
VFA	Voids filled with asphalt (%)			✓	
P ₂₀₀	Aggregate passing #200 sieve (%)	✓	✓		
P ₄	Aggregate passing #4 sieve (%)	✓	✓		
P _{3/8}	Aggregate passing 3/8-inch sieve (%)	✓	✓		
P _{3/4}	Aggregate passing 3/4-inch sieve (%)	✓	✓		
V _a	Air voids (by volume) (%)	✓	✓		
V _{beff}	Effective asphalt content (by volume) (%)	✓	✓		
A & VTS	Intercept & slope of viscosity-temperature relationship of binder	✓			
f _s	Loading frequency (Hz)	✓			
$ G^* _b$	Binder dynamic shear modulus		✓	✓	✓
δ_b	Binder phase angle		✓		

Note: OW = Original Witczak (Andrei et al. 1999), MW = Modified Witczak (Bari 2005), H = Hirsch (Christensen et al. 2003), and A = Al-Khateeb (Al-Khateeb et al. 2006).

2.6 Sample geometry and Representative Volume Element (RVE) for $|E^*|$

As stated earlier in this chapter, the most comprehensive research effort towards the complex modulus as a material property started in mid-90s as part of the NCHRP Project 9-19, and NCHRP Project 9-29 (NCHRP 9-19 2005, and NCHRP 9-29 2002). Part of this research effort was directed towards proposing new guidelines for the proper test specimen geometry and size.

Although a major cost in $|E^*|$ testing time and equipment arises from the need to core and saw gyratory compacted specimens, the research panel of the NCHRP Project 9-19 recommended using 100mm diameter cored specimens from 150mm diameter gyratory compacted specimens, with a saw cut final height of 150mm in the $|E^*|$ test. After running numerous complex modulus tests, it was found that:

1. A minimum height-to-diameter ratio of 1.5 was recommended to ensure that the response of test specimens represents a fundamental engineering property.
2. A minimum diameter of 100mm was recommended for all asphalt mixtures up to a maximum aggregate size of 37.5mm.
3. Smooth, parallel-ended specimens were recommended to eliminate bending, end friction, and boundary effects of the specimen during the test.
4. Less variability in $|E^*|$ test results were observed when 100mm diameter specimens were used, as compared to 150mm diameter specimens. The reason behind that is the large degree of nonhomogeneity of air voids within the larger specimens; which leads to variability in $|E^*|$ test results.

Kim et al. (2004) investigated the possibility of using IDT testing to measure the $|E^*|$ of existing asphalt pavements by comparing the $|E^*|$ values from the IDT tests with $|E^*|$ values from axial compression tests on standard cylindrical specimens. It was found that IDT testing is suitable for a wide range of mixtures and statistically proven to be similar to the master curves obtained from axial compression tests. Considering the relatively small thickness of IDT specimens (38mm), IDT test is a valid option for characterizing pavement materials for existing pavements (Kim et al. 2008). In addition, Kim et al. (2008) investigated prismatic specimen geometry and found that the prism and cylindrical specimens produce $|E^*|$ values that are statistically the same.

Research performed by Zofka et al. (2007) suggested the use of much smaller sample geometry to measure asphalt mixture creep compliance at low temperatures on thin mixture beams (127×12.7×6.35mm) using the Bending Beam Rheometer (BBR) testing machine. Using statistical analysis, a regression equation was derived and it was shown that this relation gives good predictions for IDT from the BBR results.

The research methodology suggested by Zofka et al. (2007) and Velasquez et al. (2009) was explored in this research study by running the BBR tests on thin beam mixtures to obtain mixture creep compliance $D(t)$. The basic theory of viscoelasticity was used to convert $|E^*|$ values obtained from the typical cylindrical test specimens (100mm×150mm) to $D(t)$ values and were then compared to $D(t)$ values measured using the BBR testing machine.

A major drawback of testing thin beam mixtures is the fact that the thickness of the beam (6.35mm) is smaller than the maximum aggregate size for most mixtures, which violates the RVE concept. The geometry and size of a test specimen play a significant role at high

temperatures when the asphalt mixture components have major different mechanical properties (Zofka et al. 2007). On the other hand, asphalt binders start behaving as brittle linear viscoelastic materials at low temperatures, and the mismatch between the aggregate and the binder modulus becomes less significant. This agrees well with Romero and Masad (2001), who reported this phenomenon and suggested that the RVE can be significantly reduced at lower temperatures.

It is desirable to study the effect of aged material properties on pavement performance. Recent research showed that current laboratory aging protocols lead to aging gradients within the regular-size (100mm diameter, 150mm tall) samples (Houston et al. 2005). Test samples become non-homogeneous and anisotropic. Such samples are no longer useful for performance testing. Therefore, once the RVE requirement is verified for the thin beam mixtures, this will serve as a foundation for the aging study since small samples will be much less susceptible to aging gradients.

3. RESEARCH METHODOLOGY

3.1 Introduction

The main objective of this research was to evaluate the complex modulus of asphalt mixture materials commonly used in the State of Michigan. A total of 64 asphalt mixtures and 44 asphalt binders were characterized in this study. A detailed description of the materials used in this research is provided in following section.

3.2 Materials used

3.2.1 Asphalt mixtures

A total of 64 asphalt mixtures (59 Hot Mix Asphalt (HMA) mixtures and 5 Warm Mix Asphalt (WMA) mixtures) commonly used in the State of Michigan were characterized in this research. Appendix A shows a list of volumetric properties and aggregate gradation for the tested asphalt mixtures. All test samples were prepared in accordance with AASHTO PP60 “*Preparation of Cylindrical Performance Test Specimens Using the Superpave Gyratory Compactor (SGC)*”. The air voids of all samples tested were within the range of $7\% \pm 0.5\%$, which is the recommended range of air voids for most performance tests in the AASHTO specifications. This air void level is typically the median air void level expected in the field right after the construction. Running the $|E^*|$ experiments at different air void levels may lead to different $|E^*|$ values, but, such investigation was not within the scope of this study. It should be noted that very limited $|E^*|$ tests at lower air void levels were run, and resulted in very similar

$|E^*|$ values as compared to the $|E^*|$ values of the samples compacted to 7% air voids. A complete list of air voids of all mixtures tested in this study is given in Appendix B.

3.2.2 Asphalt binders

A total of 44 unique asphalt binders commonly used in the State of Michigan were characterized in this study. Virgin asphalt binders, as well as modified asphalt binders were tested to obtain the dynamic shear modulus ($|G^*|$) master curve and phase angle δ of asphalt binders. The $|G^*|$ master curve and phase angle are required inputs in the M-E PDG software for prediction of asphalt mixture complex modulus.

3.3 Laboratory testing of materials collected

3.3.1 Details of laboratory $|E^*|$ tests

Figure 3.1 shows a picture of the Asphalt Mixture Performance Tester (AMPT) equipment used in this study for testing $|E^*|$ of the asphalt mixtures. The $|E^*|$ tests were conducted in accordance with AASHTO T342 “*Determining Dynamic Modulus Mastercurve of Hot Mix Asphalt (HMA)*”. The tests were conducted at temperatures of -10, 10, 21, 37 and 54 degrees C. At each temperature, tests were run at frequencies of 25, 10, 5, 1, 0.5 and 0.1 Hz. The entire series of temperatures and frequencies were run on 3 different gyratory compacted specimens. The average of the 3 replicates was used to develop the master curve representing each asphalt mixture. A detailed explanation of determination of $|E^*|$ master curves from the laboratory data can be found in AASHTO PP62-10 “*Developing Dynamic Modulus Mastercurves for Hot Mix Asphalt (HMA)*”.

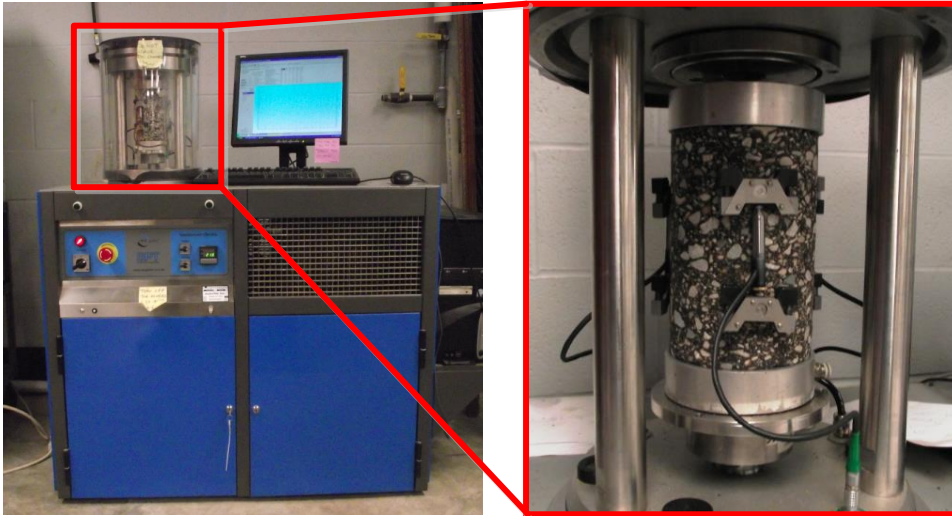


Figure 3.1: Asphalt Mixture Performance Tester (AMPT)

3.3.2 Details of laboratory $|G^*|$ tests

The $|G^*|$ tests were conducted in accordance with AASHTO T315 “*Determining the Rheological Properties of Asphalt Binder Using a Dynamic Shear Rheometer (DSR)*” on Rolling Thin Film Oven (RTFO) aged residue. Frequency sweep tests were conducted at temperatures of 15, 30, 46, 60 and 76 degrees C. At each temperature, tests were run at 11 frequencies varying between 1.0 and 100.0 Rad/sec. Three replicate asphalt binder samples were tested at each temperature and frequency. The average of the 3 replicates was used to develop the $|G^*|$ master curve.

The dynamic shear modulus ($|G^*|$) is a parameter that defines the stress-strain relationship of asphalt binders when they are subjected to cyclic shear load. The $|G^*|$ is measured using the Dynamic Shear Rheometer (DSR) shown in Figure 3.2. The $|G^*|$ is defined as:

$$|G^*| = \frac{\tau^{peak}}{\gamma^{peak}} \quad [3.1]$$

where τ^{peak} and γ^{peak} are peak shear stress and strain, respectively (see Figure 3.3). The steps in generating the $|G^*|$ master curve are identical to the steps described in the previous sections for the $|E^*|$ master curve. Because of the strong relationship between the $|G^*|$ and $|E^*|$, Levels 2 and 3 analyses in the M-E PDG software utilize the $|G^*|$ master curve (along with other inputs) to predict the $|E^*|$ master curve. Level 1 analysis in M-E PDG also requires $|G^*|$ as input, because $|G^*|$ is used to compute the viscosity-temperature relationship (a.k.a. A-VTS relationship) of the binder. The A-VTS relationship is needed in the global aging system model of the M-E PDG to predict the aging of the asphalt mixture over time.

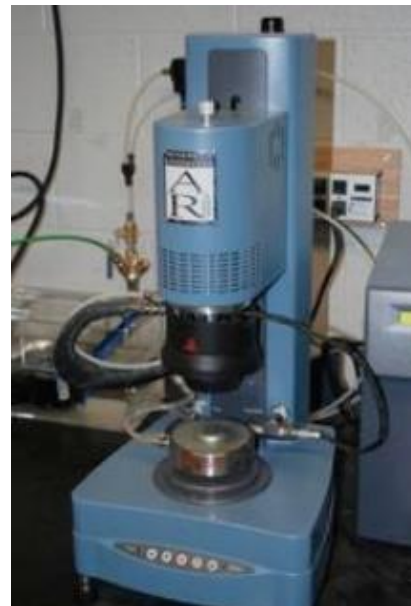
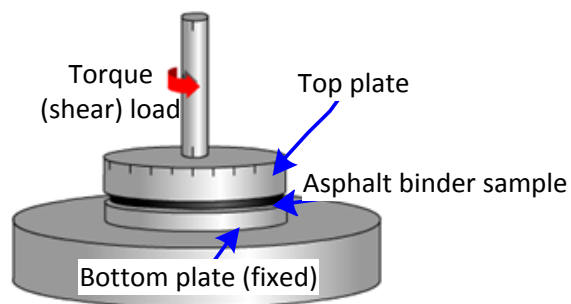


Figure 3.2: Illustration of the Dynamic Shear Rheometer (DSR) testing machine

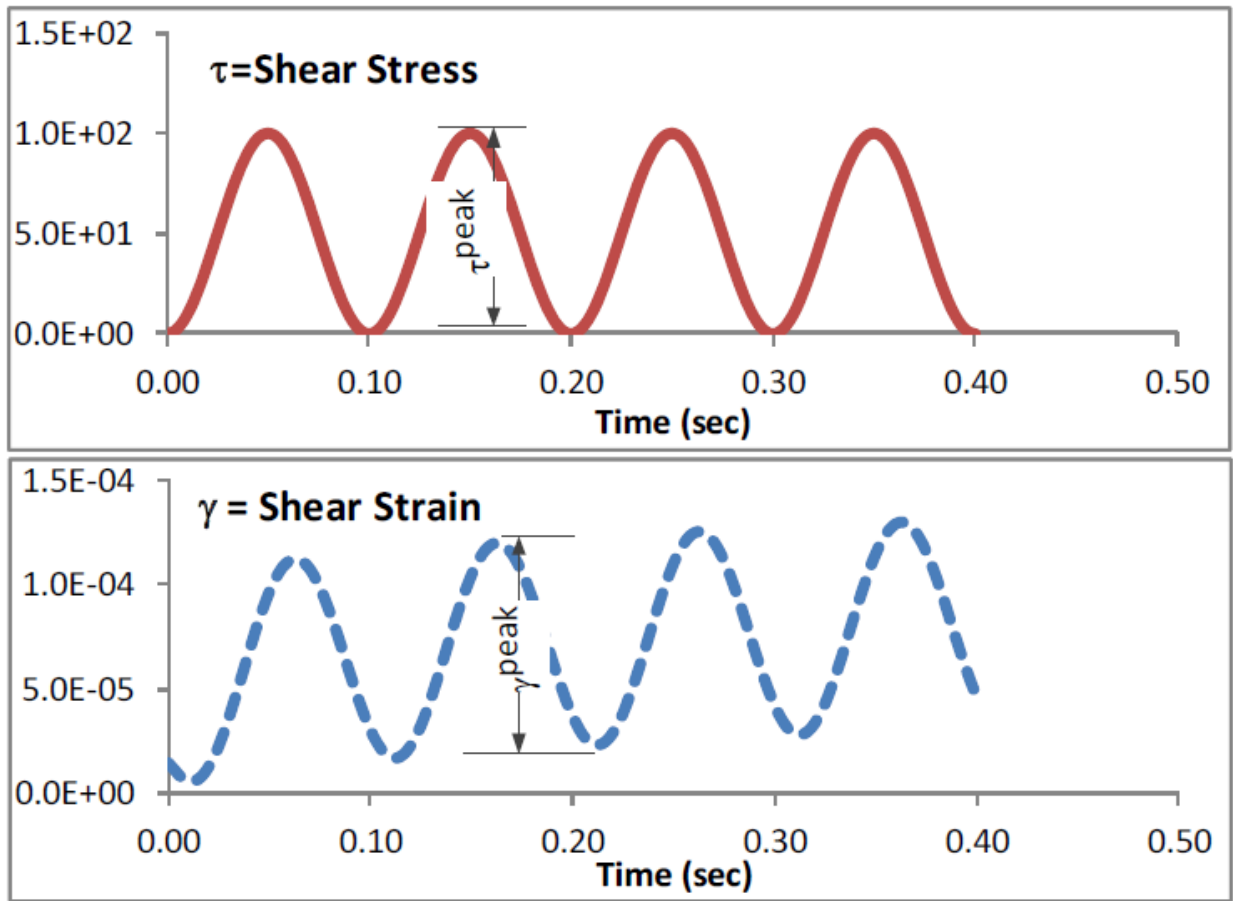


Figure 3.3: Illustration of stress-strain relationship of asphalt binders when they are subjected to cyclic shear load

3.4 Investigation of the Representative Volume Element (RVE) requirement for dynamic modulus $|E^*|$ of asphalt mixtures using Thin Beam Mixtures (TBMs)

In this study, a research methodology suggested by Zofka et al. (2007) and Velasquez et al. (2009) for low temperature applications was followed to investigate the Representative Volume Element (RVE) requirement for asphalt mixtures. Relatively small samples of asphalt mixture beams (127×12.7×6.35mm) were cut from gyratory specimens (Figure 3.4) to

investigate the possibility of obtaining the $|E^*|$ master curve from a much smaller specimen geometry as compared to the typical cylindrical test specimens (100mm diameter×150mm tall).

It is desirable to study the effect of oxidation/aging on pavement performance. Recent research showed that current laboratory aging protocols lead to aging gradients within the regular-size (100mm diameter, 150mm tall) samples. Test samples become non-homogeneous and anisotropic. Such samples are no longer useful for performance testing. Therefore, it is essential that the use of relatively smaller sample geometries be investigated since small samples will be much less susceptible to aging gradients and will experience more homogeneity after undergoing different laboratory aging processes.

The Bending Beam Rheometer (BBR) test was conducted on thin beam mixtures to obtain mixture the creep compliance $D(t)$ of the asphalt mixture. The basic theory of viscoelasticity was then used to convert $|E^*|$ values obtained from the typical cylindrical test specimens to $D(t)$ values and were then compared to $D(t)$ values measured using the BBR testing machine. Figure 3.4 below illustrates the experimental setup of the TBMs.

A total of 10 unique asphalt mixtures with varying Nominal Maximum Aggregate Sizes (NMASs) and Job Mix Formulas (JMFs) were tested. In addition, three replicates representing the same unique asphalt mixture were tested in order to account for sample-to-sample variability.



Saw cutting regular-size performance specimen in two halves



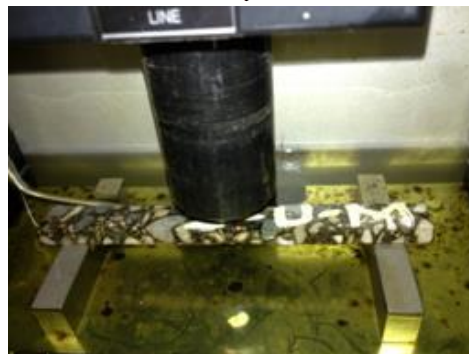
Tile saw is used for cutting three disks (center, middle, and edge)



Tile saw is used to cut a TBM from each disk



Resulting asphalt thin mixture beam



BBR testing on TBM

Figure 3.4: Illustration of Thin Beam Mixture sample preparation and testing.

4. LABORATORY TESTING: RESULTS & DISCUSSION

4.1 Complex modulus $|E^*|$ testing of asphalt mixtures

Sampling of loose mixtures was conducted by MDOT during the summers of 2011 and 2012. The loose mixtures were collected from selected pavement projects in multiple regions in the State of Michigan (North, Grand, Bay, Southwest and University Regions (NGBSU), Metro Region, and Superior Region). A total of 64 unique asphalt mixtures were sampled and a wide range of $|E^*|$ master curves that are representative of typical MDOT mixtures were obtained. A total of 213 different specimens were prepared from 64 unique asphalt mixture types. The tested asphalt mixture types are shown in Tables 4.1 through 4.4. The grey shaded cells in these tables represent the HMAs collected and tested.

Table 4.1: HMAs tested for $|E^*|$ master curve.

	Mix No:	2		3		3		4		5	
	Layer:	Base		Base		Leveling		Leveling/Top		Top	
	Mix Type	Binder PG	HMA#	Binder PG	HMA#	Binder PG	HMA#	Binder PG	HMA#	Binder PG	HMA#
<i>North, Grand, Bay, Southwest and University Regions (NGBSU)</i>											
M	E30	64-22	1	64-22	2	70-28P	3	70-28P	4	70-28P	5
HS	E30	64-22	1	64-22	2	76-28P	6	76-28P	7	76-28P	8
M	E50	64-22	9	64-22	10	70-28P	11	70-28P	12	70-28P	13
HS	E50	64-22	9	64-22	10	76-28P	14	76-28P	15	76-28P	16
M	E10	58-22	17	58-22	18	64-28	19	64-28	20	64-28	21
HS	E10	58-22	17	58-22	18	70-28P	22	70-28P	23	70-28P	24

Table 4.1 (cont'd)

	Mix No:	2		3		3		4		5	
	Layer:	Base		Base		Leveling		Leveling/Top		Top	
	Mix Type	Binder PG	HMA#	Binder PG	HMA#	Binder PG	HMA#	Binder PG	HMA#	Binder PG	HMA#
<i>North, Grand, Bay, Southwest and University Regions (NGBSU)</i>											
M	E3	58-22	25	58-22	26	64-28	27	64-28	28	64-28	29
HS	E3	58-22	25	58-22	26	70-28P	30	70-28P	31	70-28P	32
M	E03	58-22	33	58-22	34	58-28	35	58-28	36	58-28	37
HS	E03	58-22	33	58-22	34	64-28	38	64-28	39	64-28	40
M	E1	58-22	41	58-22	42	58-28	43	58-28	44	58-28	45
HS	E1	58-22	41	58-22	42	64-28	46	64-28	47	64-28	48
<i>Metro Region</i>											
M	E30	64-22	1	64-22	2	70-22P	89	70-22P	90	70-22P	91
HS	E30	64-22	1	64-22	2	76-22P	92	76-22P	93	76-22P	94
M	E50	64-22	9	64-22	10	70-22P	95	70-22P	96	70-22P	97
HS	E50	64-22	9	64-22	10	76-22P	98	76-22P	99	76-22P	100
M	E10	58-22	17	*58-22	18	64-22	101	64-22	102	64-22	103
HS	E10	58-22	17	58-22	18	70-22P	104	70-22P	105	70-22P	106
M	E3	58-22	25	58-22	26	64-22	107	64-22	108	64-22	109
HS	E3	58-22	25	58-22	26	70-22P	110	70-22P	111	70-22P	112
M	E03	58-22	33	58-22	34	58-22	113	58-22	114	58-22	115
HS	E03	58-22	33	58-22	34	64-22	116	64-22	117	64-22	118
M	E1	58-22	41	58-22	42	58-22	119	58-22	120	58-22	121
HS	E1	58-22	41	58-22	42	64-22	122	64-22	123	64-22	124
<i>Superior Region</i>											
M	E10	58-28	53	58-28	54	58-34	55	58-34	56	58-34	57
HS	E10	58-28	53	58-28	54	64-34P	58	64-34P	59	64-34P	60
M	E3	58-28	61	58-28	62	58-34	63	58-34	64	58-34	65
HS	E3	58-28	61	58-28	62	64-34P	66	64-34P	67	64-34P	68
M	E03	58-28	69	58-28	70	58-34	71	58-34	72	58-34	73
HS	E03	58-28	69	58-28	70	64-34P	74	64-34P	75	64-34P	76

Table 4.1 (cont'd)

		Mix No:		3		3		4		5	
		Layer:		Base		Base		Leveling		Leveling/Top	
		Mix Type:		Binder PG	HMA#	Binder PG	HMA#	Binder PG	HMA#	Binder PG	HMA#
<i>Superior Region</i>											
M	E1	58-28	77	58-28	78	58-34	79	58-34	80	58-34	81
HS	E1	58-28	82	58-28	83	64-34P	84	64-34P	85	64-34P	86
Note: M=Mainline, HS=High Stress											

Table 4.2: HMAs tested for |E*| master curve (GGSP and LVSP Mixtures)

HMA Type	Layer:	Leveling/Top					
	Region:	<i>North, Grand, Bay, Southwest and University Regions (NGBSU)</i>		<i>Metro</i>		<i>Superior</i>	
	Mix Type	Binder PG	HMA#	Binder PG	HMA#	Binder PG	HMA#
M	GGSP	70-28P	49	70-22P	125	-	-
HS	GGSP	76-28P	50	76-22P	126		
M	LVSP	58-28	51	58-22	127	58-34	87
HS	LVSP	64-28	52	64-22	128	64-34P	88
Note: M=Mainline, HS=High Stress							

Table 4.3: HMAs tested for |E*| master curve (SUPERPAVE) – Mixtures that do not follow MDOT specifications but are permitted to be used.

HMA Type	Mix No:	2		3		4		5	
	Layer:	Base		Base		Leveling/Top		Top	
	Mix Type	Binder PG	HMA#	Binder PG	HMA#	Binder PG	HMA#	Binder PG	HMA#
M	E10			58-28	200				
HS	E10							64-22	202
HS	E30					70-22P	203	70-22P	204
M	E3	58-28	205						
M	E1							64-22	206
M	E1							64-22	207

Note: M=Mainline, HS=High Stress

Table 4.4: HMAs tested for |E*| master curve (GGSP and LVSP Mixtures) - Mixtures that do not follow MDOT specifications but are permitted to be used.

HMA Type:	Layer:	Leveling/Top					
	Region:	NGBSU		Metro		Superior	
	Mix Type	Binder	HMA#	Binder	HMA#	Binder	HMA#
M	ASCRL	64-28	201				

Note: M=Mainline

In order to illustrate the overall range of |E*| values for all mixtures tested, the |E*| master curves were plotted in Figure 4.1. As shown, the difference between the lowest and highest |E*| values is approximately 2 orders of magnitude.

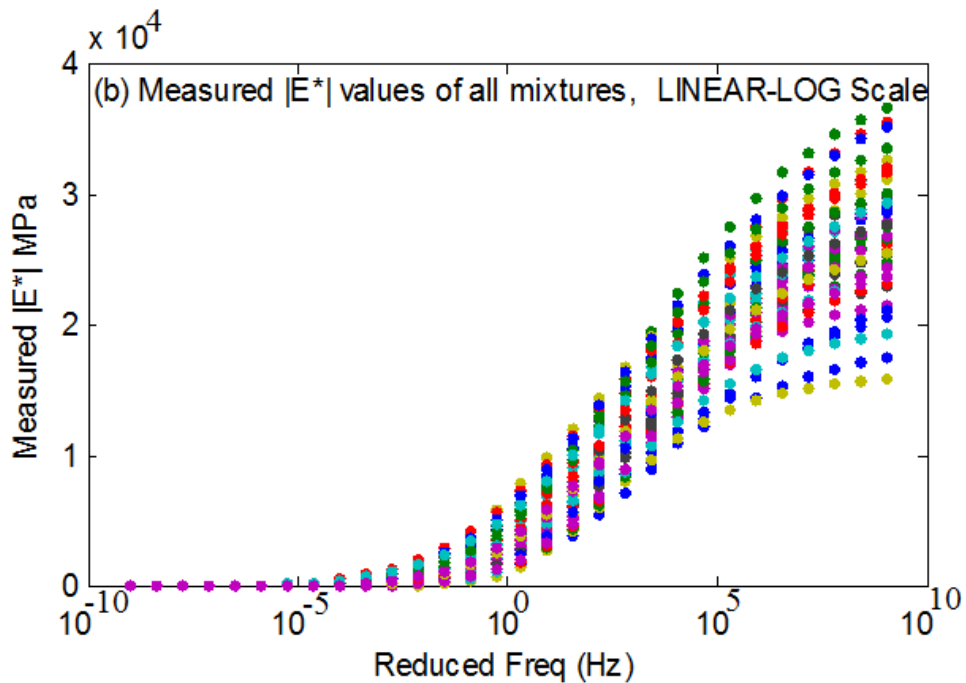
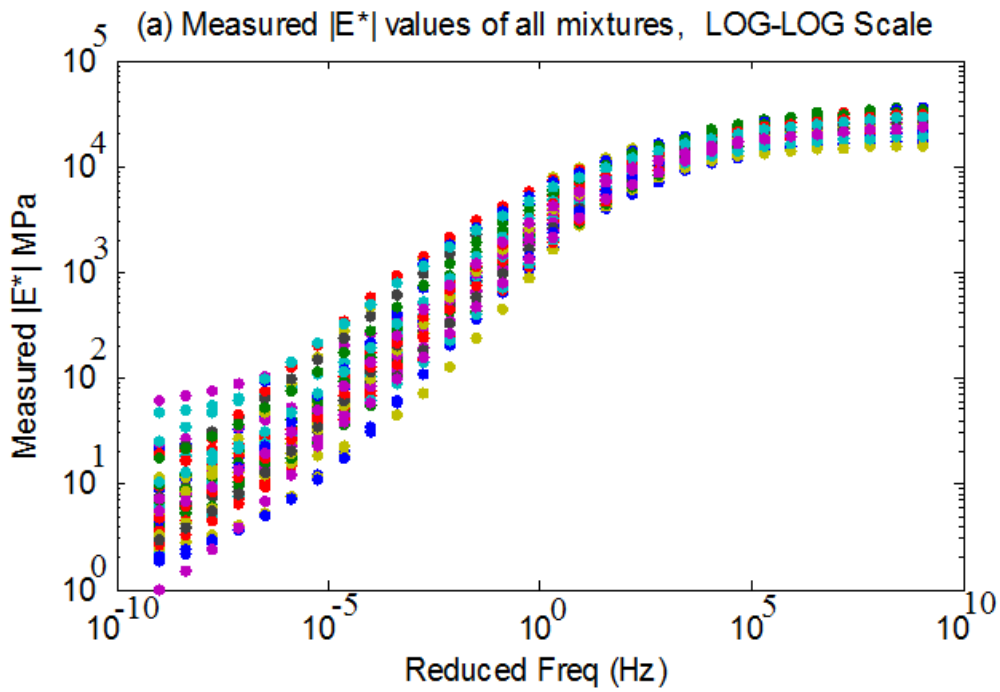


Figure 4.1: Dynamic Modulus master curves of all tested asphalt mixture specimens. The plot in log-log scale is to show the differences in low frequency/high temperature, and the plot in linear-log scale is to show the differences in high frequency/low temperature.

4.1.1 Summary of $|E^*|$ values based on MDOT mix designation for each region

Table 4.5, Table 4.6, and Table 4.7 show a summary of the $|E^*|$ values at temperatures of -10, 21 and 54°C, at a loading frequency of 10Hz. These tables are provided to illustrate the relative differences in $|E^*|$ values of various asphalt mixture types used in MI. As shown in Table 4.5, 3E mixtures are generally stiffer than 4E and 5E mixtures (e.g., compare HMA# 18 versus 20 versus 21). However the trend is not always consistent in all temperatures (e.g., HMA# 31 versus 32 at -10°C). A clear trend should not be expected since there are many variables (e.g., aggregate gradation, binder $|G^*|$ master curve, VMA, VFA...etc.) that play a role in the magnitude of $|E^*|$ at different temperatures and frequencies.

4.1.2 Comparison of variation in $|E^*|$ master curves based on MDOT mix designation

Figure 4.2 shows $|E^*|$ master curves of the 3E3 mixtures, where a single master curve is not visible. Appendix C shows the $|E^*|$ master curves of all other mixtures grouped based on the MDOT mix designation (e.g., 4E10, 3E03 etc.). The objective of plotting these graphs was to investigate if MDOT mix types for a given region (e.g., 5E10 for Metro Region) exhibit same or similar $|E^*|$ master curve values. After carefully analyzing the $|E^*|$ master curves, it was concluded that it is not appropriate to come up with a single $|E^*|$ master curve for a given MDOT mix, for a given region. The main reason is that the aggregate gradation plays a key role in $|E^*|$ master curve and it is not unique for an MDOT mix type in a region (e.g., 3E3 in Metro). For example, two 3E3 projects in Metro region may (and most probably will) have different gradations (and mix designs).

Table 4.5: Summary of |E*| values for different asphalt mixture types in NGBSU Regions

North, Grand, Bay, Southwest and University Regions (NGBSU)													
	Mix No:	3				4				5			
Mainline / High Stress	Layer:	Base				Leveling/Top				Top			
	Traffic	HMA #	E* (MPa)			HMA #	E* (MPa)			HMA#	E* (MPa)		
			10Hz, -10°C	10Hz, 21°C	10Hz, 54C		10Hz, -10°C	10Hz, 21°C	10Hz, 54C		10Hz, -10°C	10Hz, 21°C	10H, 54C
M	E30	2	24183	9108	1175	4	21668	5683	498	5			
HS	E30	2	24183	9108	1175	7				8			
M	E50	10				12				13			
HS	E50	10				15				16			
M	E10	18	26710	7668	668	20	24989	7175	698	21	19780	4893	398
HS	E10	18	26710	7668	668	23	22232	5300	475	24	15287	4133	444
M	E3	26	21470	5649	453	28	22301	5618	449	29	17958	6068	605
HS	E3	26	21470	5649	453	31	17363	4834	437	32	21282	4796	399
M	E03	34				36				37	18761	4017	214
HS	E03	34				39				40			
M	E1	42				44	20696	4833	440	45	15280	4207	429
HS	E1	42				47	20879	5707	536	48	18204	4659	369

Table 4.6: Summary of |E*| values for different asphalt mixture types in the Metro Region

Metro Region													
	Mix No:	3				4				5			
Mainline / High Stress	Layer:	Base				Leveling/Top				Top			
	Traffic	HMA #	E* (MPa)			HMA #	E* (MPa)			HMA #	E* (MPa)		
			10Hz, -10C	10Hz, 21C	10Hz, 54C		10Hz, -10C	10Hz, 21C	10Hz, 54C		10Hz, -10C	10Hz, 21C	10Hz, 54C
M	E30	2	24183	9108	1175	90	22256	7408	913	91			
HS	E30	2	24183	9108	1175	93				94			
M	E50	10				96				97	23603	7405	813
HS	E50	10				99				100			
M	E10	18	26710	7668	668	102	26014	10224	1443	103	24044	8588	849
HS	E10	18	26710	7668	668	105	21314	7375	852	106	21293	6425	656
M	E3	26	21470	5649	453	108	23374	8419	948	109	23442	7706	549
HS	E3	26	21470	5649	453	111	25192	9402	1434	112	20122	6323	705
M	E03	34				114				115			
HS	E03	34				117				118			
M	E1	42				120				121			
HS	E1	42				123				124			

Table 4.7: Summary of |E*| values for different asphalt mixture types in Superior Region

Superior Region													
Mix No:		3				4				5			
Layer:		Base				Leveling/Top				Top			
Mainline / High Stress	Traffic	HMA#	E* (MPa)			HMA#	E* (MPa)			HMA#	E* (MPa)		
			10Hz, -10C	10Hz, 21C	10Hz, 54C		10Hz, -10C	10Hz, 21C	10Hz, 54C		10Hz, -10C	10Hz, 21C	10Hz, 54C
M	E10	54				56				57			
HS	E10	54				59				60			
M	E3	62	19556	4142	241	64	19103	4519	527	*65	17663	3193	260
HS	E3	62	19556	4142	241	67	19403	3339	261	68	16849	3456	264
M	E03	70				72				73			
HS	E03	70				75				76			
M	E1	78				80	18831	3483	297	81	17265	3570	
HS	E1	83				85				86			

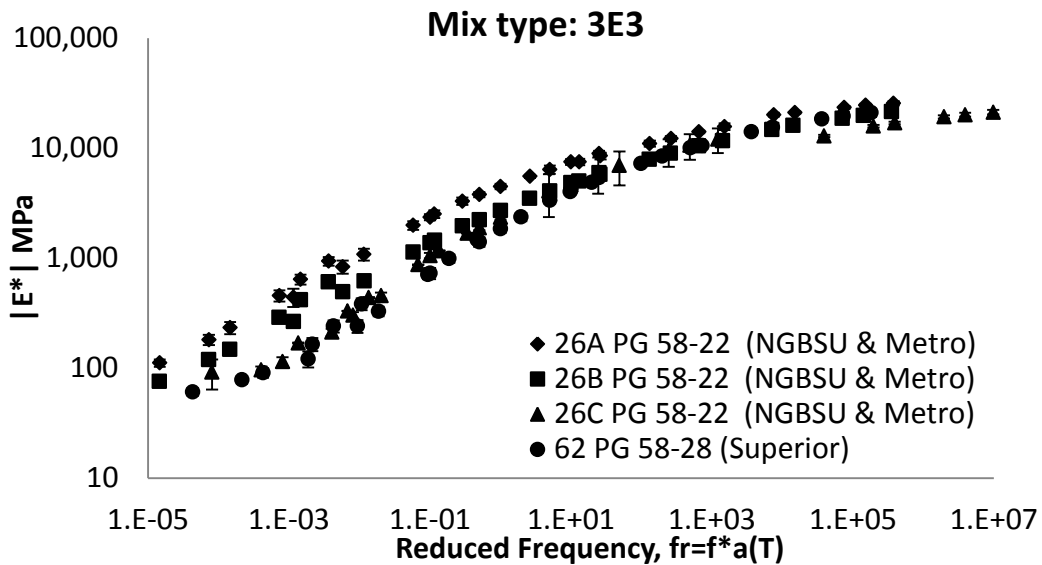


Figure 4.2: $|E^*|$ master curves of four 3E3 mixtures, 3 of which (26* mixes) are from same region. NGBSU = North, Grand, Bay, Southwest and University Regions.

As a result, $|E^*|$ can be very different. An evidence of this phenomenon is the three 3E3 mixtures (26A, 26B and 26C) that were tested as part of this study. As shown in Figure 4.2, mixtures 26A, 26B and 26C exhibited different $|E^*|$ values. In fact, 26C had a very similar $|E^*|$ master curve as 62, which has a different binder PG and was in a different region (Superior).

4.1.3 Comparison of variation in $|E^*|$ master curve for HMA and WMA asphalt mixtures

A limited number of warm mix asphalt mixtures (4 WMAs) were characterized in this study. Two graphs comparing WMA and HMA $|E^*|$ master curves are shown in Figure 4.3 and Figure 4.4. Figure 4.3 compares two different $|E^*|$ master curves for the same type of MDOT mixture (3E30) and clearly shows that the WMA is softer than the HMA. In Figure 4.4, WMA is shown as in-between HMAs (51A and 51B) of the same type of MDOT mixture (Low Volume Superpave (LVSP)). However, it should be noted that when the JMFs were compared, the gradation of 51A was much coarser than the 51B and 51C, which were almost identical (see

Figure 4.5). Therefore, it is more appropriate to compare 51B-HMA and 51C-WMA. As shown, 51C-WMA is slightly softer than the 51B-HMA.

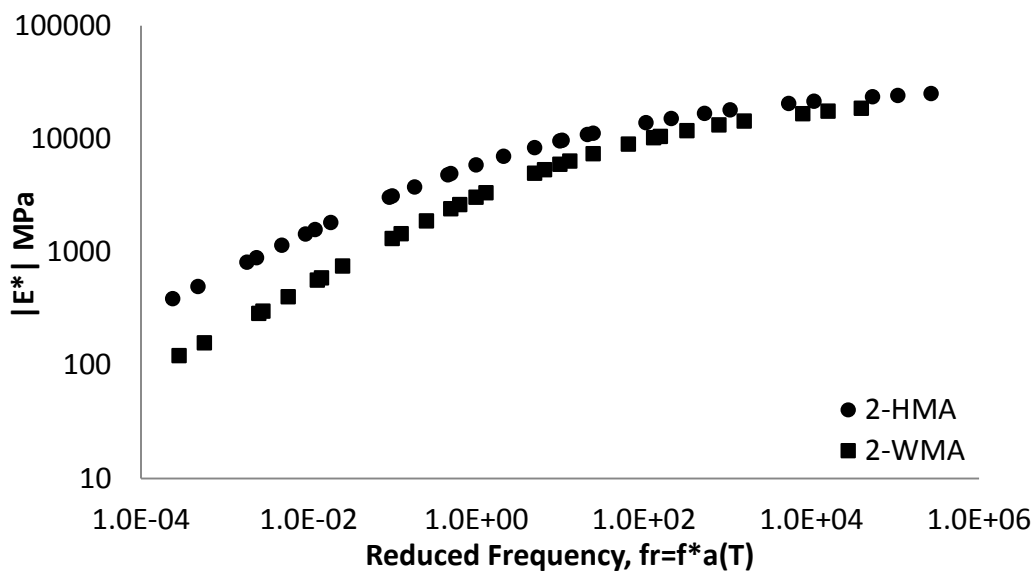


Figure 4.3: WMA versus HMA $|E^*|$ master curves for (3E30) MDOT mixture

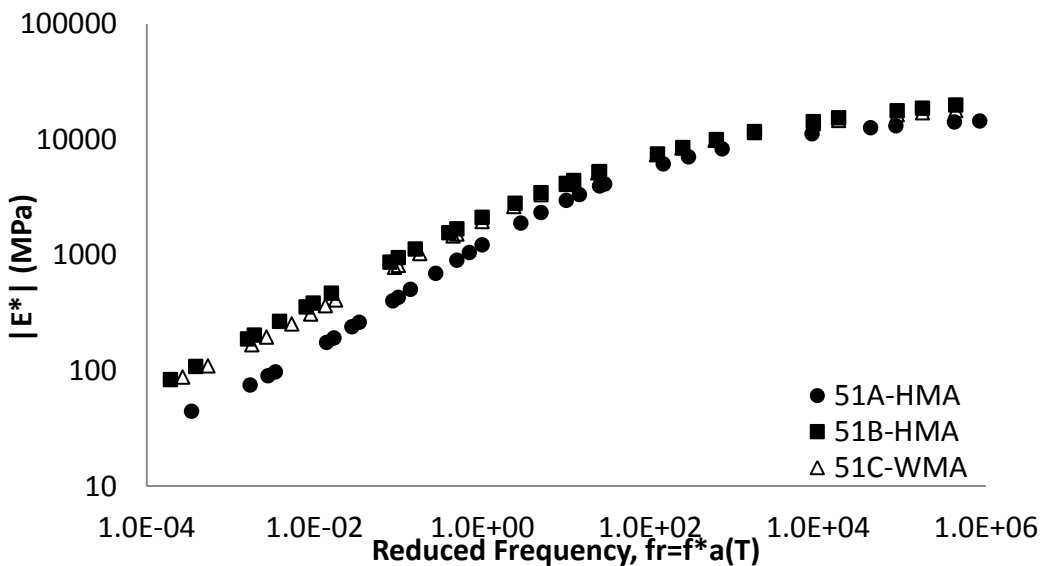


Figure 4.4: WMA versus HMA $|E^*|$ master curves for (LVSP) MDOT mixture

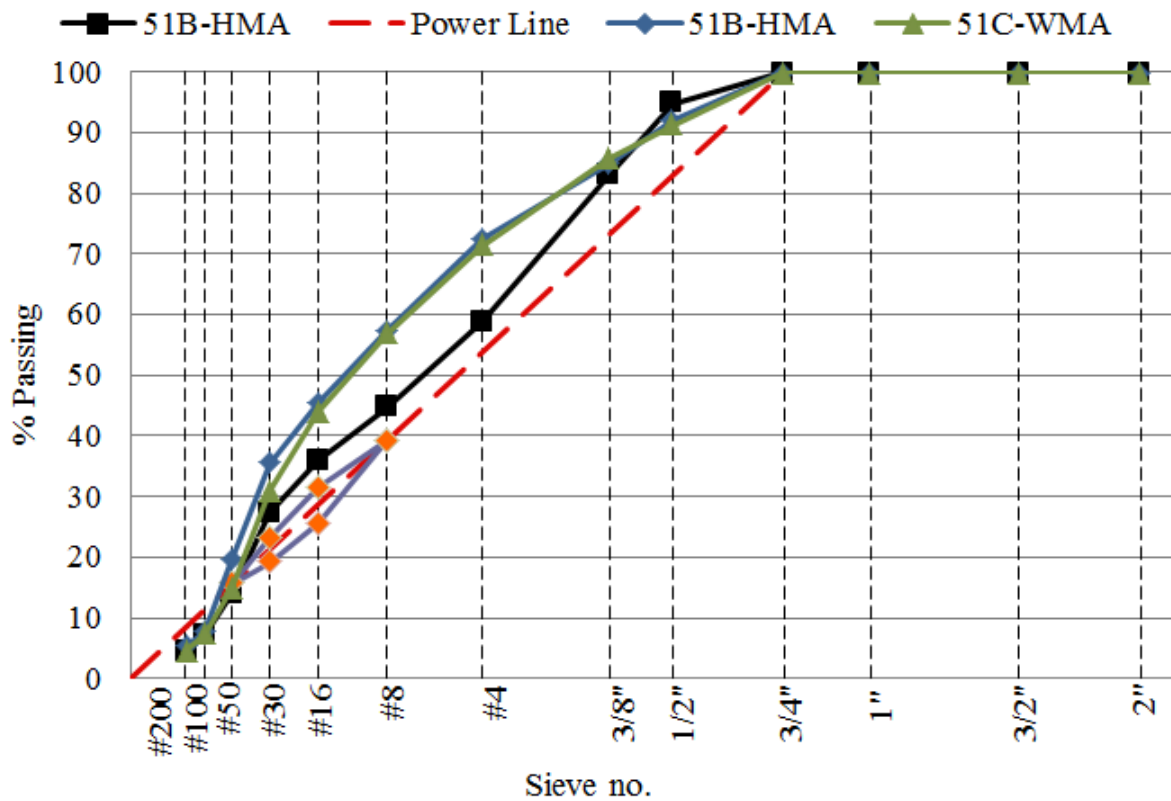


Figure 4.5: Aggregate gradation of WMA and HMA mixtures ((LVSP) MDOT mixture)

4.2 Dynamic shear modulus $|G^*|$ testing of asphalt binders

The dynamic shear modulus test was run on RTFO aged residue to obtain the $|G^*|$ of 44 unique binders commonly used in the State of Michigan. Table 4.8 shows a list of the different asphalt binder PG grades tested in this study. Frequency sweep tests were conducted at temperatures of 15, 30, 46, 60 and 76 degrees C. At each temperature, tests were run at 11 frequencies varying between 1.0 and 100.0 Rad/sec.

Table 4.8: List of binder PGs tested in this study

Binder PG Grade	Total number of binders from different locations
58-22	3
58-28	9
58-34	2
64-22	9
64-28	7
64-34P	4
70-22P	4
70-28	1
70-28P	5
TOTAL	44

4.2.1 Comparison of variation in $|G^*|$ master curves based on binder PG grade

As mentioned previously, there is a strong relationship between the binder $|G^*|$ and corresponding mixture $|E^*|$. Levels 2 and 3 in the M-E PDG utilize the $|G^*|$ master curve (along with other inputs) to predict the $|E^*|$ master curve. Also, Level 1 analysis requires $|G^*|$ as input to compute the A-VTS relationship of the binder that is needed in the global aging system model of the M-E PDG to predict the aging of the asphalt mixture over time. Figure 4.6 shows the $|G^*|$ master curves of seven different binders with same performance grade of PG 64-28. As shown, a single PG in some cases showed significant variations and did not necessarily produce the same $|G^*|$ master curve.

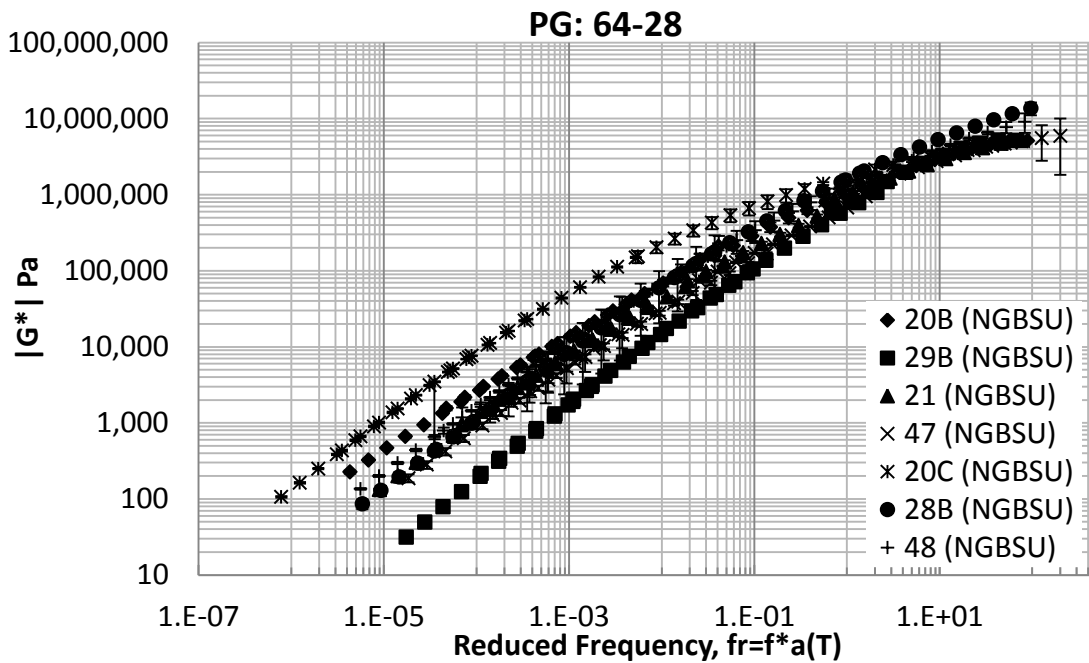


Figure 4.6: |G*| Master curves of seven different PG64-28 binders. NGBSU = North, Grand, Bay, Southwest and University Regions

In order to evaluate the effect of the $|G^*|$ master curve and phase angle (δ) on performance prediction, a sensitivity analysis was run in the M-E PDG software. A HMA over HMA base case was selected. All other inputs were held constant while the $|G^*|$ and δ were used to characterize the asphalt binder. The results showed that the variation in $|G^*|$ and δ is insignificant for cracking and International Roughness Index (IRI) (see Figure 4.7 to Figure 4.9). However, it was observed that rutting is sensitive to asphalt binder characteristics as shown in Figure 4.10. Therefore, it is recommended that $|G^*|$ master curves should not be grouped based on PG grades or regions where the material was acquired from. The $|G^*|$ master curves grouped based on the other asphalt binder PG grades tested in this study are given in Appendix D.

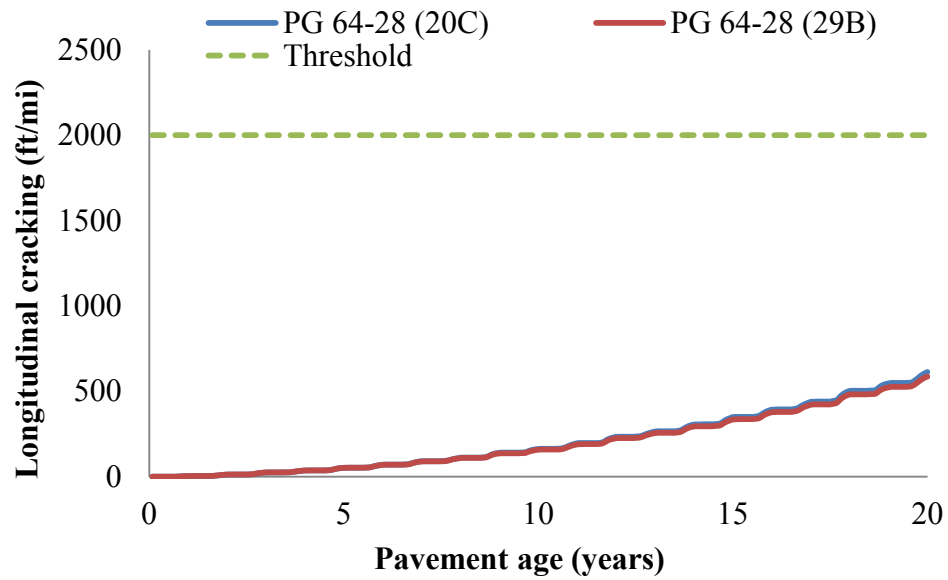


Figure 4.7: Illustration of the effect of variation in $|G^*|$ and δ on Longitudinal cracking predictions in the M-E PDG software.

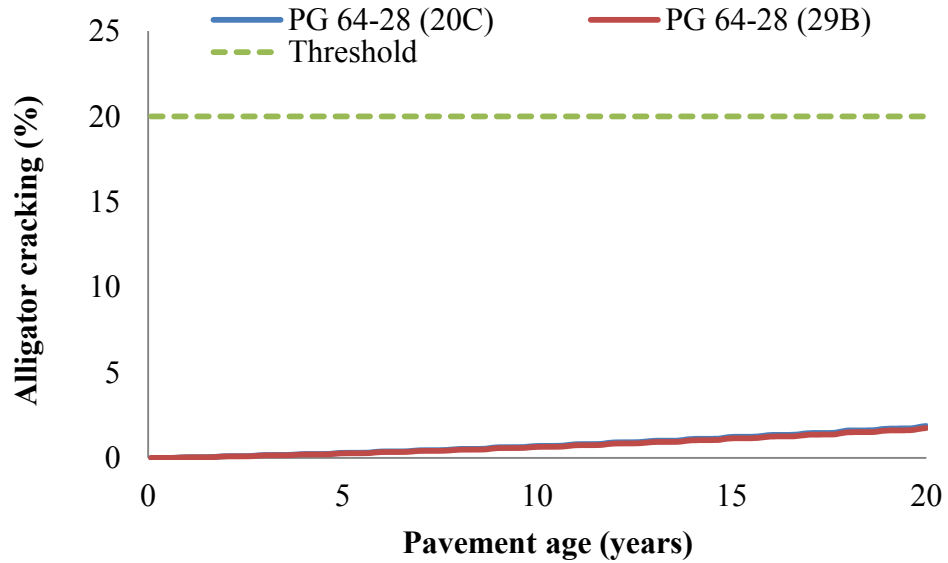


Figure 4.8: Illustration of the effect of variation in $|G^*|$ and δ on alligator cracking predictions in the M-E PDG software.

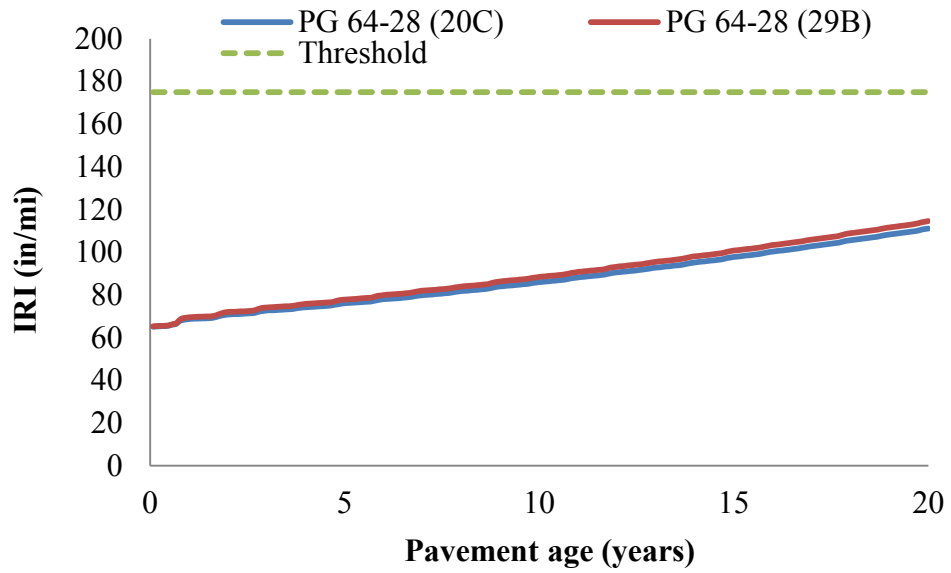


Figure 4.9: Illustration of the effect of variation in $|G^*|$ and δ on IRI predictions in the M-E PDG software.

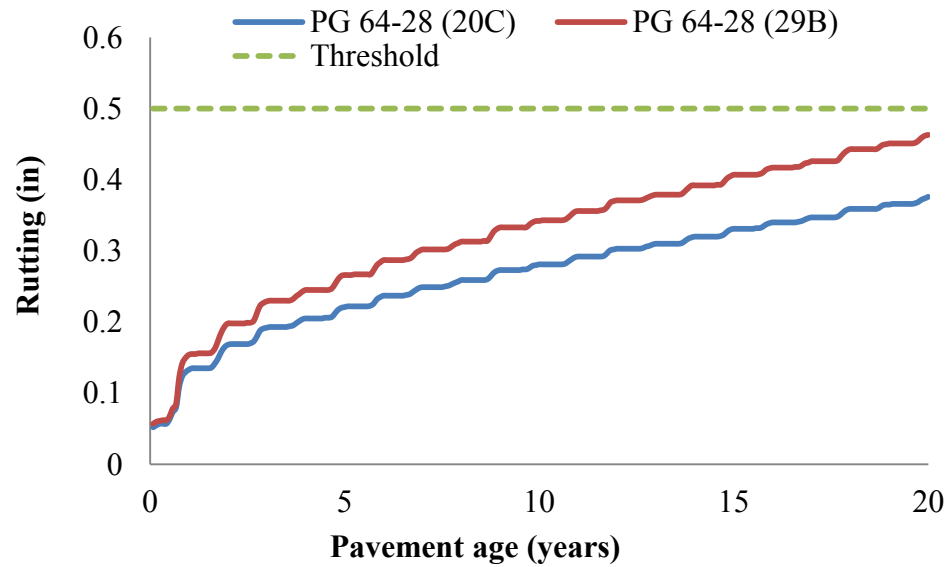


Figure 4.10: Illustration of the effect of variation in $|G^*|$ and δ on rutting predictions in the M-E PDG software.

5. |E*| PREDICTION MODELS: RESULTS AND DISCUSSION

A recent FHWA-funded research showed that the predictions of Witzczak, Hirsch and Al-Khateeb equations were inaccurate at low frequencies/high temperatures (Sakhaeifar et al. 2009, Kim et al. 2010). Independent evaluations of these models were performed in various studies (e.g., Azari et al. 2007, Robbins and Timm 2011, Singh et al. 2010). These studies consistently showed inaccuracies of statistical models at certain frequencies and temperatures. This indicated the need for either local calibration of the constants in these equations, or if necessary, employ advanced computing tools such as the Artificial Neural Networks (ANNs) to develop models for better prediction of |E*| values and use them as Level 1 inputs in the M-E PDG software. Such models were developed by Kim et al. (2010) as part of a FHWA funded study.

5.2 Evaluation and calibration of the Modified Witzczak's equation for Michigan asphalt mixtures

As seen in Table 4.1 and Table 4., there are numerous Michigan mixtures where |E*| characterization could not be done as part of this study because they were not used in a field project during the period of this research study. For these mixtures, |E*| predictive models, such as the Witzczak's model or the ANN model, may be utilized to estimate the master curves. For this, first, the modified Witzczak (Bari 2005) model, which is implemented in the M-E PDG software, was evaluated. The performance of Witzczak's model is evaluated using two different approaches; goodness-of-fit statistics, and comparison of measured and predicted values with respect to the line of equality (LOE) (visual inspection). The goodness-of-fit statistics include S_e/S_y (standard error of estimate /standard deviation), and the correlation coefficient (R^2). The

ratio of S_e/S_y is a measure of improvement in the accuracy of prediction due to the empirical model. Smaller ratio of S_e/S_y indicates better prediction by the model. On the other hand, R^2 measures model accuracy, values closer to one indicate better estimation by the model (Singh et. al. 2010). It is noted that R^2 is a better parameter for linear models with a large sample size. However, for non-linear models, such as the empirical models, ratio of S_e/S_y is a more rational measure of prediction reliability (Kim et. al 2005). The goodness-of-fit statistics (S_e/S_y , R^2) were calculated using the following equations:

$$S_e = \sqrt{\frac{\sum (y - \hat{y})^2}{(n - k)}} \quad [5.1]$$

$$S_y = \sqrt{\frac{\sum (y - \bar{y})^2}{(n - 1)}} \quad [5.2]$$

$$R^2 = 1 - \frac{(n - k)}{(n - 1)} \left(\frac{S_e}{S_y} \right)^2 \quad [5.3]$$

where:

S_e : Standard error of estimate,

S_y : Standard deviation,

R^2 : Correlation coefficient,

y : Measured dynamic modulus,

\hat{y} : Predicted dynamic modulus,

\bar{y} : Mean value of measured dynamic modulus,

n : Sample size,

k : Number of independent variables in the model. In this case, $k=21$ (Equation 5.4).

Figure 5.1 shows the predicted versus measured values based on the modified Witczak's equation developed as part of the NCHRP 1-40D, which is based on the nationally calibrated coefficients. As shown, the goodness-of-fit statistics for the linear-linear plot are $S_e/S_y = 0.5084$, and $R^2 = 0.7881$, and for the log-log plot $S_e/S_y = 0.446$, and $R^2 = 0.8369$. It should be recalled that the smaller the S_e/S_y and the larger the R^2 , the better the goodness-of-fit is. There are significant differences in $|E^*|$ values at high temperature/low frequencies (lower left side of the graph in Figure 5.1).

Using the laboratory $|E^*|$ data collected in this study, the MATLAB software was used to calibrate the coefficients of the Modified Witczak's equation. Figure 5.2 shows the predicted versus measured $|E^*|$ values using the calibrated coefficients. The goodness-of-fit statistics for the linear-linear plot are $S_e/S_y = 0.3029$, and $R^2 = 0.9248$, and for the log-log plot $S_e/S_y = 0.2053$, and $R^2 = 0.965$ which are much better than the statistics shown in Figure 5.1. In addition, the predicted values are much closer to the line of equality as compared to results shown in Figure 5.1. Table 5.1 shows a comparison between coefficients used in the original and optimized models. Each coefficient in Table 5.1 is shown in the following equation (which is the Modified Witczak equation):

$$\log_{10} |E^*| = a_1 + a_2(|G^*|_b^{a_3})^* \left(a_4 + a_5 p_{200} + a_6 (p_{200})^2 + a_7 p_4 + a_8 (p_4)^2 + a_9 p_{3/8} + a_{10} (p_{3/8})^2 + a_{11} V_a + a_{12} \left(\frac{V_{beff}}{V_{beff} + V_a} \right) \right) + \frac{a_{13} + a_{14} V_a + a_{15} \left(\frac{V_{beff}}{V_{beff} + V_a} \right) + a_{16} p_{3/8} + a_{17} (p_{3/8})^2 + a_{18} p_{3/4}}{1 + \exp(a_{19} + a_{20} \log |G^*|_b + a_{21} \log \delta_b)} \quad [5.4]$$

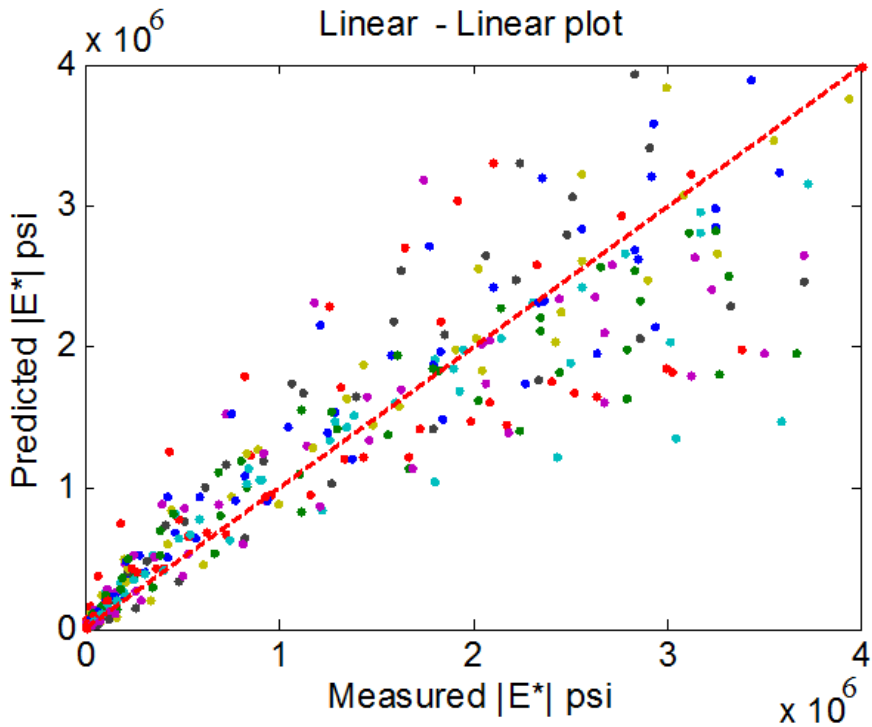
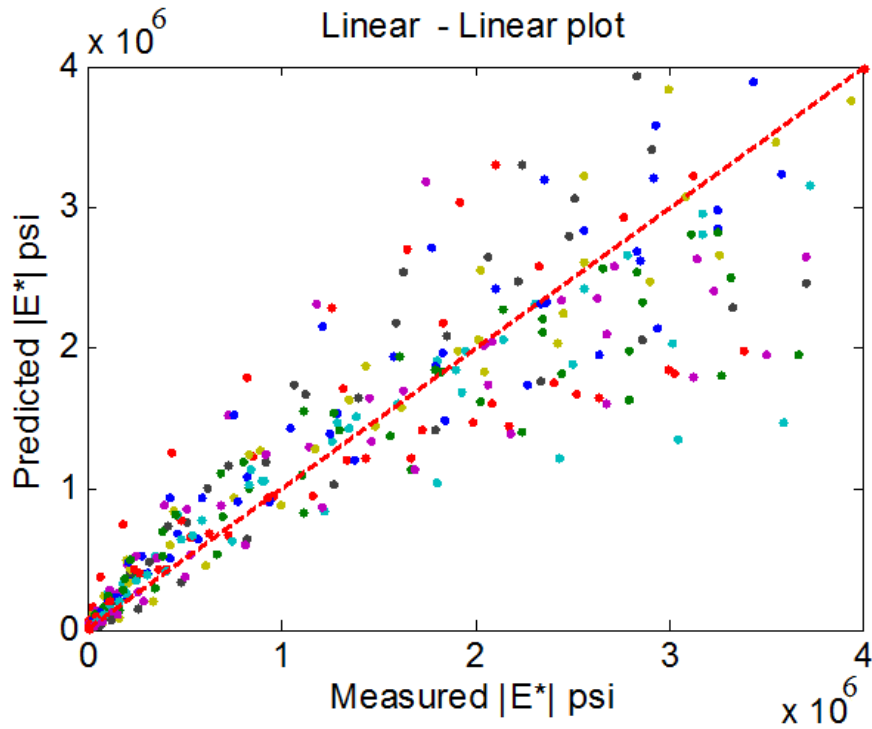


Figure 5.1: The modified Witczak's equation developed as part of the NCHRP 1-40D. The plot shows the predicted versus measured values before calibration for MDOT mixtures. $S_e/S_y = 0.5084$, $R^2 = 0.7881$ (linear-linear plot), and $S_e/S_y = 0.446$, $R^2 = 0.8369$ (log-log plot).

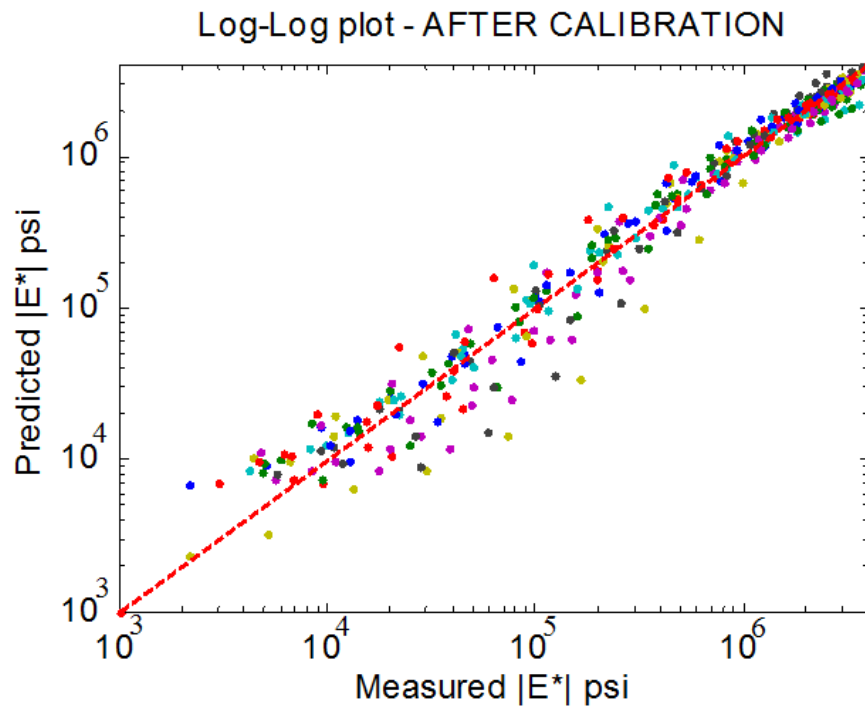
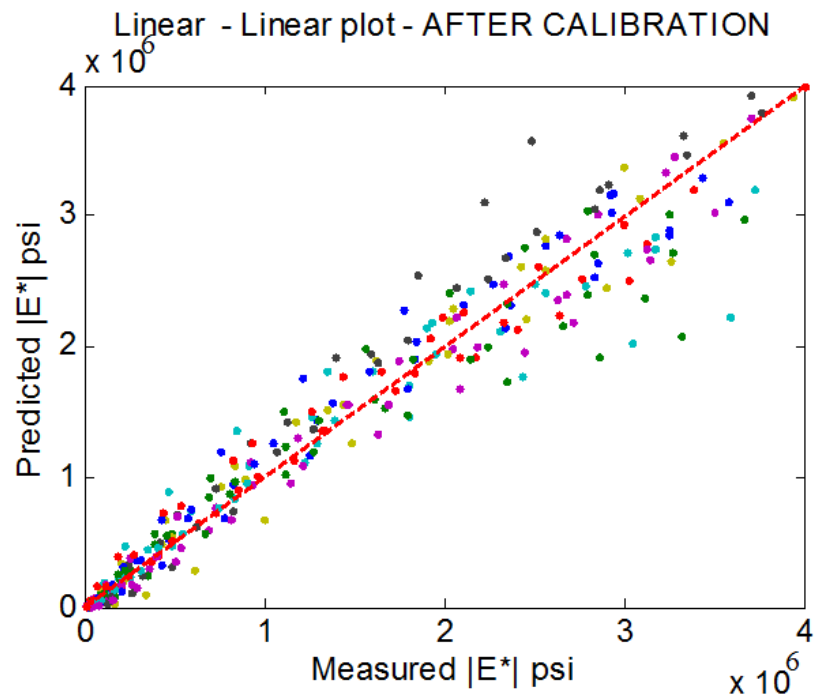


Figure 5.2: The modified Witczak's equation developed as part of the NCHRP 1-40D. The plot shows the predicted versus measured values after calibration for MDOT mixtures. $S_e/S_y = 0.3029$, $R^2 = 0.9248$ (linear-linear plot), and $S_e/S_y = 0.2053$, $R^2 = 0.965$ (log-log plot).

Table 5.1: Comparison between coefficients used in the original and optimized models.

Coefficients	E* Predictive model	
	Original model	Optimized model
a1	-0.349	-0.97535
a2	0.754	1.212316
a3	-0.0052	0.009132
a4	6.65	8.153804
a5	-0.032	-0.00188
a6	0.0027	0.001256
a7	0.011	0.006975
a8	-0.0001	-0.000019
a9	0.006	0.011852
a10	-0.00014	-0.00017
a11	-0.08	-0.22348
a12	-1.06	-4.84772
a13	2.558	1.092204
a14	0.032	0.074729
a15	0.713	2.350258
a16	0.0124	-0.03973
a17	-0.0001	0.000576
a18	-0.0098	0.014317
a19	-0.7814	0.112725
a20	-0.5785	-0.64427
a21	0.8834	0.38239

5.3 Validation of the calibrated Modified Witczak |E*| predictive model for MDOT asphalt mixtures

About 15% (9 out of 64) of the asphalt mixtures characterized in this study were used in the independent validation of the calibrated Modified Witczak predictive model. These 9 mixtures were not used during the calibration of the model shown in Figure 5.2. Figure 5.3 shows a comparison between laboratory measured |E*| values and predicted |E*| values using the model calibrated for MDOT mixtures. The calibrated model showed very good results as

compared to the measured laboratory data. The goodness-of-fit statistics for the log-log plot $S_e/S_y = 0.3749$, $R^2 = 0.885$, are better than the statistics shown in Figure 5.1.

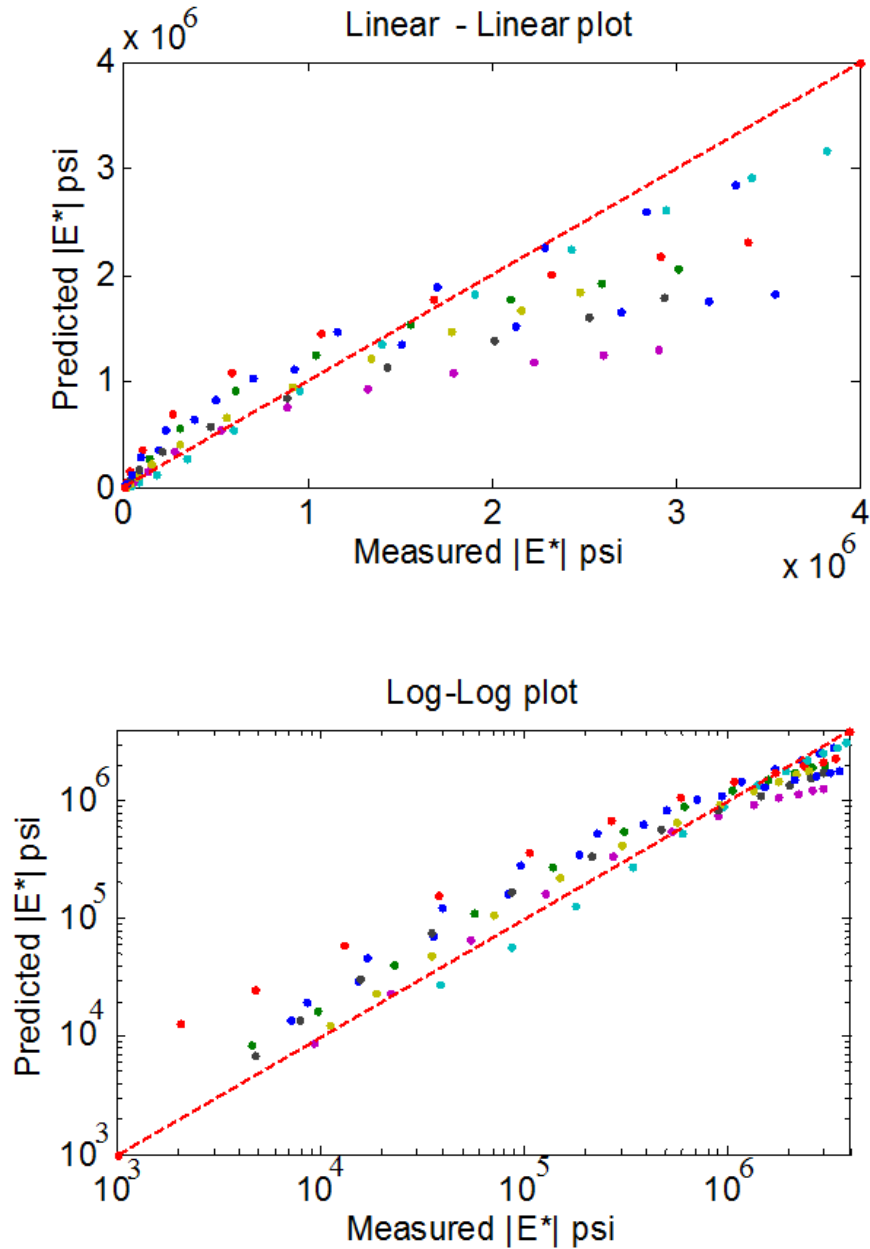


Figure 5.3: The modified Witczak’s equation developed as part of the NCHRP 1-40D. The plot shows the predicted versus measured values for MDOT mixtures using the calibrated coefficients. $S_e/S_y = 0.3749$, $R^2 = 0.885$ (log-log plot).

5.4 Evaluation of the ANNACAP software for predicting $|E^*|$ of MDOT mixtures

The ANNACAP software, which is an artificial neural network (ANN)-based $|E^*|$ prediction model developed by FHWA's Long Term Pavement Performance (LTPP) program (FHWA 2011 (web link), Kim et al. 2010) was evaluated as part of this study. The ANNACAP software was used to predict the $|E^*|$ values using the volumetric properties of the MDOT mixtures tested, then compared with the laboratory-measured $|E^*|$ values. Figure 5.4 shows the measured versus ANNACAP-predicted $|E^*|$ values, where the correlation coefficient (R^2) was 0.775. As shown, the software, which was trained (i.e., calibrated) nationally, did not perform very well in predicting $|E^*|$ values of MDOT mixtures tested in this study.

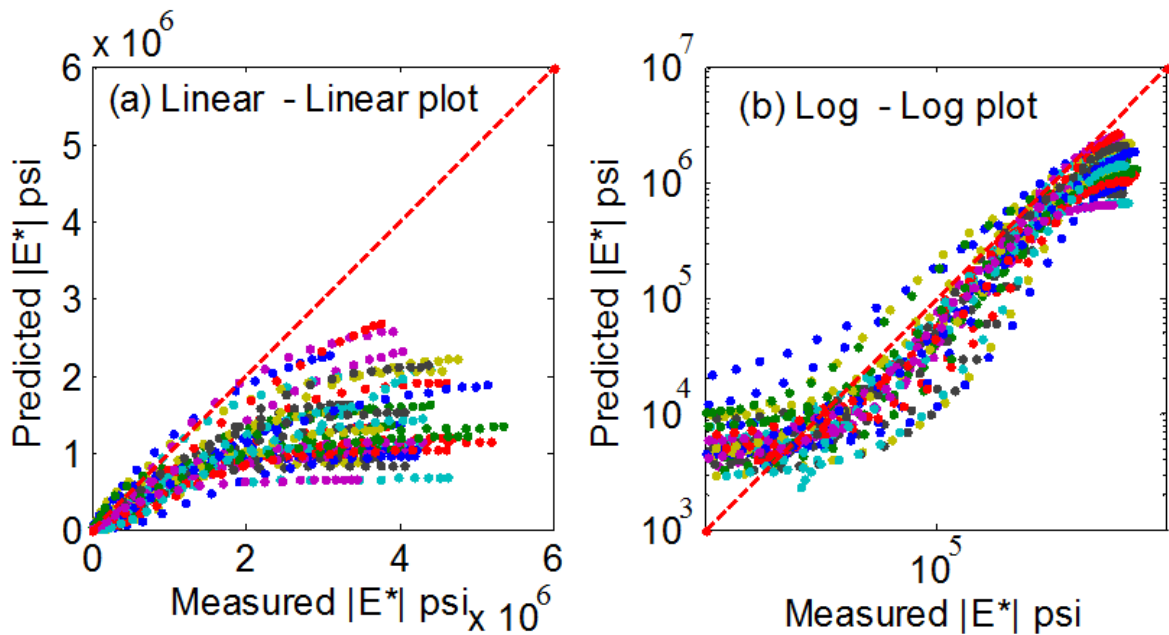


Figure 5.4: Predicted versus measured values for MDOT mixtures using the ANNACAP software: (a) Linear-Linear plot, (b) Log-Log plot.

5.5 Development and validation of a new ANN-based $|E^*|$ predictive model trained for Michigan asphalt mixtures

In the field of Computer Science, Artificial Neural Networks (ANNs) have been extensively utilized for pattern recognition in images, with special emphasis to the application of face detection (Propp and Samal 1992, Rowley et al. 1998, Sung and Poggio 1998). For road materials, ANNs have been employed to classify aggregates size (Kim et al. 2004), predict pavement layer moduli (Ceylan et al. 2007; Kim and Kim 1998), simulate rutting and fatigue performance of asphalt mixtures (Huang et al., 2007; Tarefder et al. 2005a), estimate the thickness of the pavement layers (Gucunski and Krstic 1996), approximate the resilient modulus of base materials (Tutumluer and Seyhan 1998), and relate mixture variables to permeability and roughness (Choi et al. 2004; Tarefder et al. 2005b). ANN models are very useful in predicting certain engineering outputs (e.g., $|E^*|$) from a number of input variables (e.g., asphalt volumetric properties).

In an effort to develop an improved $|E^*|$ predictive model for the future MDOT mixtures that are not similar to the ones tested in this study, an ANN model was developed using the data generated as part of this study. In this study, an ANN was developed to predict $|E^*|$ at different temperatures and frequencies using the following inputs:

- (i) p_{200} = Percentage of aggregate passing #200 sieve
- (ii) p_4 = Cumulative percentage of aggregate retained in #4 sieve
- (iii) $p_{3/8}$ = Cumulative percentage of aggregate retained in 3/8-inch sieve
- (iv) $p_{3/4}$ = Cumulative percentage of aggregate retained in 3/4-inch sieve

- (v) V_a = Percentage of air voids (by volume of mix)
- (vi) V_{beff} = Percentage of effective asphalt content (by volume of mix)
- (vii) $|G^*|_b$ = Dynamic shear modulus of asphalt binder (psi)
- (viii) δ_b = Binder phase angle associated with $|G^*|_b$ (degrees)
- (ix) f = reduced frequency (Hz) corresponding to each $|G^*|_b$ and δ_b .

It is noted that the ANN-algorithm developed in this study automatically generates the $|E^*|$ master curve and determines the shift factor polynomial coefficients (i.e., a_1 and a_2 of $aT(T)$ – see Equation [2.11]) and uses them to calculate the reduced frequency (i.e., the input (ix) above).

5.5.1 Structure of the ANN

A feed-forward (back-propagation) network of one hidden layer and one output layer was determined to be the optimum network for the ANN model (Figure 5.5). This ANN structure was obtained by a trial and error process that involves trial of many ANN structures (Demuth and Beale 2004).

The steps below describe how the ANN shown in Figure 5.5 calculates output y (which is the $|E^*|$ in this case) from a set of 9 inputs (which are p_{200} , p_4 , $|G^*|$, etc. shown in the previous page). These steps are herein called “forward computation”.

- 1) Compute the output of the Hidden Layer (\mathbf{a}^H) using Equations [5.5] and [5.6]. The variables in bold letters in these equations indicate that they are matrices (or vectors)

and the multiplication and summation in the equation are matrix operations. The *tansig* function in Equation [5.6], however, is applied to each element of the vector.

$$\mathbf{n}^H = \mathbf{W}^H \mathbf{p} + \mathbf{b}^H \quad [5.5]$$

$$\mathbf{a}^H = \text{tansig}(\mathbf{n}^H) \quad [5.6]$$

where \mathbf{p} is the input vector (9×1), \mathbf{W}^H is the weight matrix (8×9) and \mathbf{b}^H is the bias vector (8×1) of the Hidden Layer, and the *tansig* is the transfer function given as:

$$\text{tansig}(x) = \frac{2}{1 + \exp(-2x)} - 1 \quad [5.7]$$

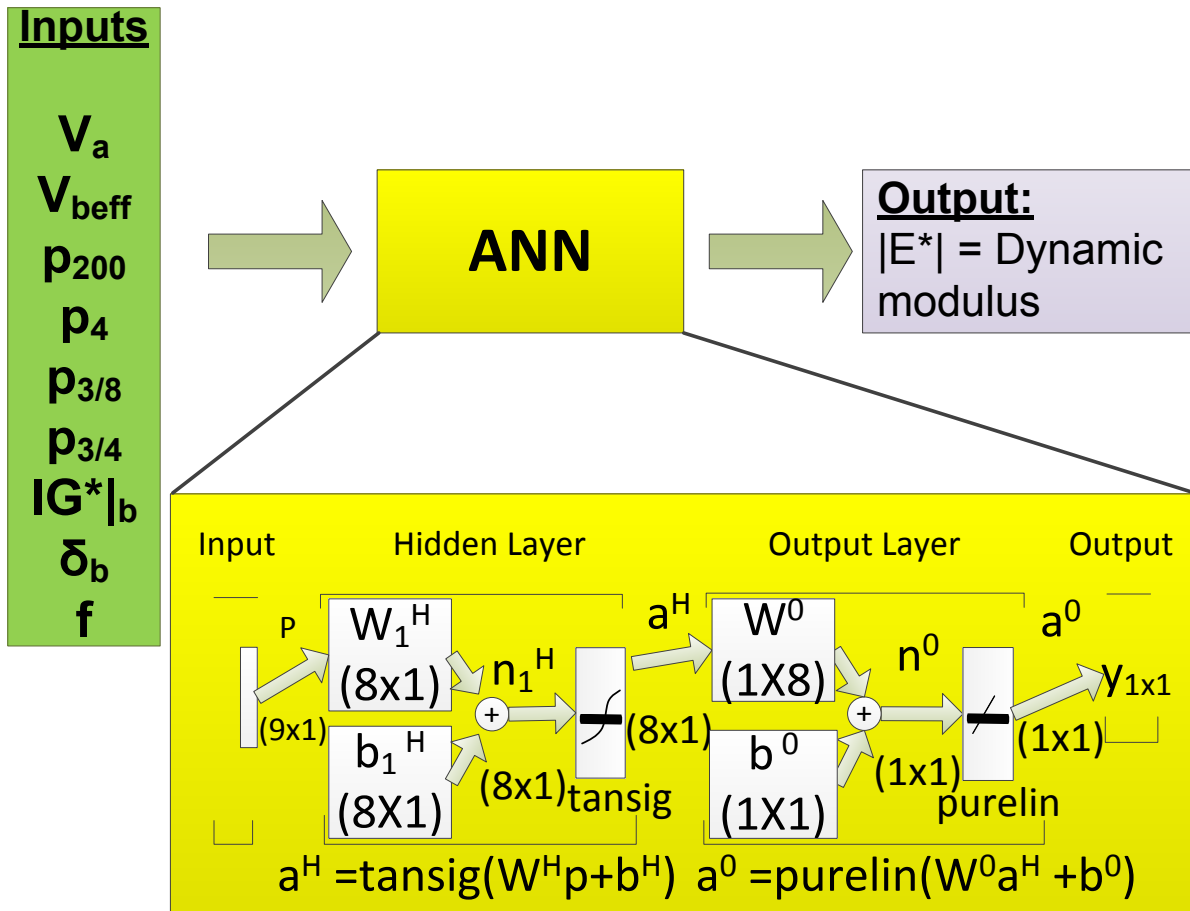


Figure 5.5: Structure of the ANN model.

2) Compute the output of the Output Layer by using the output of the Hidden Layer ()

as follows:

$$n^o = \mathbf{W}^o \mathbf{a}^H + b^o \quad [5.8]$$

$$y = \text{purelin}(n^o) = n^o \quad [5.9]$$

where y is the positive or negative scalar output of the entire network, \mathbf{a}^H is the output of the Hidden Layer (8×1), \mathbf{W}^o is the weight matrix (1×8) and b^o is the bias constant of the Output Layer.

5.5.2 Training the ANN

The training initiates with random weights (i.e., \mathbf{W}^H and \mathbf{W}^o) and biases (i.e., \mathbf{b}^H and b^o). The forward computation described in the previous section is repeated many times while adjusting these weights and biases. Each repetition is called an *epoch*, which continues until the error between the predicted output from the ANN (i.e., $y = |E^*|_{\text{predicted}}$) and actual target output (i.e., $y_{\text{target}} = |E^*|_{\text{measured}}$) is minimized. The ANN model was trained by using 41 different Job Mix Formulas (JMFs). It is noted that a JMF is the mix design the contractor uses when paving a particular mix. For each JMF, 12 $|G^*|$ values and 12 phase angle values were used to cover a wide range of frequencies and temperatures, which makes 492 data points. MATLAB's ANN toolbox was used for this purpose. In this toolbox, the mean square error between the measured and predicted $|E^*|$ decreases as the number of epochs increases. It is noted that the training dataset is divided into three subsets: *Training* (80% of the dataset), *Validation* (10% of the dataset), and *Test* (10% of the dataset). The ANN primarily uses the information from the

Training dataset and adjusts the weights and biases accordingly. While doing so, it also looks at the prediction accuracy of *Validation* dataset and makes sure that error in *Validation* data set is close to the error from the *Training* dataset. If the error in *Validation* dataset is significantly larger than the error in *Training* dataset, it means that the ANN is over trained to the *Training* dataset and memorized the *Training* dataset rather than learning the overall interrelation between the input and output. Lastly, the *Testing* dataset, which is not used during adjusting weights and biases, is used as an independent validation of the model.

Figure 5.6 shows the change in the mean squared error as the epochs increase. As shown, all curves (Training, Validation and Test) are close to each other, which means that the ANN developed in this study learned from the training data, it did not memorize. Performance of the ANN model was evaluated from the plot of the predicted versus measured values of $|E^*|$ for the training, validation and testing datasets as shown in Figure 5.7. Coefficient of determination (R^2) with respect to the line of equality was computed, which is used to measure the goodness-of-fit of the trend. As shown in Figure 5.7, ANN predictions lay around the line-of-equality with R^2 s ranging from 0.951 to 0.963. Considering the sample-to-sample variability and other factors, this is a good result and better than the Modified Witczak model (see Figure 5.3) and the ANNACAP (see Figure 5.4). It should be noted that ANN models are trained and validated for local material properties used in each developed model. Therefore ANN models that are developed nationally, are not expected and will not provide $|E^*|$ predictions that are as accurate as those of models that are independently developed for materials used in a specific State. Therefore; the ANN-based $|E^*|$ prediction model developed in this study may not perform as well as shown above in predicting $|E^*|$ values for materials used in other regions.

In order to further validate the ANN model developed in this study, 9 different asphalt mixtures were set aside and not used in any of the ANN development process. Then these 9 mixtures were used in forward computation of $|E^*|$ values using the ANN developed. Figure 5.8 presents the predicted versus measured values using the independent data set. As shown, independent validation of the ANN model exceeds the accuracy of the calibrated Modified Witczak model (see Figure 5.3).

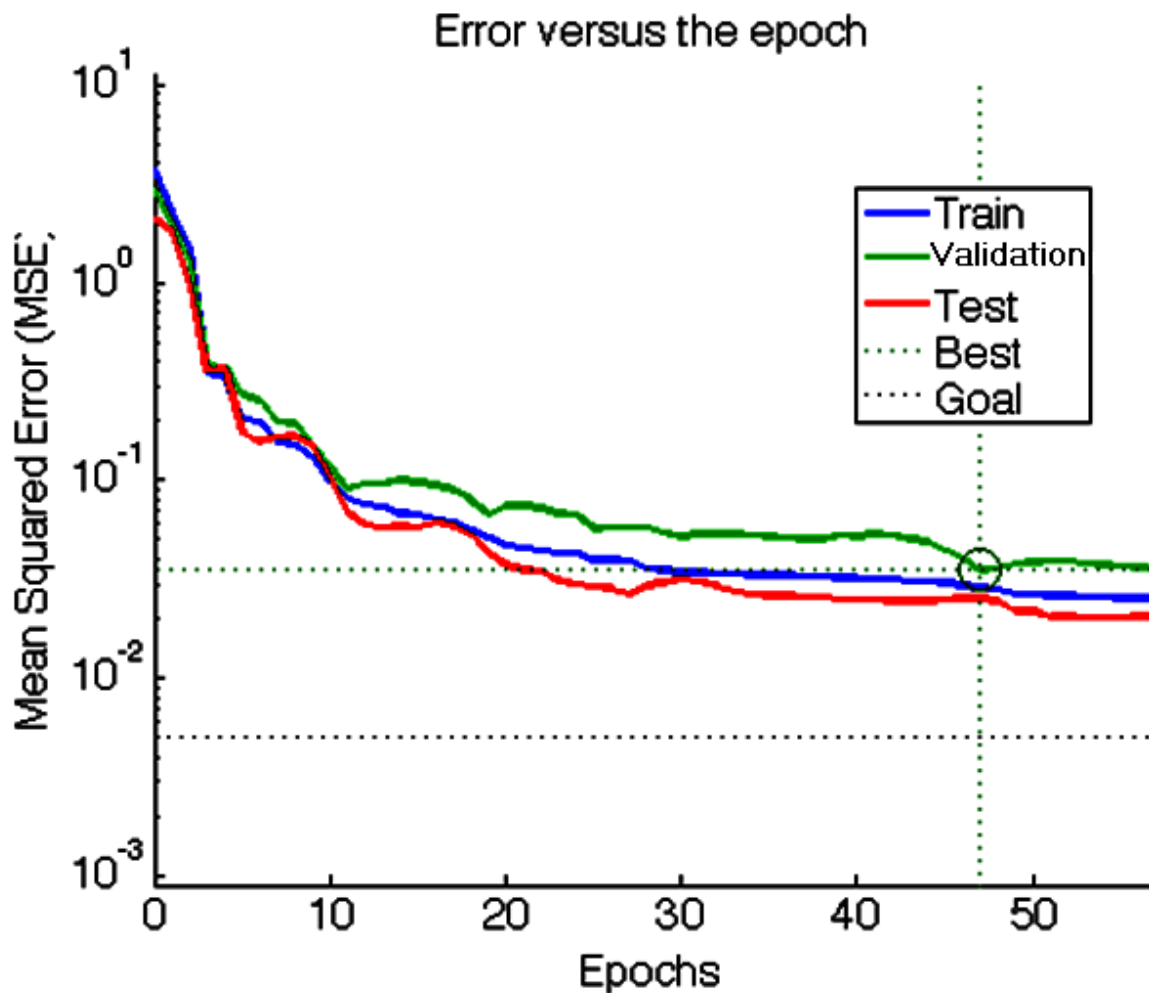


Figure 5.6: Error versus the epochs in the ANN model developed in this study

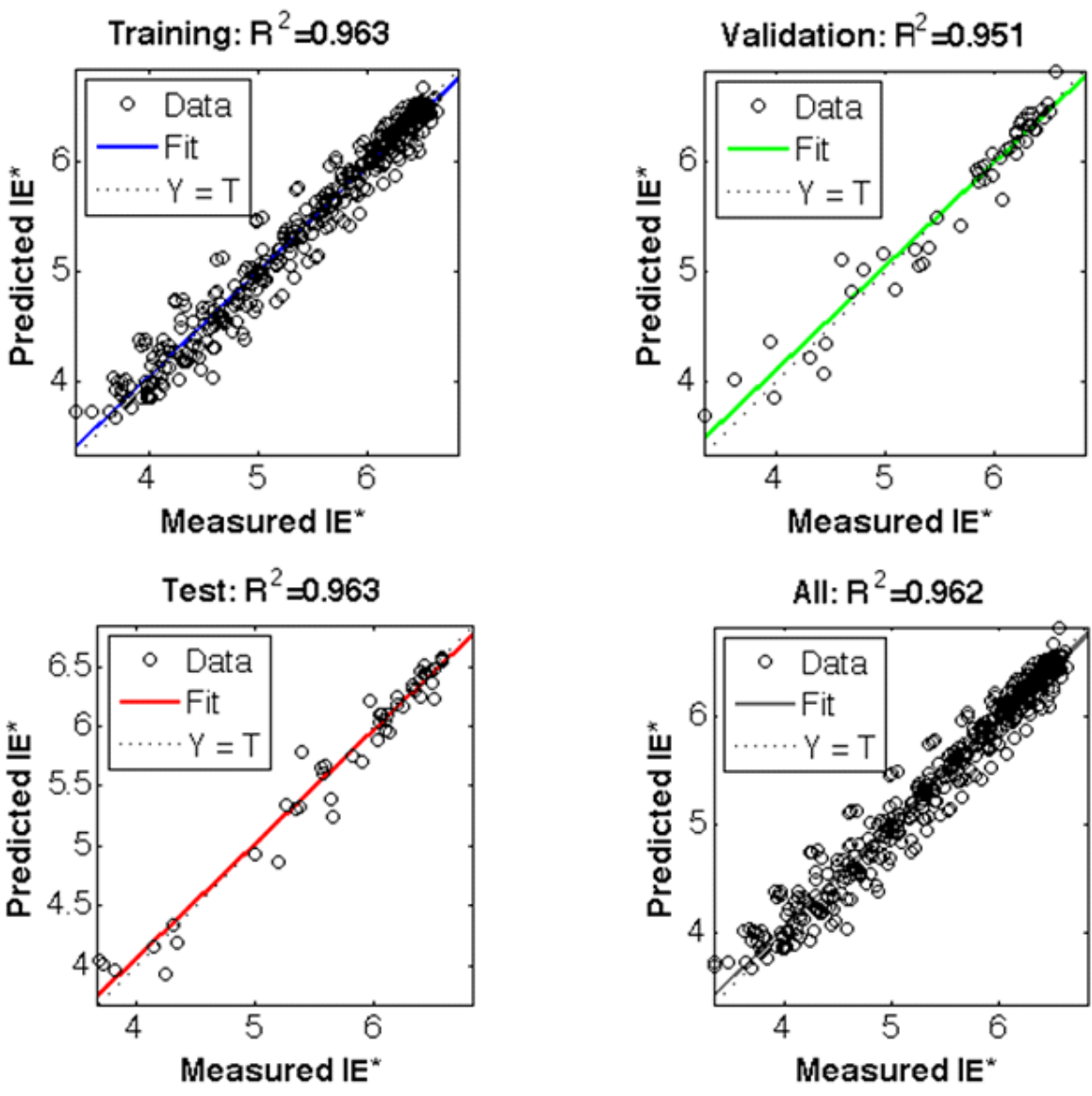


Figure 5.7: Predicted versus measured $|E^*|$ values for Training, Validation and Testing datasets as well as all the data (for mixtures used during development of the model).

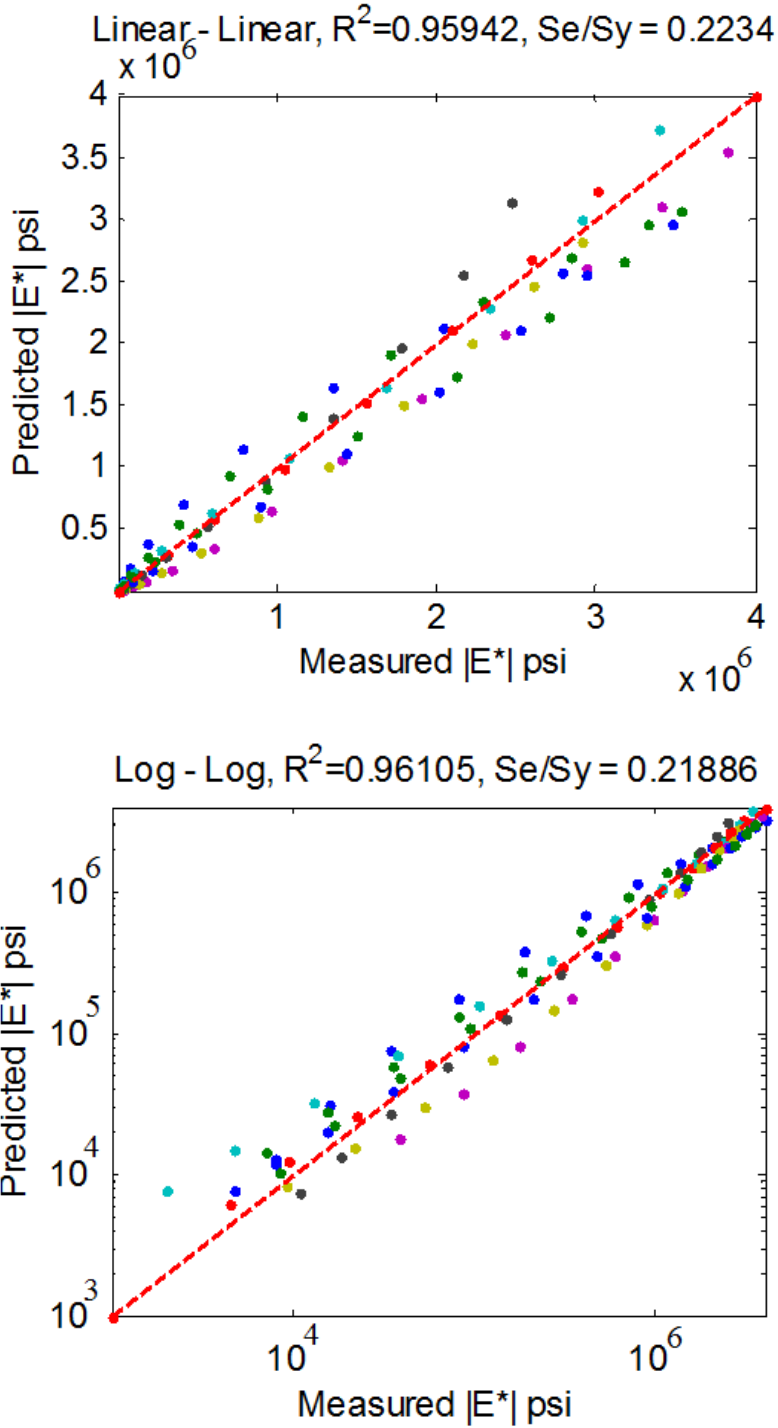


Figure 5.8: Predicted versus measured values for MDOT mixtures using the MSU-ANN model for mixtures not used during development of the model

6. INVESTIGATION OF SAMPLE GEOMETRY & RVE

REQUIREMENT FOR $|E^*|$ USING THIN BEAM MIXTURES (TBMs)

It is desirable to study the effect of aged material properties on pavement performance. Recent research showed that current laboratory aging protocols lead to aging gradients within the regular-size (100mm diameter, 150mm tall) samples (Houston et al. 2005). Test samples become non-homogeneous and anisotropic. Such samples are no longer useful for performance testing, especially for tests that are used to calibrate advanced models. Therefore, it is suggested in this study that relatively smaller test geometries be used for that purpose. Thin Beam Mixtures (TBMs) (127×12.7×6.35mm) were obtained from typical gyratory cored asphalt mixture specimens to investigate the possibility of obtaining the complex modulus $|E^*|$ master curve from the creep compliance $D(t)$ using the Bending Beam Rheometer (BBR) testing machine and in efforts of verifying the RVE requirement for asphalt mixtures. Once the RVE requirement is verified for the thin beam asphalt mixtures, this will serve as a foundation for the aging study since small samples will be much less susceptible to aging gradients. A similar study (NCHRP-IDEA 151) by Marasteanu et al. (2012) showed the feasibility of using TBM samples for low temperature cracking analysis.

6.1 Materials Used

As previously mentioned in the Chapter 3 (Research Methodology), it was intended to verify the applicability of this methodology on a wider range of asphalt mixtures. Therefore; 10 asphalt mixtures commonly used in the State of Michigan with varying Nominal Maximum

Aggregate Sizes (NMASs) were tested. In addition, three replicates representing the same asphalt mixture were tested in order to account for sample-to-sample variability which brings the total up to 30 tested asphalt mixture beams as shown below in Table 6.1.

6.2 Bending Beam Rheometer (BBR) testing on Thin Beam Mixtures (TBMs)

As part of the binder PG specification; the BBR is used to determine the creep compliance of asphalt binders using the 3-point bending setup commonly used in mechanics (Zofka et al. 2007). This test method follows the method developed at the University of Minnesota to determine the creep stiffness of thin mixture beams using the BBR testing equipment used to determine the PG grade of asphalt binders. This procedure was developed into a draft standard procedure under a NCHRP IDEA project led by Dr. Marasteanu.

Similar to BBR testing of asphalt binders, a constant force is applied in the middle of the beam, and deflections with time are measured throughout the test. Using the deflections measured during the test, and knowing the dimensions of the beam, the applied force and stress; the resulting strain and creep compliance $D(t)$ can be computed.

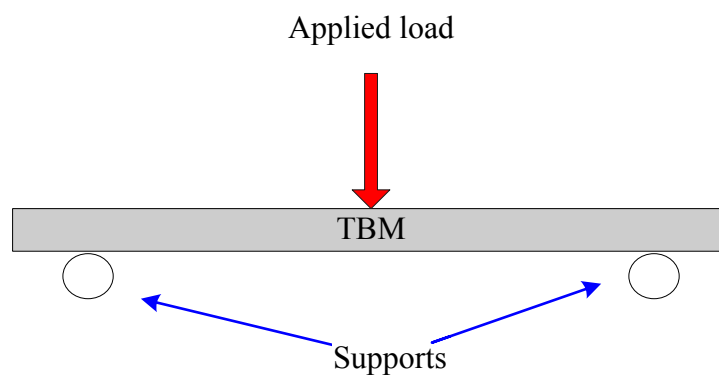


Figure 6.1: 3-point testing concept on asphalt mixtures.

Table 6.1: List of TBMs tested along with their volumetric properties and NMAS

NMAS (mm)	HMA ID	Binder PG	Maximum Specific Gravity Gmm	TBM ID	Air Voids (AV) (%)
25.0	205	58-28	2.502	205-U-C	14.09
				205-U-M	11.85
				205-U-E	12.66
19.0	2	64-22	2.545	2-U-C	12.23
				2-U-M	8.49
				2-U-E	9.03
	18A	58-22	2.534	18A-U-C	8.63
				18A-U-M	7.21
				18A-U-E	5.82
	26B	58-28	2.415	26B-U-C	9.79
				26B-U-M	8.77
				26B-U-E	6.50
12.5	80	58-34	2.511	80-U-C	N/M*
				80-U-M	N/M*
				80-U-E	9.39
	90	70-22	2.547	90-U-C	10.85
				90-U-M	4.11
				90-U-E	8.03
	64	58-34	2.462	64-U-C	12.81
				64-U-M	8.40
				64-U-E	9.30
9.5	206	64-22	2.503	206-U-C	9.94
				206-U-M	8.28
				206-U-E	6.22
	21	64-28	2.481	21-U-C	9.18
				21-U-M	10.34
				21-U-E	12.47
	29A	64-28	2.457	29A-U-C	13.31
				29A-U-M	12.71
				29A-U-E	10.38

N/M: Not measured

Once the $D(t)$ tests are completed at different temperatures, the Time-Temperature Superposition (TTS) principle is used to compute the $D(t)$ master curve. It should be noted that the theory of viscoelasticity states that if one of the linear viscoelastic properties (i.e., complex modulus $|E^*|$, creep compliance $D(t)$, and relaxation modulus $E(t)$) is known, the remaining properties can be calculated through numerical inter-conversion procedures (Park and Schapery, 1999). Once the $D(t)$ master curve is determined, the $|E^*|$ master curve can be computed using the methods described by Park and Schapery (1999).

6.3 Results and Discussion

Due to the availability of limited samples; the TBM tests were only conducted at one temperature (-10°C). This did not produce enough data points to obtain $|E^*|$ values for the studied mixtures through inter-conversion processes. Instead, using the basic theory of viscoelasticity; $|E^*|$ laboratory measurements on regular size specimens of the 10 HMAs under study were converted to $D(t)$ values and compared with the values measured using the BBR machine on the TBMs.

Figure 6.2 through Figure 6.6 show comparisons between $|E^*|$ -based $D(t)$ values and TBM-based $D(t)$ values for all TBMs tested in this study based on the NMAS of each asphalt mixture. Visual inspection with respect to the line of equality (LOE) do not show a good correlation between measured $D(t)$ values using the TBM and $D(t)$ values converted from $|E^*|$ data run on the regular size specimens. A trend in $D(t)$ values obtained from the BBR test on TBMs was observed. On the other hand; the factor between $|E^*|$ -based and TBM-based $D(t)$

values was inconsistent and ranged between 1.5 and 4 factors. This was observed for all NMASs used in this study.

Figure 6.2 shows a comparison between $|E^*|$ -based $D(t)$ values and TBM-based $D(t)$ values for HMA #205 with a NMAS of 25.0mm. The factor between $|E^*|$ -based, and TBM-based $D(t)$ values was approximately 3 factors. Figure 6.3 shows comparisons for 19.0mm NMAS thin beams. The factor between $|E^*|$ -based, and TBM-based $D(t)$ values ranged between 1.5 and approximately 4 factors. The data shown in Figure 6.2 for the 25.0mm NMAS represents one asphalt mixture only. This is the reason why the 25.0mm NMAS showed less variability as compared to the 19.0mm NMAS mixtures. Figure 6.4 shows comparisons for 12.5mm NMAS thin beams. The factor between $|E^*|$ -based, and TBM-based $D(t)$ values ranged between 1.5 and less than 3 factors. Figure 6.5 shows comparisons for 9.5mm NMAS thin beams. The difference between $|E^*|$ -based, and TBM-based $D(t)$ values ranged between 1.6 and approximately 2 factors. In addition, Figure 6.6 shows a comparison between $|E^*|$ -based $D(t)$ values and TBM-based $D(t)$ values for all TBMs tested in this study. The overall plot shows a difference between $|E^*|$ -based and TBM-based $D(t)$ values that range between 1.5 and approximately 3 factors. It should be noted that the variation could have also been caused by the different air void levels for each TBM.

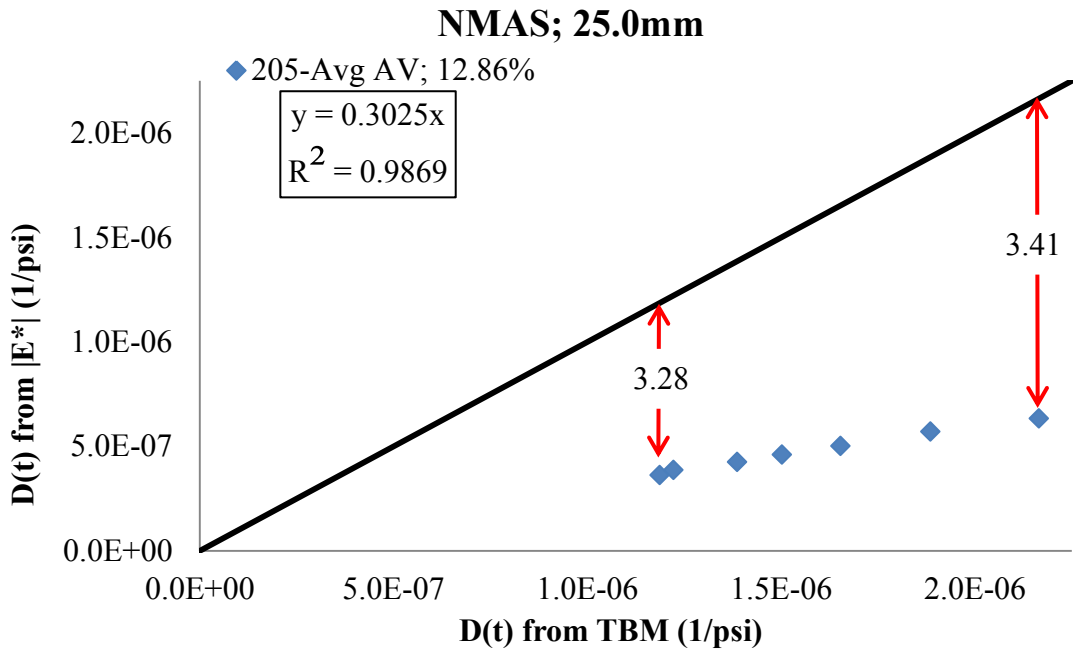


Figure 6.2: Comparison between $|E^*|$ -based $D(t)$ values and TBM-based $D(t)$ values for 25.0mm NMAS.

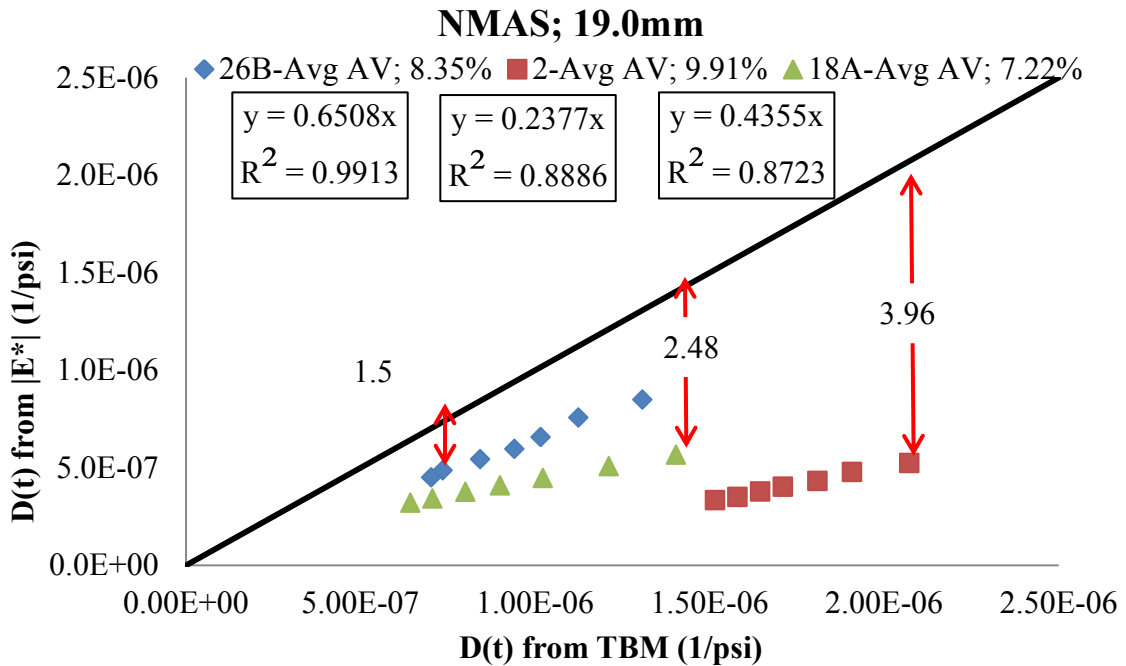


Figure 6.3: Comparison between $|E^*|$ -based $D(t)$ values and TBM-based $D(t)$ values for 19.0mm NMAS.

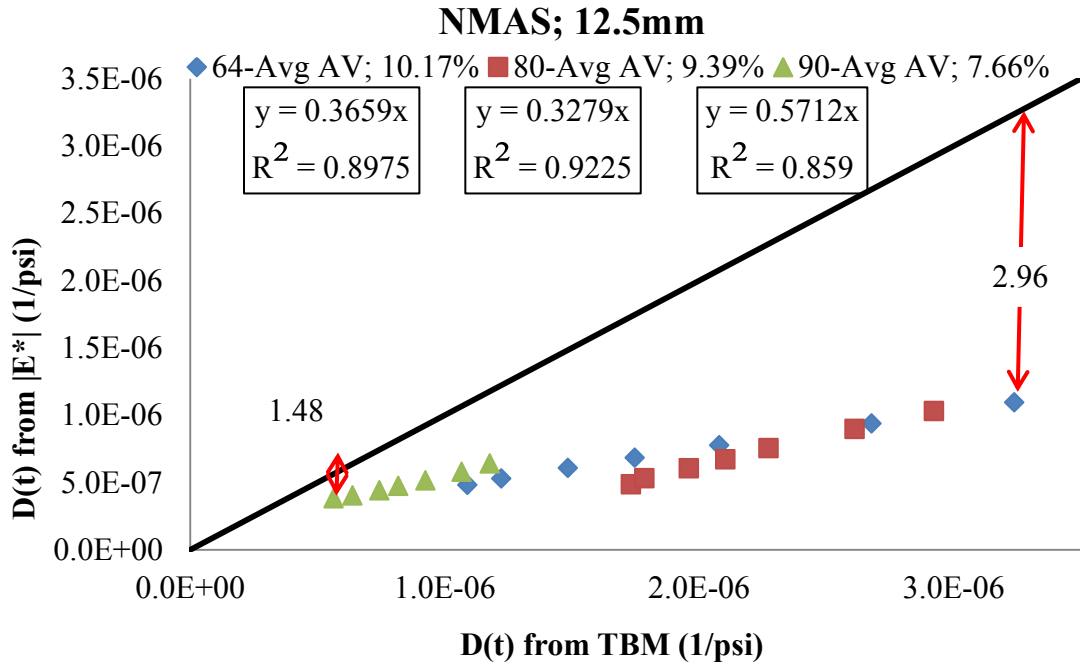


Figure 6.4: Comparison between $|E^*|$ -based $D(t)$ values and TBM-based $D(t)$ values for 12.5mm NMAS.

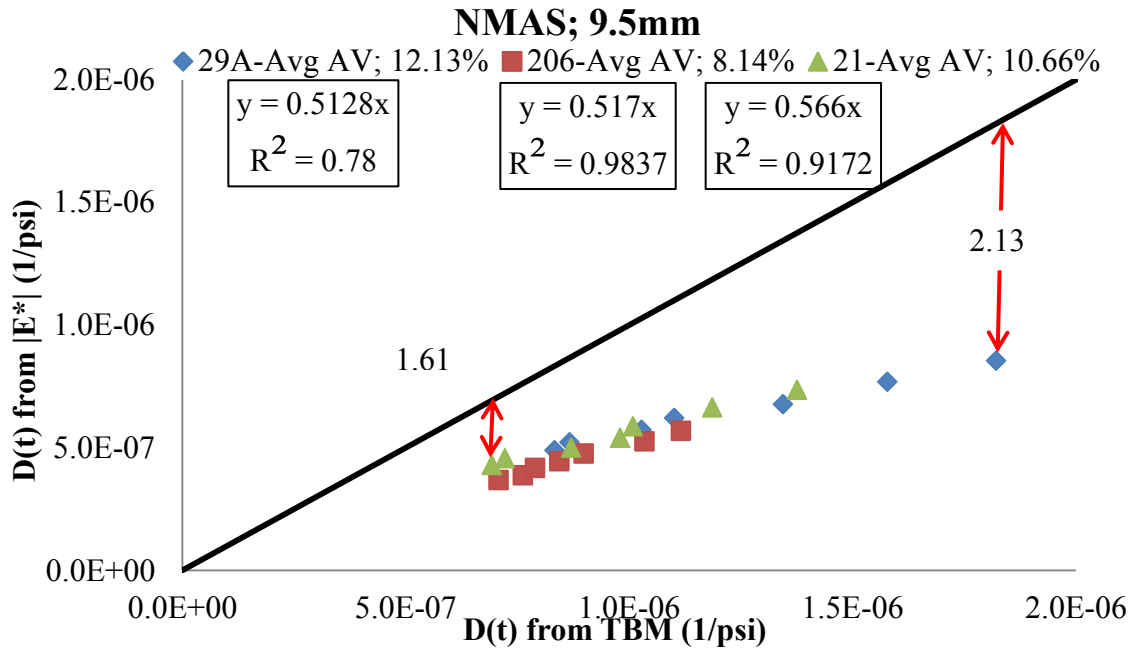


Figure 6.5: Comparison between $|E^*|$ -based $D(t)$ values and TBM-based $D(t)$ values for 9.5mm NMAS.

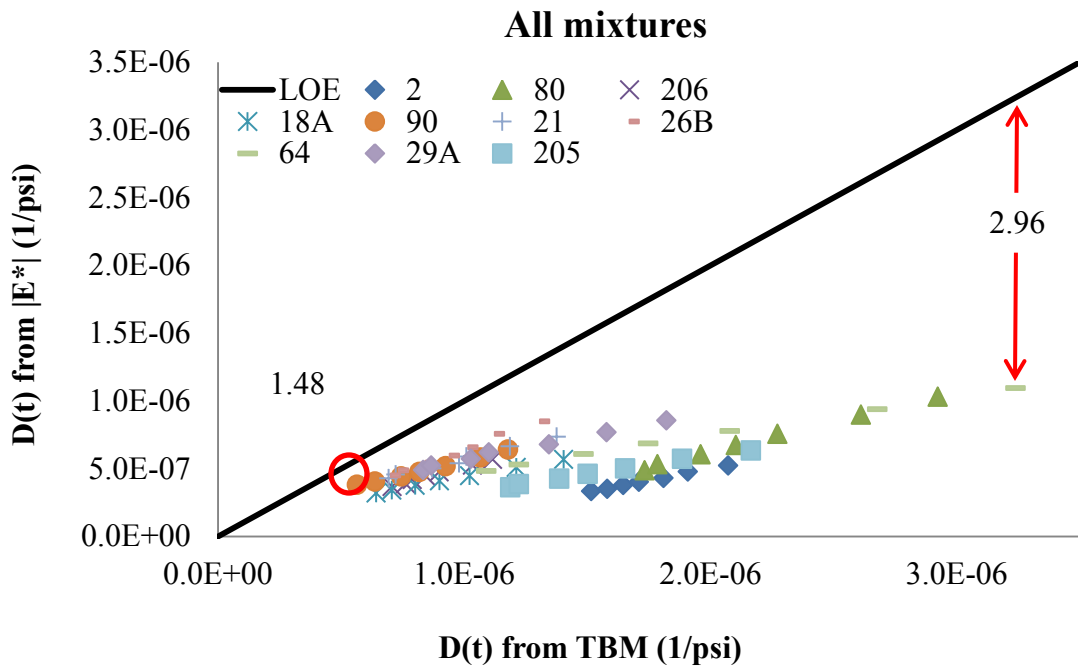


Figure 6.6: Comparison between $|E^*|$ -based $D(t)$ values and TBM-based $D(t)$ values for all mixtures and NMASSs.

As shown from the simple analysis, $D(t)$ values obtained from the BBR test are not very comparable to the values obtained from regular size $|E^*|$ test specimens. It should be noted that the BBR testing on TBMs is a bending mode of testing, and the $|E^*|$ testing on regular-size performance specimens is a compression mode of testing. Therefore, the factors between $|E^*|$ -based and TBM-based $D(t)$ values are expected. In a similar study, Zofka et al. (2007) compared $D(t)$ values obtained from the BBR machine with $D(t)$ values obtained from the Indirect Tensile Strength (IDT) test. The difference in magnitude was close to the difference obtained in this study at intermediate temperatures (-10°C). The difference observed was much less at lower temperatures. The $D(t)$ values obtained from the BBR test should correlate even better with those obtained from the IDT test since it is a tension mode of testing. A trend was observed in TBM-

based $D(t)$ values, but inconsistent factors of difference between $|E^*|$ -based and TBM-based values do not support the use of this experimental procedure for producing fundamental engineering material properties of asphalt mixtures.

Based on the limited analysis carried out in this study, it is concluded that the BBR test is not very feasible for estimation of mixture creep compliance and therefore; not very reliable for estimation of other linear viscoelastic properties (i.e., complex modulus $|E^*|$, and relaxation modulus $E(t)$) through numerical inter-conversion.

Better results were observed for asphalt mixtures with a NMAS of 12.5mm and less. It should be noted that this experimental procedure was only conducted at one temperature (-10° C). Variability in test data is expected to be less for test temperature less than -10° C. On the other hand, much higher variability in the test data will probably be observed for materials tested at higher temperatures. Further analysis is indeed required to form a better understanding and validation of this experimental procedure.

7. CONCLUSIONS & RECOMMENDATIONS

This research investigated the linear viscoelastic characteristics of typical asphalt mixtures and binders commonly used in the State of Michigan. Such material characterization is very important for implementation of the M-E PDG in Michigan and for accurate predictions of flexible pavement performance in the field. The Modified Witczak $|E^*|$ predictive model was locally calibrated for Michigan, and an analytical model was developed to better predict distresses for flexible pavements in Michigan through an Artificial Neural Network (ANN) that was developed and trained for typical asphalt mixtures in Michigan. In addition, the Representative Volume Element (RVE) requirement for dynamic modulus $|E^*|$ of asphalt mixtures was investigated and verified. This study showed that the BBR testing machine is not always feasible for obtaining mixture Creep Compliance ($D(t)$) of thin beams of asphalt mixtures (0.5"×0.25"×4.5"), and therefore it may not be very reliable for estimation of other linear viscoelastic properties (i.e, complex modulus $|E^*|$, and relaxation modulus $E(t)$) through numerical inter-conversion. Following is a summary of conclusions and recommendations that were observed based on this study:

1. The Modified-Witczak (MW) model was calibrated for use in $|E^*|$ prediction of asphalt mixtures commonly used in the State of Michigan to be used in the Level 1 analysis of the M-E PDG software. The calibrated model performed well in comparison with the laboratory measured data.
2. The ANNACAP software, which was developed by the FHWA's LTPP program, was evaluated for use in the $|E^*|$ prediction of asphalt mixtures commonly used in the State of Michigan. The software did not perform well for MDOT mixtures in predicting $|E^*|$.

3. A new ANN-based model was developed as part of this research. The new ANN-based model did very well in predicting $|E^*|$ values of Michigan mixtures.
4. ANN models that are developed nationally are not expected and will not provide $|E^*|$ predictions that are as accurate as those of models that are independently developed for materials used in a specific State. Therefore; the ANN-based $|E^*|$ prediction model developed in this study may not perform as well as shown above in predicting $|E^*|$ values for materials used in other regions.
5. A summary of $|E^*|$ values based on MDOT mix designation was provided. As expected, 3E mixtures were generally stiffer than 4E and 5E mixtures. However the trend was not always consistent in all temperatures. A clear trend should not be expected since there are many variables that play a role in the magnitude of $|E^*|$ at different temperatures and frequencies.
6. A comparison of variation in $|E^*|$ master curves based on MDOT mix designations (e.g., 3E10) was carried out. Grouping mixtures based on MDOT mix designation and using the average of $|E^*|$ values for the given designation is not recommended.
7. This study showed that the TBM-based $D(t)$ values obtained from the BBR testing machine do not match very well to $|E^*|$ -based $D(t)$ values.
8. $D(t)$ values obtained from the BBR testing machine showed a trend in estimated values but the factor (ratio) between $|E^*|$ -based and TBM-based $D(t)$ values was inconsistent.
9. Further investigation is needed for use of TBMs.

APPENDICES

*APPENDIX A: VOLUMETRIC PROPERTIES AND AGGREGATE GRADATION
OF THE TESTED ASPHALT MIXTURES.*

Table A.1: Volumetric properties and aggregate gradation of the tested asphalt mixtures.

<i>Sample ID</i>	<i>PG Grade</i>	<i>% Asphalt (Given)</i>	<i>VMA</i>	<i>VFA</i>	<i>Angularity</i>	<i>Gmm</i>	<i>Gmb</i>	<i>Gb</i>	<i>Gse</i>	<i>Gsb</i>	<i>Pbe</i>
2A	64-22	4.90	13.94	78.47	46.00	2.545	2.469	1.027	2.755	2.728	4.55
2-WMA	64-28	4.90	14.02	78.67	46.00	2.508	2.433	1.029	2.708	2.691	
4	70-28	5.31	15.04	73.51	45.30	2.510	2.410	1.025	2.732	2.686	4.70
18A	58-22	5.20	14.16	78.81	46.00	2.534	2.458	1.018	2.760	2.715	4.62
18B	58-22	5.04	13.52	77.81	41.30	2.502	2.427	1.023	2.710	2.665	
20A	64-28	5.23	15.05	73.49	45.20	2.506	2.406	1.029	2.722	2.684	4.72
20B	64-28	5.53	14.97	73.28	45.00	2.485	2.386	1.029	2.710	2.651	4.73
20C	64-28	5.58	14.83	76.40	45.20	2.489	2.402	1.032	2.715	2.663	
21	64-28	6.01	16.34	75.58	45.30	2.481	2.382	1.029	2.727	2.676	5.33
23	70-28	4.94	14.40	75.69	46.00	2.578	2.488	1.030	2.796	2.763	
24A	70-28	6.29	16.04	75.06	45.40	2.426	2.329	1.031	2.668	2.599	5.33
24B	70-28	5.78	15.94	78.04	45.00	2.531	2.422	1.030	2.779	2.737	
26A	58-22	5.60	14.17	78.83	45.00	2.538	2.462	1.018	2.785	2.708	4.62
26B	58-28	5.30	13.80	78.17	42.10	2.490	2.415	1.020	2.709	2.653	4.55
26C	58-28	5.43	13.72	18.14	41.10	2.473	2.398	1.017	2.694	2.629	4.55
28A	64-28	5.40	14.75	72.87	41.20	2.471	2.372	1.028	2.686	2.632	4.66
28B	64-28	5.43	15.06	73.44	41.70	2.490	2.390	1.028	2.711	2.661	4.76
29A	64-28	5.99	15.74	74.59	43.40	2.457	2.359	1.028	2.696	2.632	5.12
29B	64-28	5.92	16.07	75.11	43.00	2.463	2.364	1.028	2.700	2.650	5.24
31A	70-28	5.62	15.27	73.76	41.20	2.471	2.372	1.017	2.701	2.642	4.83
31B	70-28	5.40	14.71	72.81	41.20	2.472	2.373	1.031	2.686	2.632	4.66
32A	70-28	5.99	15.71	74.54	43.40	2.458	2.360	1.031	2.696	2.632	5.12
32B	70-28	6.08	16.20	75.31	41.70	2.450	2.352	1.017	2.696	2.636	5.27
37	58-28	6.01	16.52	75.78	42.60	2.494	2.395	1.032	2.743	2.696	5.39
44	58-28	5.35	15.07	73.46	42.10	2.475	2.376	1.020	2.692	2.648	4.75

Table A.1 (cont'd)

<i>Sample ID</i>	<i>1-1/2"</i>	<i>1"</i>	<i>3/4"</i>	<i>1/2"</i>	<i>3/8"</i>	<i>No. 4</i>	<i>No. 8</i>	<i>No. 16</i>	<i>No. 30</i>	<i>No. 50</i>	<i>No. 100</i>	<i>No. 200</i>
2A	100.00	100.00	100.00	83.00	72.30	47.30	34.90	26.00	18.20	9.30	6.10	5.00
2-WMA	100.00	100.00	100.00	88.10	77.10	57.60	40.90	27.70	19.50	12.70	7.50	4.50
4	100.00	100.00	100.00	98.80	88.60	73.20	56.30	38.00	25.20	14.70	7.80	4.90
18A	100.00	100.00	100.00	84.50	73.40	49.40	34.70	25.70	20.20	11.50	6.90	5.20
18B	100.00	100.00	98.10	88.80	84.30	65.80	46.20	33.90	25.50	16.30	7.40	4.40
20A	100.00	100.00	100.00	98.80	89.50	71.10	53.50	36.30	23.50	13.10	7.40	4.70
20B	100.00	100.00	100.00	93.40	90.40	83.40	56.20	36.70	25.60	15.80	8.40	5.80
20C	100.00	100.00	100.00	93.20	88.60	73.50	54.00	40.70	30.80	19.40	8.60	4.60
21	100.00	100.00	100.00	100.00	99.20	83.60	66.30	46.50	31.20	17.30	8.70	5.40
23	100.00	100.00	100.00	91.60	83.00	68.30	50.00	35.90	25.60	14.40	6.80	4.30
24A	100.00	100.00	100.00	100.00	95.70	80.10	58.00	39.90	28.70	16.20	7.70	5.80
24B	100.00	100.00	100.00	100.00	97.80	86.80	61.80	44.30	32.30	18.30	9.00	5.60
26A	100.00	100.00	100.00	88.10	78.40	52.60	33.00	22.10	15.60	10.90	7.20	5.20
26B	100.00	100.00	100.00	89.80	80.70	63.60	46.30	35.60	26.60	13.90	6.50	4.40
26C	100.00	100.00	100.00	86.10	80.70	63.30	49.00	41.40	32.60	14.20	6.20	4.50
28A	100.00	100.00	100.00	98.90	89.60	71.50	57.00	46.30	35.90	15.60	7.00	5.40
28B	100.00	100.00	100.00	90.10	84.40	71.20	55.70	44.20	32.20	16.10	7.40	5.10
29A	100.00	100.00	100.00	100.00	97.90	80.30	59.60	44.90	32.90	15.20	7.20	5.40
29B	100.00	100.00	100.00	100.00	96.90	77.40	59.00	46.40	33.20	16.10	7.10	4.90
31A	100.00	100.00	100.00	93.90	87.80	72.00	56.70	43.90	32.60	16.30	6.90	4.70
31B	100.00	100.00	100.00	98.90	89.60	71.50	57.00	46.30	35.90	15.60	7.00	5.40
32A	100.00	100.00	100.00	100.00	97.90	80.30	59.60	44.90	32.90	15.20	7.20	5.40
32B	100.00	100.00	100.00	100.00	96.70	77.80	58.20	45.10	34.20	191.00	7.40	5.00
37	100.00	100.00	100.00	100.00	92.50	70.10	58.60	50.30	41.10	21.90	8.70	5.90
44	100.00	100.00	100.00	93.70	86.20	73.30	54.80	41.80	30.60	16.10	6.60	4.40

Table A.1 (cont'd)

<i>Sample ID</i>	<i>PG Grade</i>	<i>% Asphalt (Given)</i>	<i>VMA</i>	<i>VFA</i>	<i>Angularity</i>	<i>Gmm</i>	<i>Gmb</i>	<i>Gb</i>	<i>Gse</i>	<i>Gsb</i>	<i>Pbe</i>
45	58-28	5.98	16.22	75.38	42.40	2.454	2.356	1.020	2.695	2.644	5.29
47	64-28	5.29	14.88	73.12	42.60	2.504	2.404	1.029	2.722	2.675	4.66
48	64-28	5.91	16.02	75.03	41.90	2.474	2.375	1.029	2.713	2.661	5.21
49A	70-28	6.18	17.59	77.35	48.90	2.535	2.434	1.025	2.808	2.771	5.72
49B	70-28	6.16	18.19	78.01	46.30	2.489	2.390	1.018	2.750	2.741	6.05
49C	70-28	6.12	17.94	77.70	48.70	2.543	2.441	1.035	2.810	2.793	
51A	58-28	6.24	16.51	75.80		2.474	2.375	1.032	2.727	2.667	5.44
51B	58-28	5.36	14.72	76.22		2.483	2.396	1.024	2.701	2.659	
51C-WMA	58-28	5.60	15.37	77.33		2.468	2.382	1.024	2.693	2.657	
62	58-28	4.89	14.17	78.82	42.90	2.589	2.512	1.032	2.807	2.783	4.59
64	58-34	5.40	15.00	73.30	41.00	2.462	2.364	1.023	2.679	2.629	4.74
65	58-34	6.00	16.10	75.20	43.20	2.468	2.369	1.023	2.712	2.655	5.24
67	64-34	5.10	15.40	74.10	42.10	2.565	2.463	1.026	2.789	2.764	4.75
68	64-34	5.46	15.78	75.65	42.80	2.537	2.436	1.026	2.773	2.734	4.96
80	58-34	5.45	15.20	73.70	41.80	2.511	2.411	1.026	2.740	2.688	4.77
81	58-34	5.66	16.11	75.20	42.80	2.523	2.422	1.026	2.765	2.724	5.13
85	64-34	5.48	15.20	77.00	43.20	2.497	2.410	1.033	2.721	2.686	
86	64-34	6.14	16.00	81.20	42.50	2.471	2.397	1.033	2.718	2.678	
90	70-22	4.98	14.73	76.23	47.00	2.547	2.458	1.023	2.763	2.739	
97	70-22	5.49	15.92	74.88	46.00	2.537	2.436	1.023	2.776	2.738	
102	64-22	5.20	14.96	73.25	46.00	2.550	2.448	1.027	2.776	2.729	4.60
103	64-22	5.60	16.06	75.10	45.00	2.498	2.398	1.027	2.730	2.697	5.17
105	70-22	5.08	15.23	73.74	46.00	2.536	2.434	1.025	2.753	2.726	4.73
106	70-22	5.70	16.02	75.04	46.30	2.489	2.389	1.025	2.724	2.683	5.16
108	64-22	5.21	15.05	73.43	46.00	2.541	2.439	1.027	2.765	2.722	4.65

Table A.1 (cont'd)

<i>Sample ID</i>	<i>1-1/2"</i>	<i>1"</i>	<i>3/4"</i>	<i>1/2"</i>	<i>3/8"</i>	<i>No. 4</i>	<i>No. 8</i>	<i>No. 16</i>	<i>No. 30</i>	<i>No. 50</i>	<i>No. 100</i>	<i>No. 200</i>
45	100.00	100.00	100.00	100.00	96.60	77.40	57.80	45.10	34.40	18.60	8.00	5.40
47	100.00	100.00	100.00	93.50	87.10	76.40	57.20	41.30	29.90	16.60	8.00	5.30
48	100.00	100.00	100.00	100.00	99.70	83.30	6.30	49.80	36.70	20.00	9.20	6.10
49A	100.00	100.00	100.00	94.60	70.00	26.60	20.50	16.60	13.00	10.40	8.90	8.20
49B	100.00	100.00	99.90	92.50	77.10	27.40	19.00	15.30	12.70	10.70	9.30	8.20
49C	100.00	100.00	100.00	96.10	79.70	31.80	22.10	17.80	14.40	11.80	9.70	8.10
51A	100.00	100.00	100.00	94.80	83.20	58.70	44.60	35.90	27.40	14.00	7.10	4.70
51B	100.00	100.00	100.00	91.90	84.80	72.40	57.20	45.40	35.50	19.50	7.90	5.20
51C-WMA	100.00	100.00	100.00	91.20	85.70	71.40	56.70	43.90	30.80	14.80	7.30	4.50
62	100.00	100.00	100.00	86.50	76.10	56.90	45.40	34.40	23.10	14.60	6.10	3.50
64	100.00	100.00	100.00	95.00	86.90	72.50	56.70	43.50	32.20	15.50	6.20	4.50
65	100.00	100.00	100.00	100.00	97.40	75.20	56.70	42.50	31.10	15.50	6.60	4.80
67	100.00	100.00	100.00	95.90	84.30	64.80	56.20	45.00	30.90	20.10	8.20	5.00
68	100.00	100.00	100.00	100.00	95.40	73.60	59.90	47.80	33.90	21.60	8.80	5.20
80	100.00	100.00	100.00	98.20	89.90	69.30	54.00	41.10	30.00	18.60	8.40	5.60
81	100.00	100.00	100.00	100.00	97.40	75.20	56.40	43.60	31.00	16.80	8.60	5.80
85	100.00	100.00	100.00	93.70	84.40	66.40	53.50	42.60	26.90	11.20	7.00	5.40
86	100.00	100.00	100.00	100.00	97.00	80.20	62.20	47.80	33.80	18.20	8.20	5.70
90	100.00	100.00	100.00	98.20	85.60	63.60	44.20	31.00	22.00	14.00	7.50	5.60
97	100.00	100.00	100.00	100.00	99.70	77.70	53.90	37.20	26.20	14.80	9.10	6.20
102	100.00	100.00	100.00	98.50	88.60	65.10	45.00	30.30	21.50	13.50	7.80	5.60
103	100.00	100.00	100.00	100.00	99.90	75.90	54.70	39.10	29.50	18.00	9.80	6.00
105	100.00	100.00	100.00	99.30	88.30	63.00	42.20	28.10	19.40	12.90	7.70	5.50
106	100.00	100.00	100.00	100.00	99.50	76.20	47.70	32.70	23.20	14.70	7.90	5.40
108	100.00	100.00	100.00	98.70	87.30	65.10	46.50	32.30	23.30	14.90	8.10	5.70

Table A.1 (cont'd)

<i>Sample ID</i>	<i>PG Grade</i>	<i>% Asphalt (Given)</i>	<i>VMA</i>	<i>VFA</i>	<i>Angularity</i>	<i>Gmm</i>	<i>Gmb</i>	<i>Gb</i>	<i>Gse</i>	<i>Gsb</i>	<i>Pbe</i>
109	64-22	5.50	16.08	75.12	45.00	2.493	2.393	1.027	2.719	2.695	5.18
111	70-22	5.31	15.09	73.50	46.00	2.544	2.443	1.025	2.775	2.724	4.66
112	70-22	5.80	16.39	75.59	45.00	2.489	2.389	1.025	2.729	2.692	5.31
127	58-22	5.43	15.23	73.74		2.522	2.421	1.022	2.754	2.701	4.74
200	58-28	5.20	13.70	78.22	43.20	2.513	2.438	1.024	2.731	2.678	4.50
201	64-28	3.30			3.30	2.734		1.026	2.835	2.775	2.54
202	64-22	6.03	16.19	75.36	45.60	2.482	2.383	1.031	2.728	2.672	5.29
203	70-22	4.99	14.85	73.07	47.00	2.510	2.410	1.025	2.717	2.689	4.62
204	70-22	5.80	15.77	74.63	47.00	2.524	2.423	1.025	2.774	2.710	4.98
205	58-28	4.90	13.23	77.32	42.10	2.502	2.427	1.020	2.704	2.660	4.31
206	64-22	5.40	16.08	75.13	45.00	2.503	2.403	1.027	2.727	2.709	5.16
207	64-22	6.21	16.04	75.06	43.70	2.503	2.403	1.025	2.767	2.684	5.14
208WMA	64-22	5.60	14.75	76.27		2.461	2.375	1.034	2.680	2.630	
209A-HMA	64-22	6.21	15.89	77.97	45.00	2.476	2.389	1.209	2.730	2.664	
209B-WMA	64-22	6.21	15.89	77.97	45.00	2.476	2.389	1.209	2.730	2.664	

Table A.1 (cont'd)

<i>Sample ID</i>	<i>1-1/2"</i>	<i>1"</i>	<i>3/4"</i>	<i>1/2"</i>	<i>3/8"</i>	<i>No. 4</i>	<i>No. 8</i>	<i>No. 16</i>	<i>No. 30</i>	<i>No. 50</i>	<i>No. 100</i>	<i>No. 200</i>
109	100.00	100.00	100.00	100.00	99.60	75.60	51.40	36.50	27.40	17.60	9.60	6.40
111	100.00	100.00	100.00	98.90	87.60	66.50	47.30	33.90	24.40	15.80	8.20	5.70
112	100.00	100.00	100.00	100.00	99.90	75.80	54.90	39.20	29.10	18.20	8.40	6.10
127	100.00	100.00	100.00	92.50	86.80	79.20	58.50	43.20	32.60	20.90	10.30	5.60
200	100.00	100.00	99.90	88.90	82.60	65.00	48.40	34.10	22.50	12.00	7.30	5.10
201	100.00	100.00	96.00	59.50	30.20	14.70	11.50	9.10	7.20	6.00	4.60	3.60
202	100.00	100.00	100.00	100.00	99.70	84.10	66.70	46.80	31.50	16.60	8.70	6.00
203	100.00	100.00	100.00	96.40	87.10	52.30	33.60	22.40	15.90	10.90	7.10	5.50
204	100.00	100.00	100.00	100.00	99.70	76.40	53.20	36.60	24.30	13.70	8.70	6.10
205	100.00	100.00	90.00	73.50	69.70	57.40	44.50	35.30	25.50	12.60	5.90	4.40
206	100.00	100.00	100.00	100.00	99.70	78.00	53.90	38.60	29.10	18.00	9.60	6.40
207	100.00	100.00	100.00	99.60	97.80	85.50	63.50	46.40	33.30	20.30	9.70	5.30
208WMA	100.00	100.00	100.00	94.20	86.10	65.20	48.70	39.40	32.40	15.60	6.40	4.50
209A-HMA	100.00	100.00	100.00	100.00	97.80	77.60	52.70	37.40	25.90	14.20	7.30	4.90
209B-WMA	100.00	100.00	100.00	100.00	97.80	77.60	52.70	37.40	25.90	14.20	7.30	4.90

APPENDIX B: A LIST OF ASPHALT MIXTURE SAMPLES TESTED IN THIS STUDY ALONG WITH THE CORRESPONDING AIR VOID LEVEL OF EACH SAMPLE

Table B.1: List of HMAs tested and their air voids.

Unique HMA#	Sample#	HMA ID	Sample ID	AV%	Core Avg. AV%	STDEV AV	COV (%)	Compaction method
1	1	18-S1	18-1	5.7	5.7	0.3	5.9	Slab-Shearbox
	2		18-2	6.1				
	3		18-3	5.4				
	4	18-S2	18-4	7.9	7.37	0.005	6.4	Gyratory
	5		18-5	7.1				
	6		18-6	7.1				
2	7	28(B)-S1	28-1	6.6	6.7	0.2	2.7	Slab-Shearbox
	8		28-2	6.9				
	9		28-3	6.5				
3	10	29(A)-S1	29-1	8.9	9.1	0.4	4	Slab-Shearbox
	11		29-3	9.4				
	12	29(A)-S2	29-1	7.5	7.57	0.001	1.3	Gyratory
	13		29-2	7.6				
	14		29-3	7.6				
4	15	44-S1	44-1	8.0	8.3	0.4	4.3	Slab-Shearbox
	16		44-2	8.2				
	17		44-3	8.7				
	18	44-S2	44-4	7.0	7.0	0	0.6	Slab-Shearbox
	19		44-5	7.0				
	20		44-6	6.9				
5	21	49A-S1	49A-1	4.2	4.4	0.3	7.5	Slab-Shearbox
	22		49A-2	4.6				
	23	49A-S2	49A-1	6.4	7.03	0.7	9.8	Gyratory
	24		49A-2	6.9				
	25		49A-3	7.8				
6	26	203-S1	203-1	3.8	4.1	0.3	8	Slab-Shearbox
	27		203-2	4.4				
	28		203-3	4.2				
	29	203-GYRO	203-GYRO	4.7	4.7	-	-	Gyratory
	30	203-S2	203-4	6.5	6.4	0.2	2.9	Slab-Shearbox
	31		203-5	6.2				
	32		203-6	6.6				

Table B.1 (cont'd)

Unique HMA#	Sample#	HMA ID	Sample ID	AV%	Core Avg. AV%	STDEV AV	COV (%)	Compaction method
7	33	204-S1	204-1	6.4	6.3	0.1	1.9	Slab-Shearbox
	34		204-2	6.2				
	35		204-3	6.2				
	36	204-S2	204-1	6.9	6.86	0.07	1	Gyratory
	37		204-2	6.8				
8	38	205-S1	205-1	9.0	8.8	0.2	2.7	Slab-Shearbox
	39		205-2	8.8				
	40		205-3	8.6				
	41	205-GYRO	205-GYRO	8.9	8.9	-	-	Gyratory
	42	205	205-1	7.0	6.74	0.27	4	Gyratory
	43		205-2	6.7				
	44		205-3	6.5				
9	45	24A	24A-1	6.7	6.9	0.2	2.8	Gyratory
	46		24A-2	7.1				
	47		24A-3	6.7				
	48		24A-4	7.0				
10	49	32B	32-1	8.2	7.1	0.7	10.2	Gyratory
	50		32B-2	7.2				
	51		32B-3	6.6				
	52		32B-4	6.6				
11	53	37	37-1	7.3	7.3	0.29	3.9	Gyratory
	54		37-2	7.6				
	55		37-3	7.0				
12	56	67	67-1	6.7	7.2	0.5	6.9	Gyratory
	57		67-2	7.7				
	58		67-3	7.2				
13	59	81	81-1	8.3	8.0	0.4	5.2	Gyratory
	60		81-2	7.6				
	61		81-3	8.2				
14	62	51A	51A-1	7.7	7.3	0.4	5.6	Gyratory
	63		51A-2	6.9				
	64		51A-3	7.2				

Table B.1 (cont'd)

Unique HMA#	Sample#	HMA ID	Sample ID	AV%	Core Avg. AV%	STDEV AV	COV (%)	Compaction method
15	65	64	64-1	6.1	7	0.8	11.4	Gyratory
	66		64-2	7.7				
	67		64-3	7.2				
16	68	102	102-1	7.2	7.8	0.6	7.6	Gyratory
	69		102-2	7.9				
	70		102-3	8.4				
17	71	103	103-1	7.0	7.2	0.2	3.1	Gyratory
	72		103-2	7.3				
	73		103-3	7.4				
18	74	109	109-1	7.8	7.6	0.2	2.2	Gyratory
	75		109-2	7.5				
	76		109-3	7.6				
19	77	105	105-1	6.4	6.8	0.4	6.2	Gyratory
	78		105-2	7.1				
	79		105-3	7.1				
20	80	111	111-1	7.5	7.2	0.8	10.6	Gyratory
	81		111-2	7.7				
	82		111-3	6.3				
21	83	48	48-1	7.3	7.2	0.2	2.3	Gyratory
	84		48-2	7.3				
	85		48-3	7.0				
22	86	31B	31B-1	7.2	7.5	0.3	3.5	Gyratory
	87		31B-2	7.5				
	88		31B-3	7.7				
23	89	45	45-1	7.2	7.2	0.1	0.8	Gyratory
	90		45-2	7.2				
	91		45-3	7.1				
24	92	21	21-1	7.4	7.4	0.16	2.2	Gyratory
	93		21-2	7.2				
	94		21-3	7.6				

Table B.1 (cont'd)

Unique HMA#	Sample#	HMA ID	Sample ID	AV%	Core Avg. AV%	STDEV AV	COV (%)	Compaction method
25	95	62	62-1	6.4	6.7	0.3	3.8	Gyratory
	96		62-2	6.7				
	97		62-3	6.9				
26	98	112	112-1	7.6	7.5	0.2	2.2	Gyratory
	99		112-2	7.3				
	100		112-3	7.4				
27	101	206	206-1	7.4	7.7	0.3	3.6	Gyratory
	102		206-2	8.0				
	103		206-3	7.8				
28	104	108	108-1	7.4	7.5	0.1	1.4	Gyratory
	105		108-2	7.6				
	106		108-3	7.5				
29	107	68	68-1	7.3	7.6	0.4	4.8	Gyratory
	108		68-2	8.0				
	109		68-3	7.3				
30	110	207	207-1	7.6	7.6	0.1	1.7	Gyratory
	111		207-2	7.5				
	112		207-3	7.7				
31	113	47	47-1	6.2	6.83	0.68	10	Gyratory
	114		47-2	6.8				
	115		47-3	7.5				
32	116	127	127-1	7.5	7.5	0.05	0.6	Gyratory
	117		127-2	7.5				
	118		127-3	7.6				
33	119	106	106-1	6.8	7.52	0.64	8.5	Gyratory
	120		106-2	7.9				
	121		106-3	7.9				
34	122	4	4--1	6.8	6.95	0.19	2.7	Gyratory
	123		4--2	7.0				
	124		4--3	7.1				

Table B.1 (cont'd)

Unique HMA#	Sample#	HMA ID	Sample ID	AV%	Core Avg. AV%	STDEV AV	COV (%)	Compaction method
35	125	20A	20A-1	7.6	7.33	0.35	4.8	Gyratory
	126		20A-2	7.5				
	127		20A-3	6.9				
36	128	2	2-1	7.7	7.38	0.26	3.5	Gyratory
	129		2-2	7.3				
	130		2-3	7.2				
37	131	20B	20B-1	6.2	6.4	0.28	4.4	Gyratory
	132		20B-2	6.7				
	133		20B-3	6.4				
38	134	23	23-1	7.2	7.01	0.2	2.8	Gyratory
	135		23-2	6.9				
	136		23-3	7.0				
39	137	24B	24B-1	6.8	6.84	0.2	3.1	Gyratory
	138		24B-2	6.7				
	139		24B-3	7.1				
40	140	26A	26A-1	6.8	7.06	0.3	3.8	Gyratory
	141		26A-2	7.0				
	142		26A-3	7.3				
41	143	26B	26B-1	6.4	7.04	0.9	12.3	Gyratory
	144		26B-2	7.7				
42	145	26C	26C-1	7.6	7.53	0.4	5	Gyratory
	146		26C-2	7.1				
	147		26C-3	7.9				
43	148	31A	31A-1	7.2	7.49	0.3	3.5	Gyratory
	149		31A-2	7.6				
	150		31A-3	7.7				
44	151	32A	32A-1	7.4	6.92	0.4	6	Gyratory
	152		32A-2	6.7				
	153		32A-3	6.7				
45	154	51B	51B-1	7.1	7.44	0.28	3.8	Gyratory
	155		51B-2	7.7				
	156		51B-3	7.5				

Table B.1 (cont'd)

Unique HMA#	Sample#	HMA ID	Sample ID	AV%	Core Avg. AV%	STDEV AV	COV (%)	Compaction method
46	157	65	65-1	6.8	7.2	0.46	6.4	Gyratory
	158		65-2	7.7				
	159		65-3	7.1				
47	160	80	80-1	7.4	7.15	0.28	4	Gyratory
	161		80-2	6.8				
	162		80-3	7.2				
48	163	97	97-1	7.0	6.82	0.12	1.8	Gyratory
	164		97-2	6.8				
	165		97-3	6.7				
49	166	200	200-1	8.0	7.25	0.63	8.7	Gyratory
	167		200-2	6.8				
	168		200-3	7.0				
50	169	201	201-1	11.4	11.4	0.12	1.1	Gyratory
	170		201-2	11.5				
	171		201-3	11.2				
51	172	202	202-1	7.4	7.57	0.3	4	Gyratory
	173		202-2	7.4				
	174		202-3	7.9				
52	175	WMA	WMA-1	6.8	7.27	0.45	6.2	Gyratory
	176		WMA-2	7.3				
	177		WMA-3	7.7				
53	178	90	90-1	7.48	7.25	0.66	9.1	Gyratory
	179		90-2	6.50				
	180		90-3	7.77				
54	181	208	208-1	7.29	6.86	0.003	5.5	Gyratory
	182		208-2	6.70				
	183		208-3	6.59				
55	184	49C	49C-1	7.23	6.97	0.003	4.9	Gyratory
	185		49C-2	6.58				
	186		49C-3	7.11				

Table B.1 (contd')

Unique HMA#	Sample#	HMA ID	Sample ID	AV%	Core Avg. AV%	STDEV AV	COV (%)	Compaction method
56	187	85	85-1	7.53	7.47	0.0006	0.9	Gyratory
	188		85-2	7.41				
	189		85-3	7.46				
57	190	86	86-1	7.73	6.70	0.009	13.3	Gyratory
	191		86-2	6.22				
	192		86-3	6.15				
58	193	51C	51C-1	7.36	7.21	0.0024	3.4	Gyratory
	194		51C-2	7.33				
	195		51C-3	6.93				
59	196	2B	2B-1	7.33	7.25	0.0007	1.04	Gyratory
	197		2B-2	7.24				
	198		2B-3	7.18				
60	199	209A	209A-1	6.88	7.07	0.17	2.4	Gyratory
	200		209A-2	7.21				
	201		209A-3	7.11				
61	202	209B	209B-1	7.19	7.153	0.119	1.7	Gyratory
	203		209B-2	7.25				
	204		209B-3	7.02				
62	205	49B	49B-1	6.15	6.35	0.24	4.0	Gyratory
	206		49B-2	6.61				
	207		49B-3	6.28				
63	208	29B	29B-1	8.86	9.12	0.4	4.0	Gyratory
	209		29B-2	9.38				
64	211	20C	20C-1	7.42	7.53	0.1	1.0	Gyratory
	212		20C-2	7.57				
	213		20C-3	7.61				

APPENDIX C: $|E^|$ MASTER CURVES OF THE TESTED ASPHALT MIXTURES
GROUPED BASED ON THE MDOT MIX DESIGNATION*

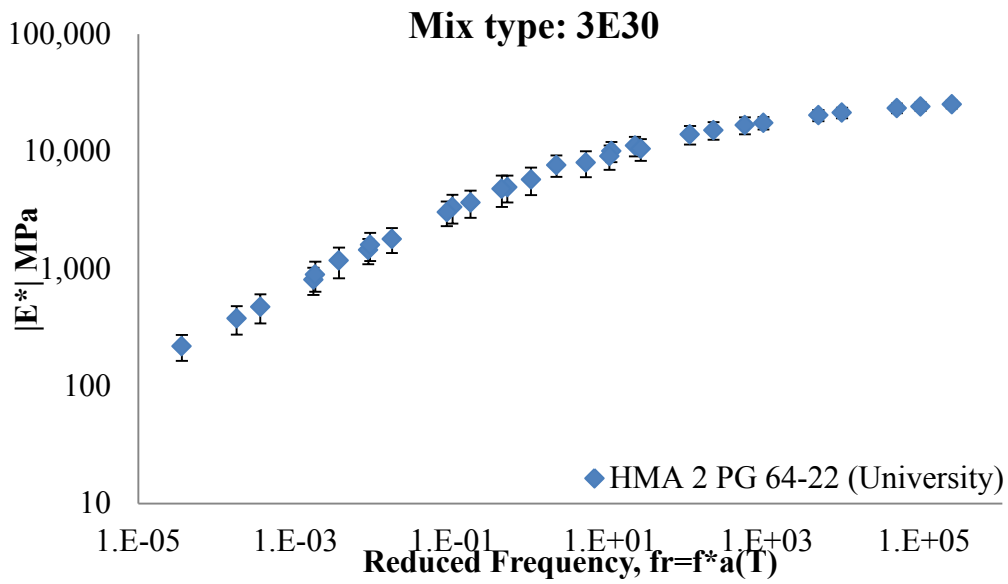


Figure C.1: Dynamic modulus $|E^*|$ master curves for 3E30 mixes.

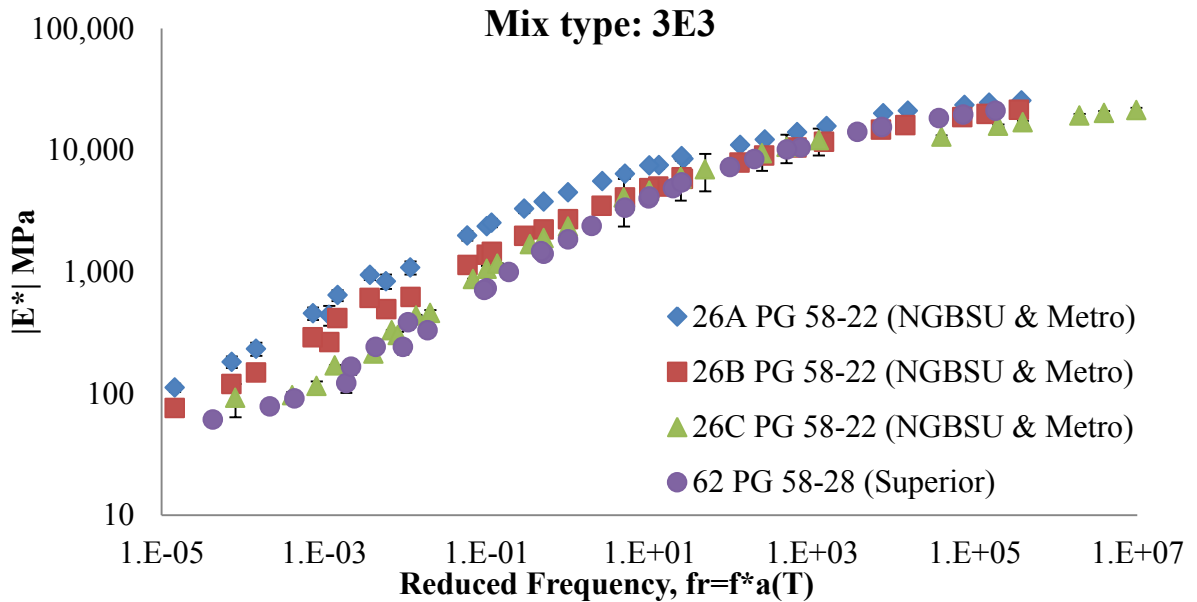
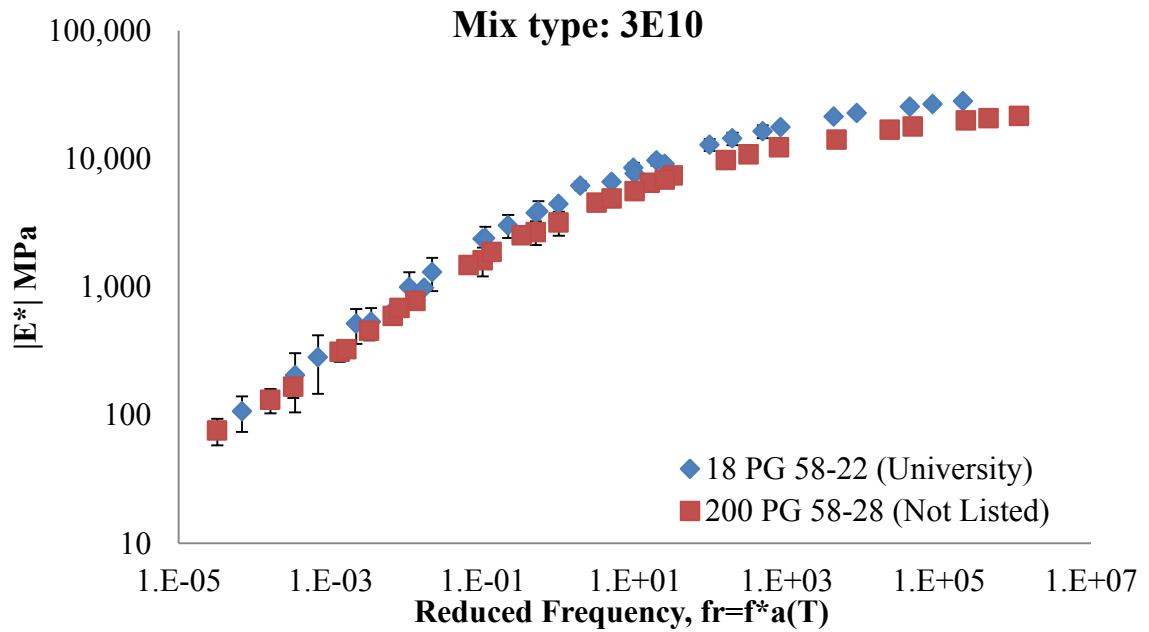
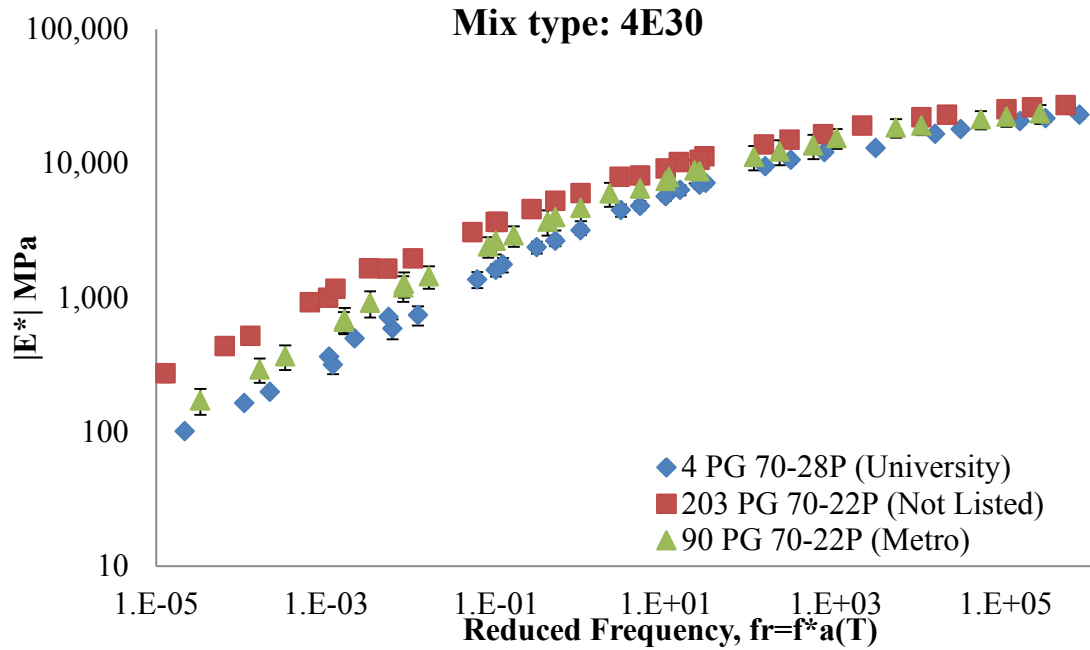


Figure C.2: Dynamic modulus $|E^*|$ master curves for 3E3 mixes.



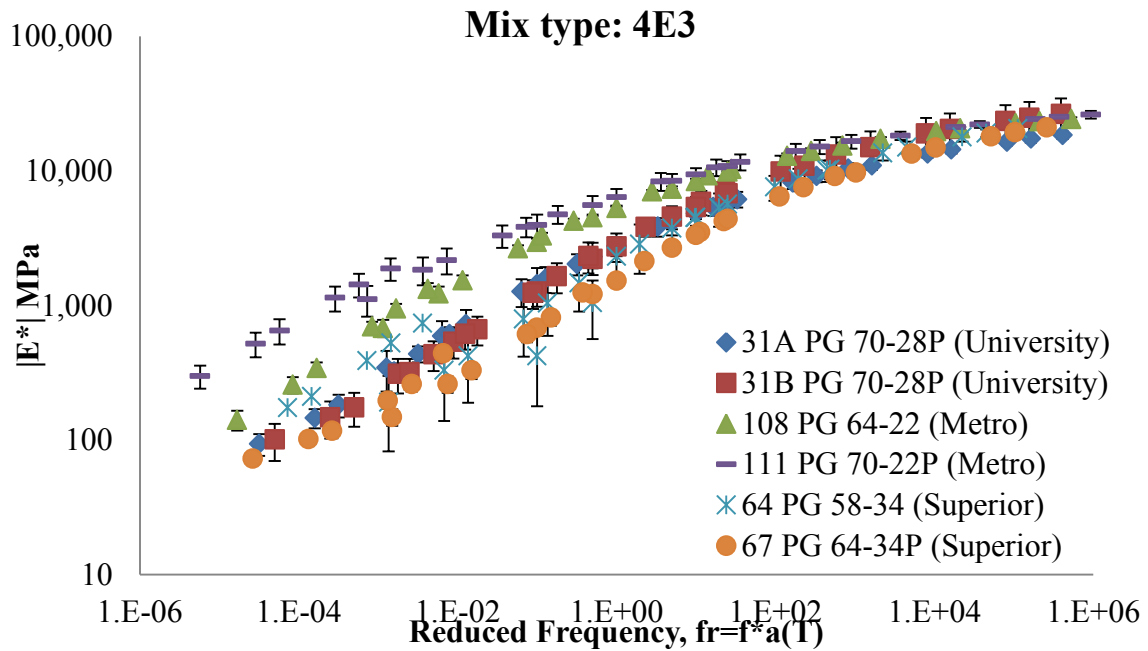


Figure C.5: Dynamic modulus $|E^*|$ master curves for 4E3 mixes.

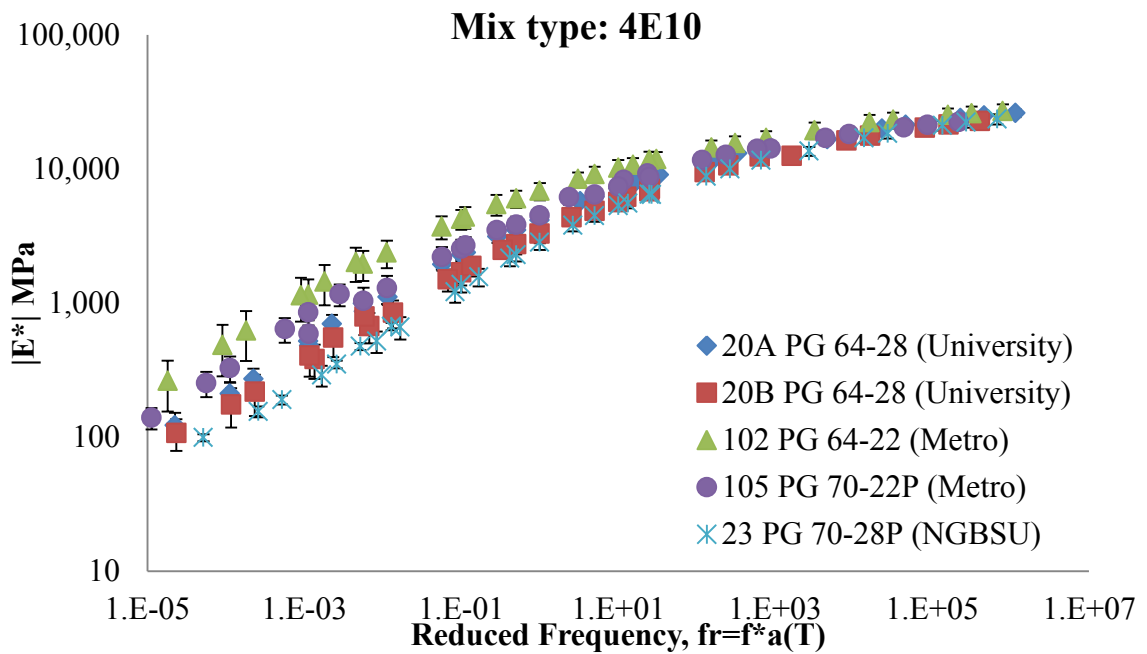


Figure C.6: Dynamic modulus $|E^*|$ master curves for 4E10 mixes.

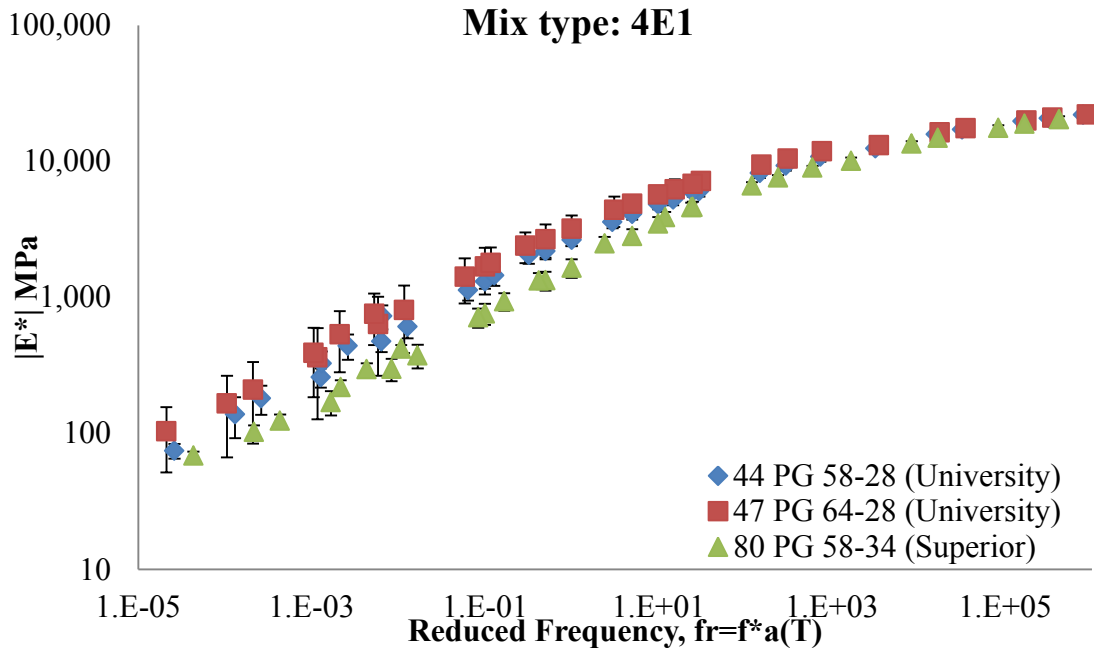


Figure C.7: Dynamic modulus $|E^*|$ master curves for 4E1 mixes.

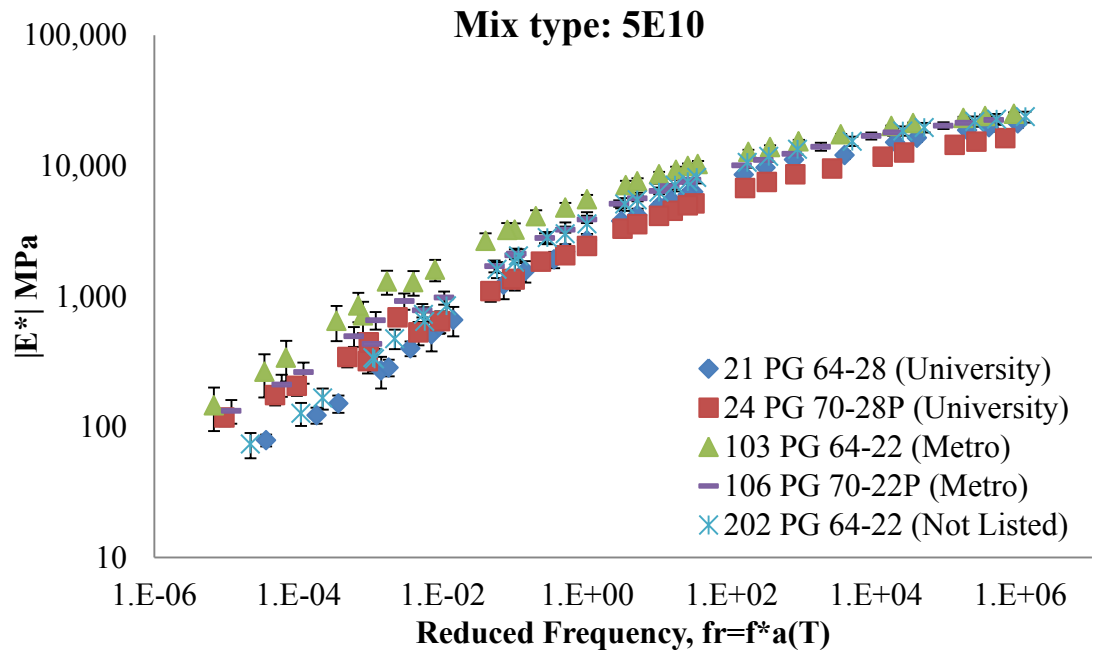


Figure C.8: Dynamic modulus $|E^*|$ master curves for 5E10 mixes.

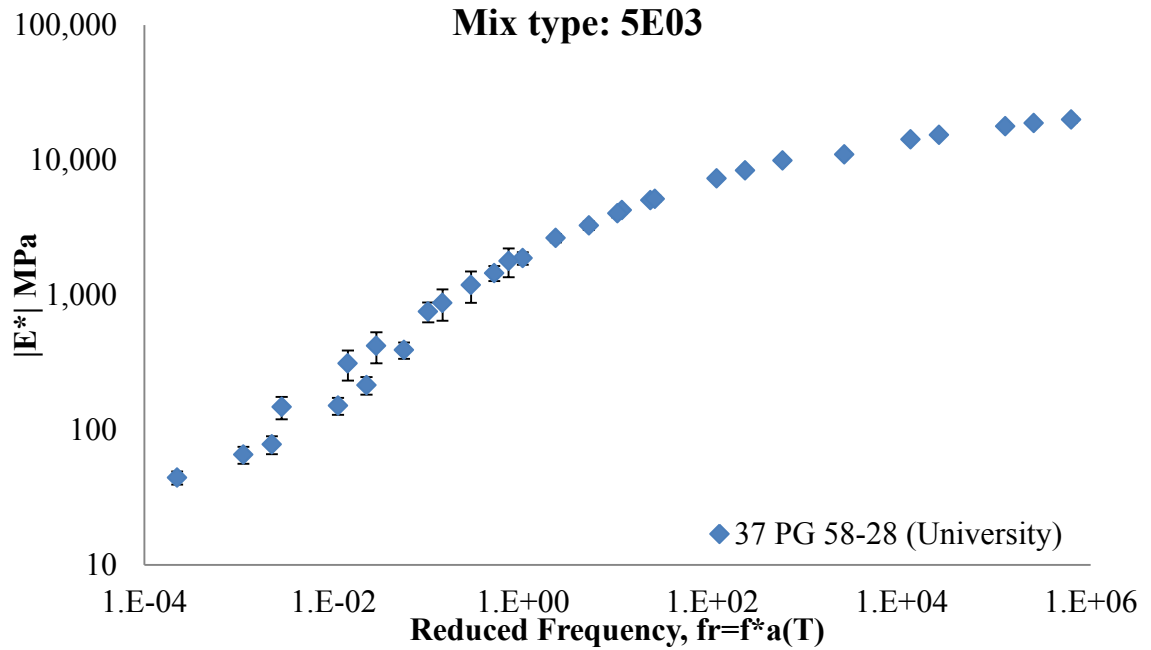


Figure C.9: Dynamic modulus $|E^*|$ master curves for 5E03 mixes.

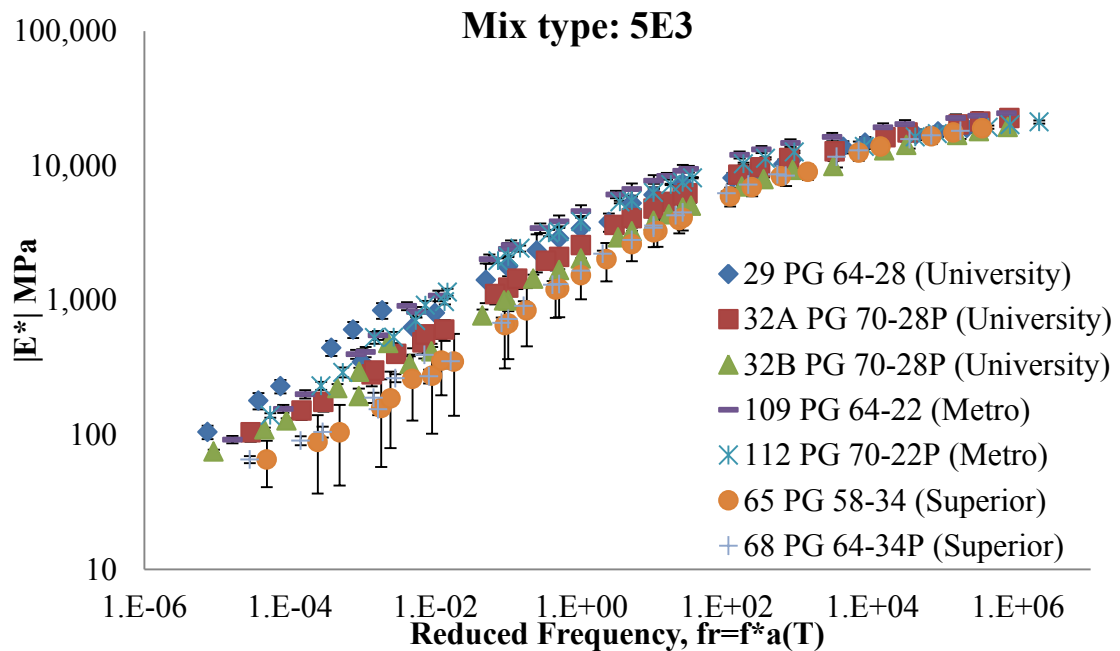


Figure C.10: Dynamic modulus $|E^*|$ master curves for 5E3 mixes.

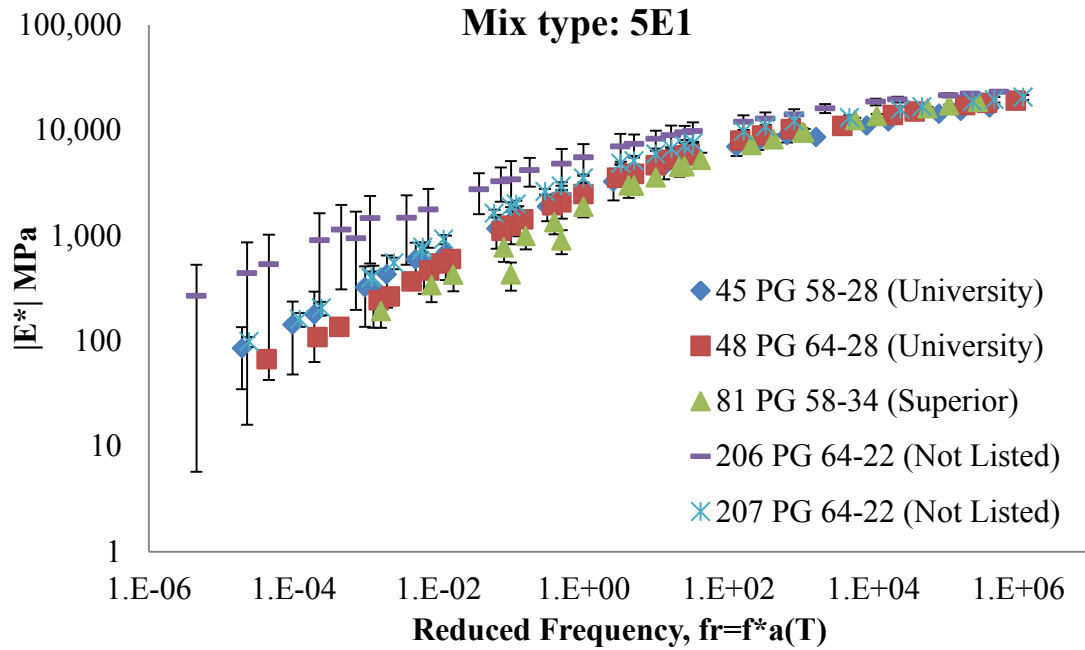


Figure C.11: Dynamic modulus $|E^*|$ master curves for 5E1 mixes.

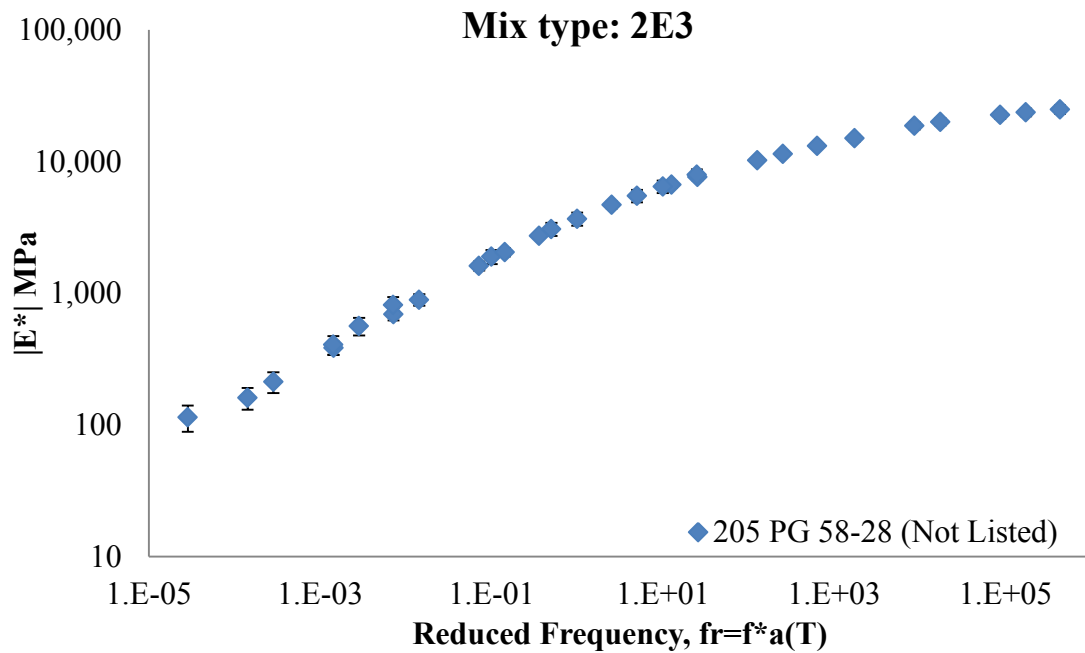


Figure C.12: Dynamic modulus $|E^*|$ master curves for 2E3 mixes.

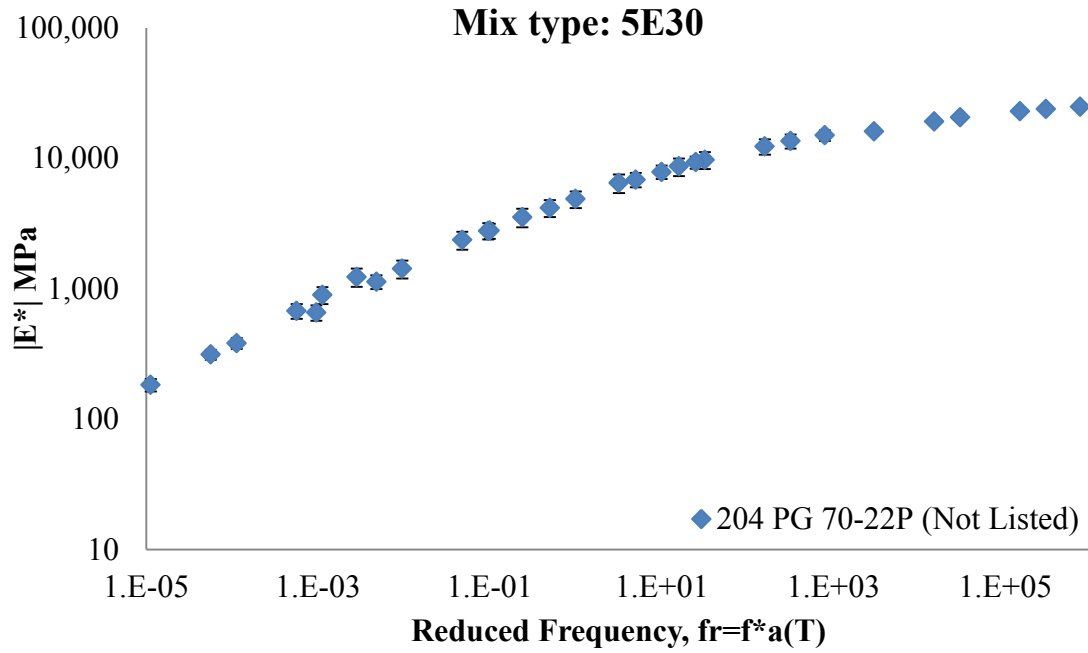


Figure C.13: Dynamic modulus $|E^*|$ master curves for 5E30 mixes.

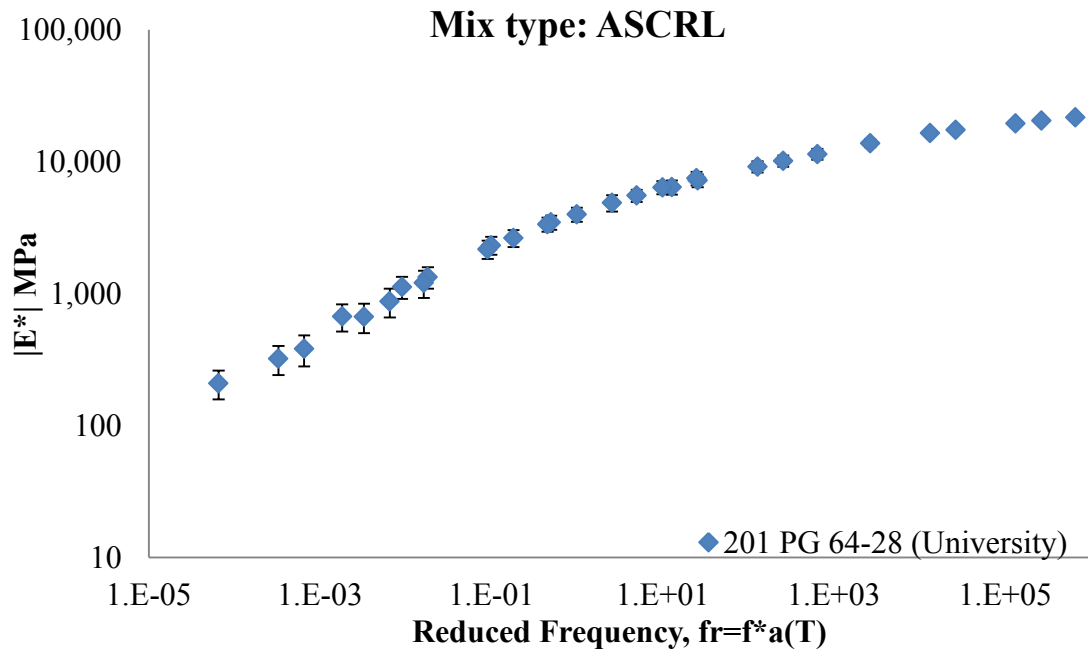


Figure C.14: Dynamic modulus $|E^*|$ master curves for ASCRL mixes.

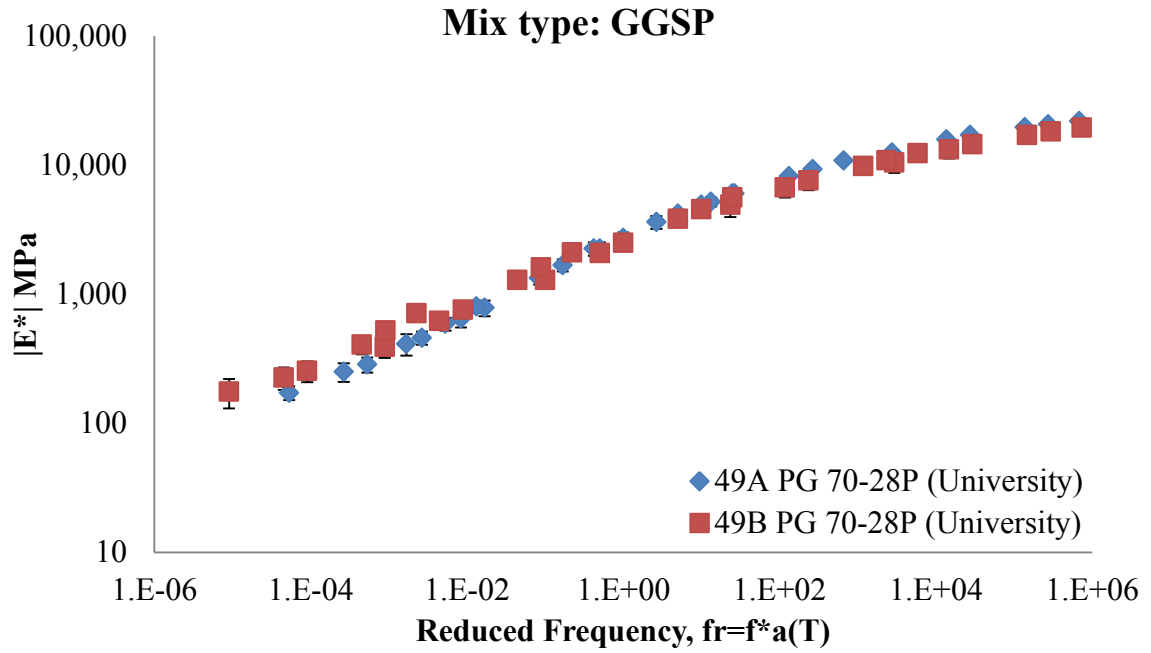


Figure C.15: Dynamic modulus $|E^*|$ master curves for GGSP mixes.

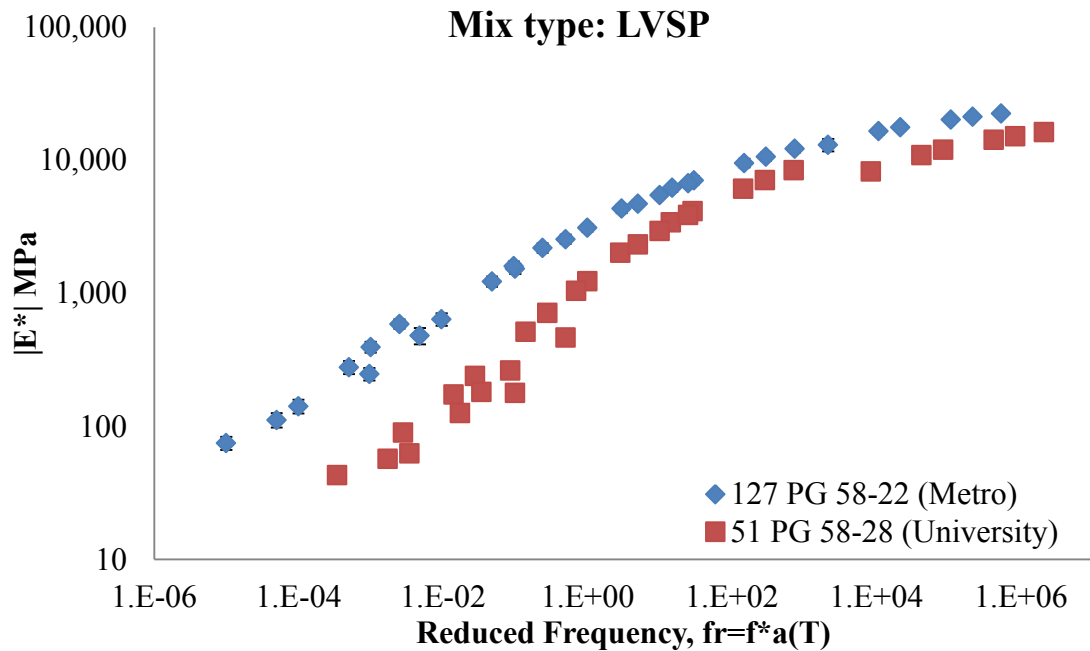


Figure C.16: Dynamic modulus $|E^*|$ master curves for LVSP mixes.

APPENDIX D: $|G^|$ MASTER CURVES GROUPED BASED ON THE PG
GRADE*

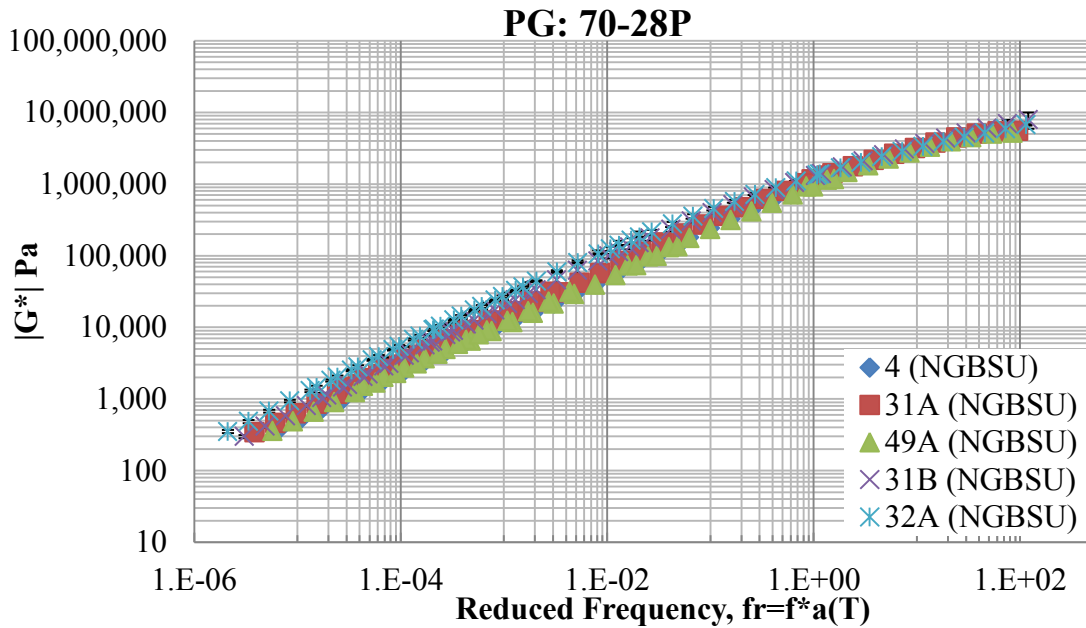


Figure D.1: $|G^*|$ master curves of different PG70-28P binders. NGBSU = North, Grand, Bay, Southwest and University Regions.

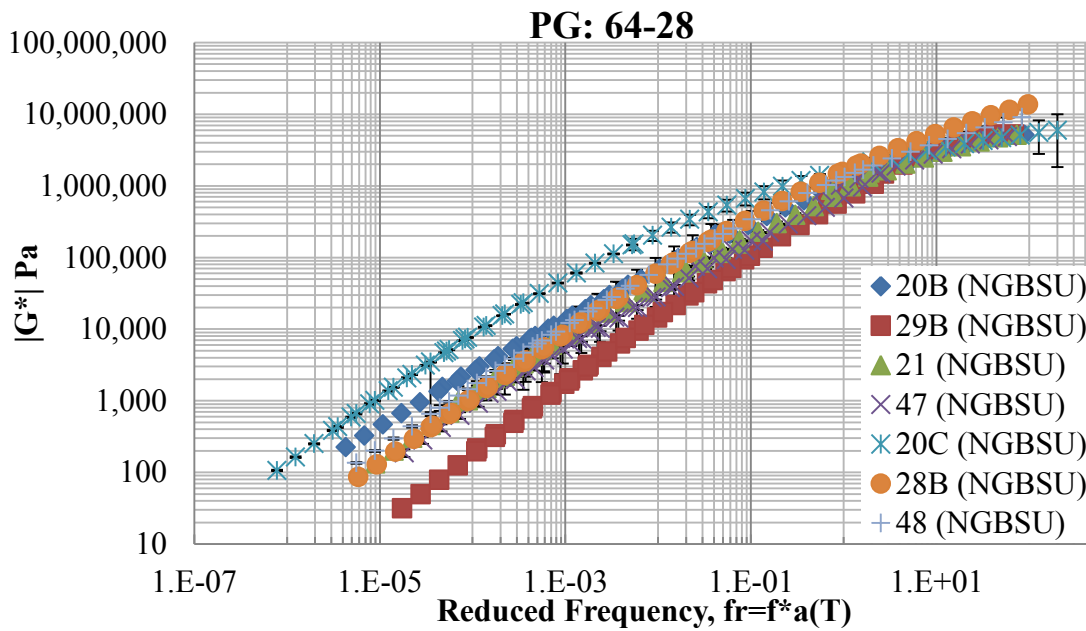


Figure D.2: $|G^*|$ master curves of different PG64-28 binders. NGBSU = North, Grand, Bay, Southwest and University Regions.

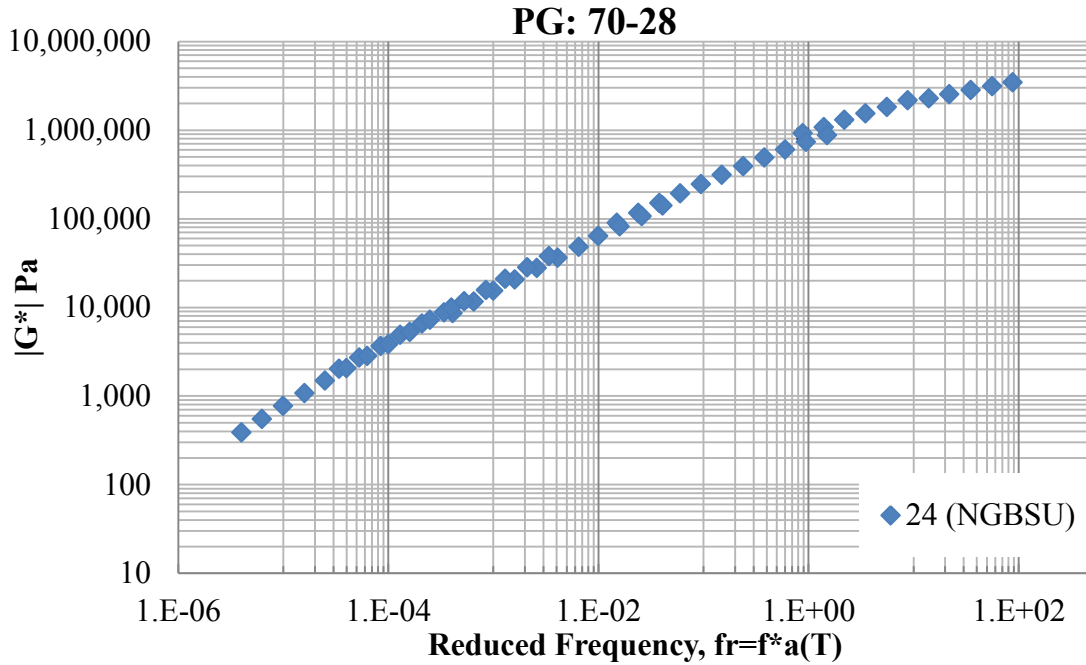


Figure D.3: $|G^*|$ master curve of a PG70-28 binder. NGBSU = North, Grand, Bay, Southwest and University Regions.

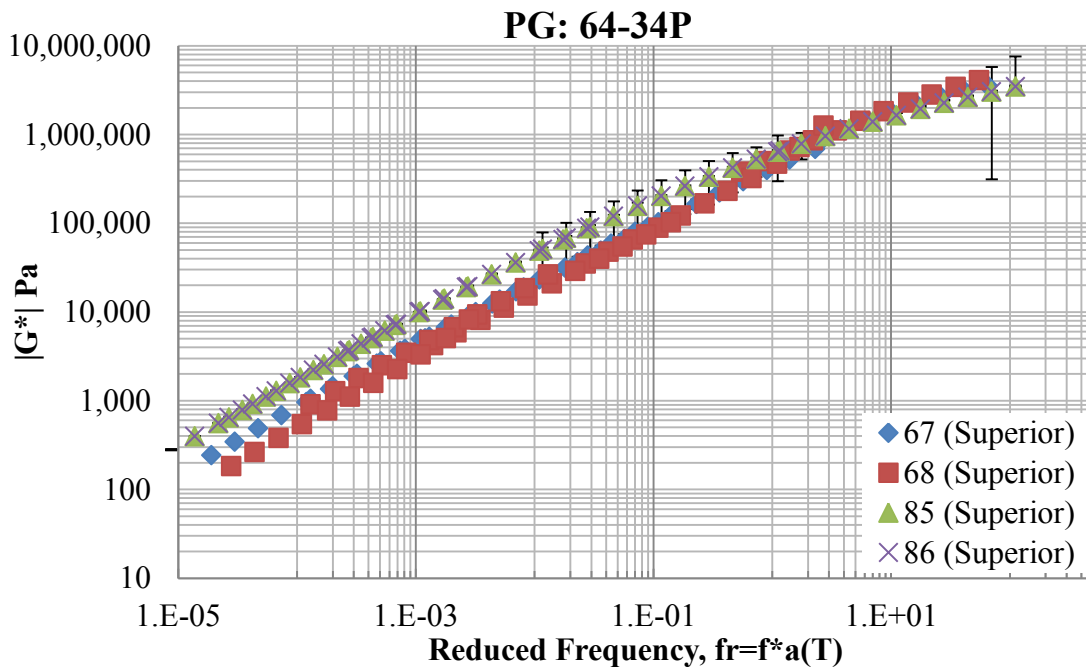


Figure D.4: $|G^*|$ master curves of different PG64-34P binders. NGBSU = North, Grand, Bay, Southwest and University Regions.

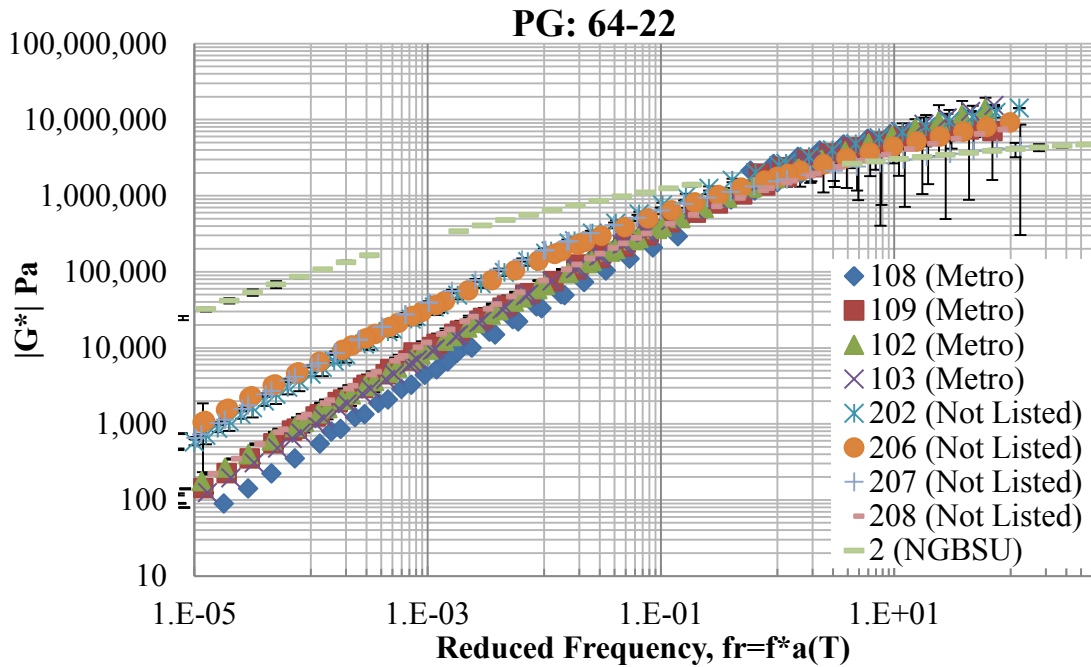


Figure D.5: $|G^*|$ master curves of different PG64-22 binders. NGBSU = North, Grand, Bay, Southwest and University Regions.

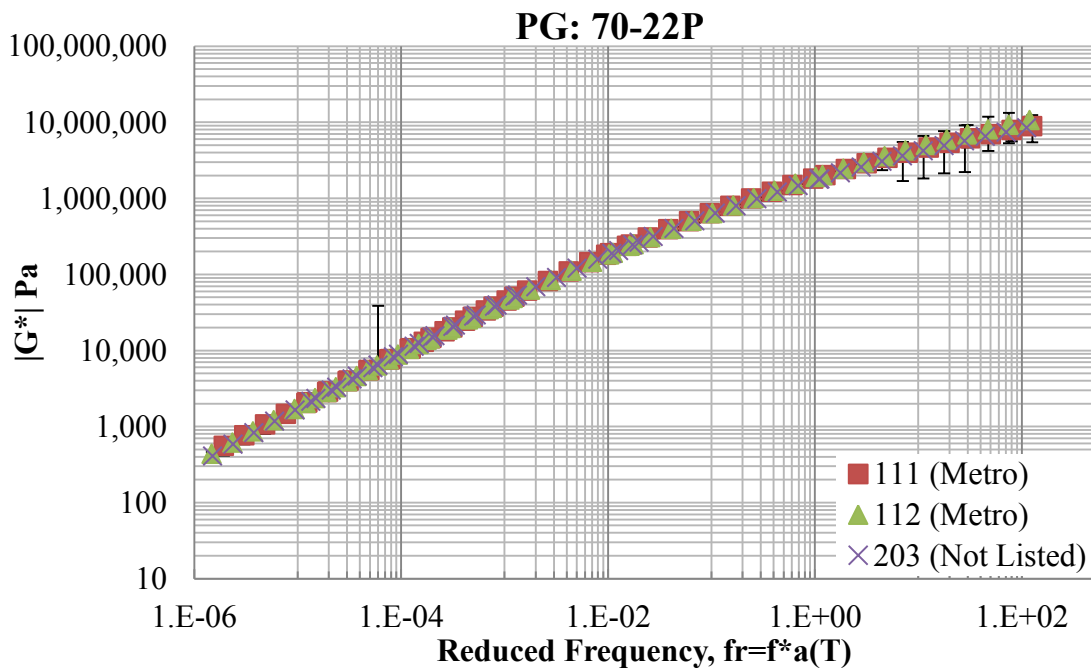


Figure D.6: $|G^*|$ master curves of different PG70-22P binders.

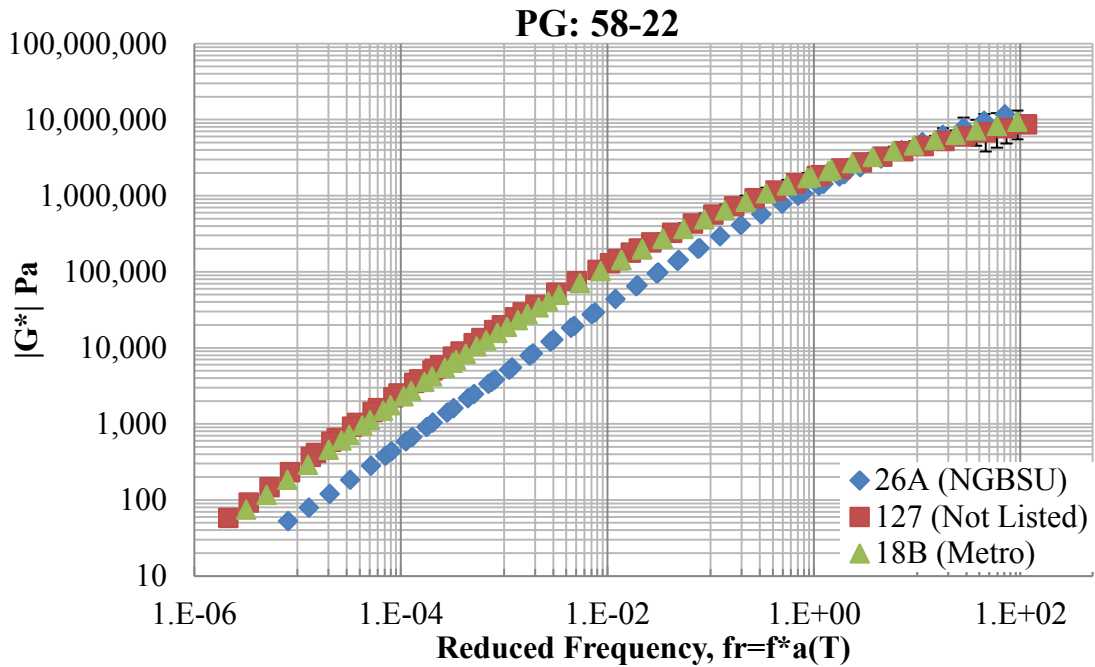


Figure D.7: $|G^*|$ master curves of different PG58-22 binders. NGBSU = North, Grand, Bay, Southwest and University Regions.

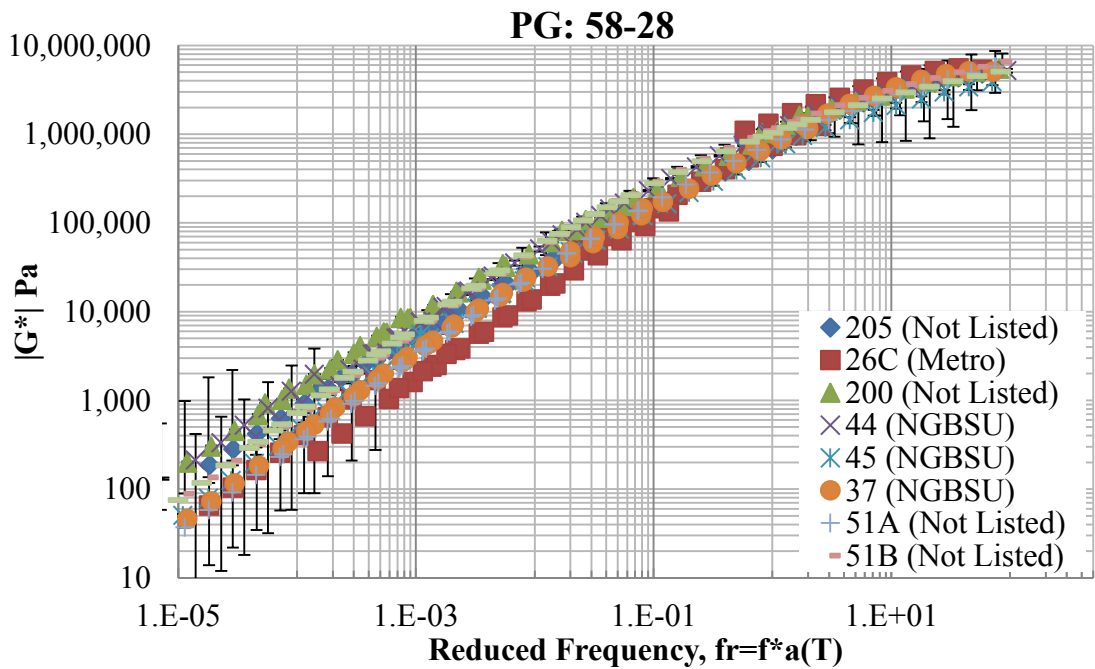


Figure D.8: $|G^*|$ master curves of different PG58-28 binders. NGBSU = North, Grand, Bay, Southwest and University Regions.

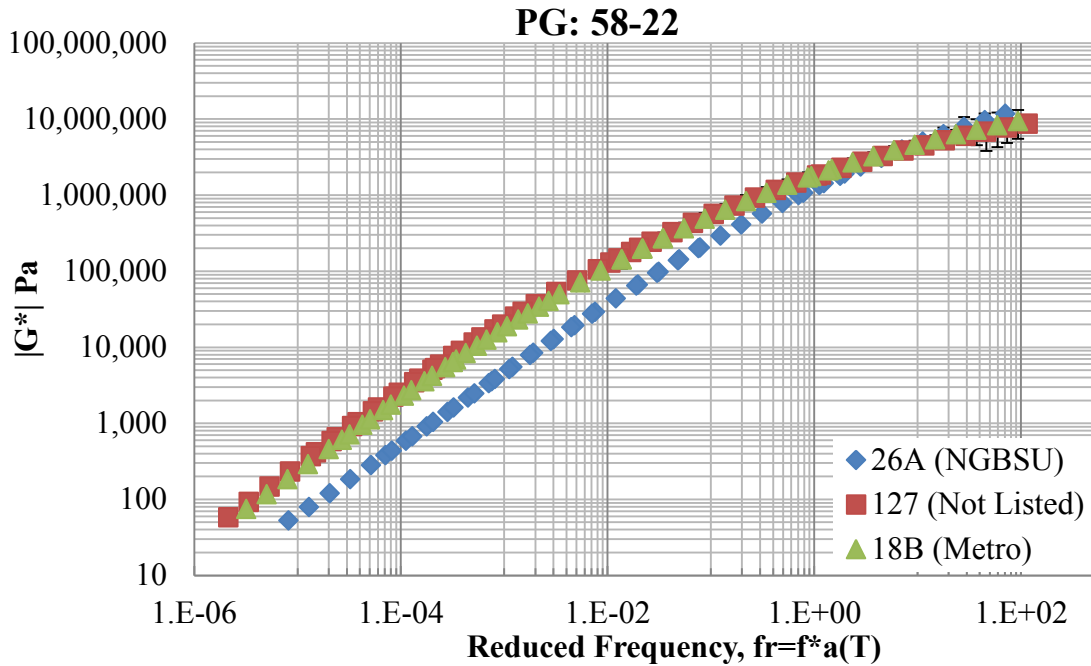


Figure D.9: $|G^*|$ master curves of different PG58-22 binders. NGBSU = North, Grand, Bay, Southwest and University Regions.

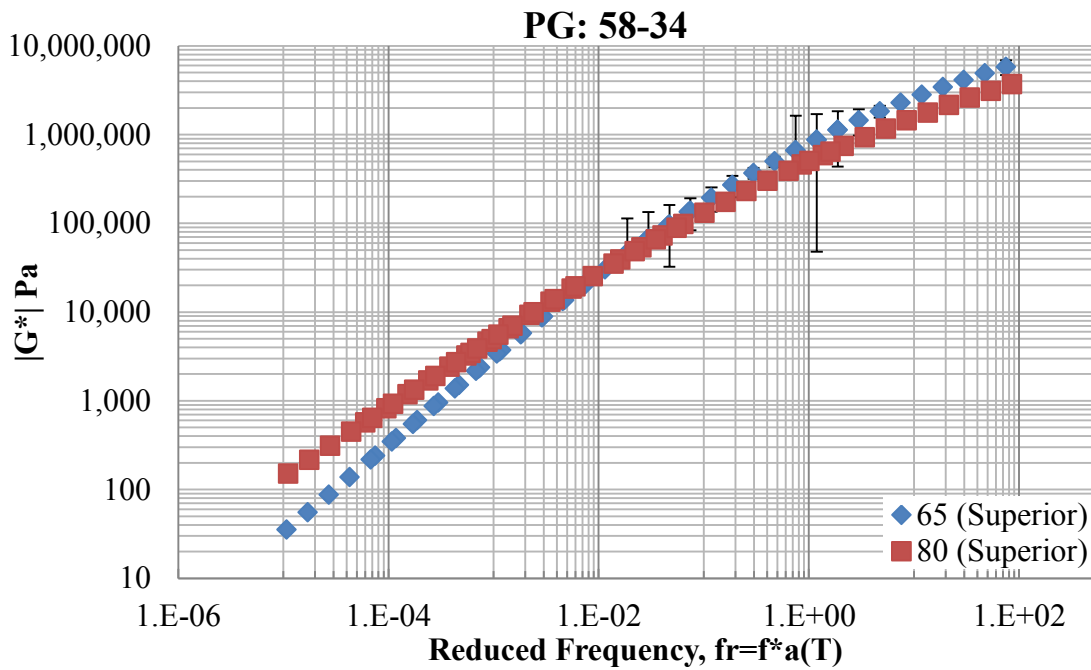


Figure D.10: $|G^*|$ master curves of different PG58-34 binders.

REFERENCES

REFERENCES

- AASHTO PP 60-09 Preparation of Cylindrical Performance Test Specimens Using the Superpave Gyratory Compactor (SGC), in AASHTO PP 60-09. 2011, American Association of State Highway and Transportation Officials, Washington, D.C.
- AASHTO PP 61-10 Developing Dynamic Modulus Master Curves for Hot Mix Asphalt (HMA) Using the Asphalt Mixture Performance Tester (AMPT), in AASHTO PP 61-10. 2011, American Association of State Highway and Transportation Officials, Washington, D.C.
- AASHTO PP 62-10 Developing Dynamic Modulus Master Curves for Hot Mix Asphalt (HMA), in AASHTO PP 62-10. 2011, American Association of State Highway and Transportation Officials, Washington, D.C.
- AASHTO T 166-11 Bulk Specific Gravity of Compacted Hot Mix Asphalt (HMA) Using Saturated Surface-Dry Specimens, in AASHTO T 166-11. 2011, American Association of State Highway and Transportation Officials, Washington, D.C.
- AASHTO 240-09 Effect of Heat and Air on a Moving Film of Asphalt Binder (Rolling Thin-Film Oven Test), in AASHTO T 240-09. 2011, American Association of State Highway and Transportation Officials, Washington, D.C.
- AASHTO T 240-09 Effect of Heat and Air on a Moving Film of Asphalt Binder (Rolling Thin-Film Oven Test), in AASHTO T 240-09. 2011, American Association of State Highway and Transportation Officials, Washington, D.C.
- AASHTO T 313-10 Determining the Flexural Creep Stiffness of Asphalt Binder Using the Bending Beam Rheometer (BBR), in AASHTO T 313-10. 2011, American Association of State Highway and Transportation Officials, Washington, D.C.
- AASHTO T 315-10 Determining the Rheological Properties of Asphalt Binder Using a Dynamic Shear Rheometer (DSR), in AASHTO T 315-10. 2011, American Association of State Highway and Transportation Officials, Washington, D.C.
- AASHTO T 322-07 Determining the Creep Compliance and Strength of Hot-Mix Asphalt (HMA) Using the Indirect Tensile Test Device, in AASHTO T 322-07. 2007, American Association of State Highway and Transportation Officials, Washington, D.C.
- AASHTO T 342-11 Determining Dynamic Modulus of Hot Mix Asphalt (HMA), in AASHTO T 342-11. 2011, American Association of State Highway and Transportation Officials, Washington, D.C.
- AASHTO, "Mechanistic-Empirical Pavement Design Guide: A Manual of Practice: Interim Edition," American Association of State Highway and Transportation Officials 2008.

- Advanced Research Associates. (2004). 2002 Design Guide: Design of New and Rehabilitated Pavement Structures, NCHRP 1-37A Project, National Cooperative Highway Research Program, National Research Council, Washington, DC.
- Al-Khateeb, G., A. Shenoy, N. Gibson, T. Harman. (2006). A New Simplistic Model for Dynamic Modulus Predictions of Asphalt Paving Mixtures. Association of Asphalt Paving Technologists Annual Meeting. Paper Preprint CD.
- Al-Khateeb, G., Shenoy, A., Gibson, N., and Harman, T. "A New Simplistic Model for Dynamic Modulus Predictions of Asphalt Paving Mixtures", Journal of the AAPT, Vol. 75E, 2006.
- Andrei, D., Witzcak, M.W., and W. Mirza. (1999) "Development of Revised Predictive Model for the Dynamic (Complex) Modulus of Asphalt Mixtures," Interteam Technical Report, NCHRP Project 1-37A, University of Maryland.
- ASTM D 2493-09. (2009). Viscosity-Temperature Chart for Asphalts, ASTM International, West Conshohocken, PA.
- Azari, H., Al-Khateeb, G. Shenoy, A. and Gibson, N. H. (2007) "Comparison of Simple Performance Test $|E^*|$ of Accelerated Loading Facility Mixtures and Prediction $|E^*|$: Use of NCHRP 1-37A and Witzcak's New Equations", Transportation Research Record: Journal of the Transportation Research Board, Vol. 1998, pp 1-9.
- Bari, J. (2005). Development of a New Revised Version of the Witzcak E^* Predictive Models for Hot Mix Asphalt Mixtures. PhD Dissertation. Arizona State University.
- Bari, J. and Witzcak, M.W. (2007) "New Predictive Models for the Viscosity and Complex Shear Modulus of Asphalt Binders for Use with the Mechanistic-Empirical Pavement Design Guide", Transportation Research Record: Journal of the Transportation Research Board, No 2001, pp 9-19.
- Bari, J., and Witzcak, M.W. "Development of a New Revised Version of the Witzcak E^* Predictive Model for Hot Mix Asphalt Mixtures", 2005.
- Birgisson, B., G. Sholar, and R. Roque (2005) Evaluation of Predicted Dynamic Modulus for Florida Mixtures, Journal of the Transportation Research Board, TRR 1929, Washington, D.C.
- Bonnaure, F., G. Gest, A. Garvois, and P. Uge. (1977) "A New Method of Predicting the Stiffness of Asphalt Paving Mixes," Journal of the Association of Asphalt Paving Technologists, Vol. 46
- Ceylan, H., Gopalakrishnan, K. and Guclu A. (2007). "Advanced Approaches to Characterizing Nonlinear Pavement System Responses." *Transportation Research Record: Journal of the Transportation Research Board*, No. 2005: 86-94.

- Choi, J.-H., Adams, T.M. and Bahia, H.U. (2004). "Pavement roughness modeling using back-propagation neural networks." *Computer-Aided Civil and Infrastructure Engineering*, Vol. 19 (4): 295-303.
- Christensen Jr., D. W., T. K. Pellinen, and R. F. Bonaquist. (2003). Hirsch Model for Estimating the Modulus of Asphalt Concrete. *Journal of the Association of Asphalt Paving Technologists (AAPT)*, Vol. 72.
- Clyne, T.R., Li, X., Marasteanu, M.O., and Skok, E.L. Dynamic and Resilient Modulus of MN DOT Asphalt Mixtures. MN/RC-2003-09. Minnesota Department of Transportation, Minneapolis, 2003.
- Demuth, H. and Beale, M., 2004. *Neural Network Toolbox for use with Matlab (User's guide). Version 4*, The Mathworks, Inc., Natick, MA.
- Ekingen, E.R., (2004). Determining Gradation And Creep Effects In Mixtures Using The Complex Modulus Test. M.Sc Thesis. University Of Florida.
- FHWA (2011): Web site:
<http://www.fhwa.dot.gov/publications/research/infrastructure/pavements/ltp/10035/012.cfm>
- Flintsch, G., Loulizi, A., Diefenderfer, S. D., Diefenderfer, B. K., and Galal, K. (2008) "Asphalt Materials Characterization In Support Of The Mechanistic-Empirical Pavement Design Guide Implementation Efforts In Virginia" *Transportation Research Record: Journal of the Transportation Research Board*, Issue 2057, pp 114-125.
- Flintsch, G.W., Al-Qadi, I.L., Loulizi, A., and Mokarem, D. Laboratory Tests for Hot-Mix Asphalt Characterization in Virginia. VTRC 05-CR22. Virginia Transportation Research Council, Charlottesville, 2005.
- Gucunski, N. and Krstic, V. (1996). "Backcalculation of pavement profiles from spectral-analysis-of-surface-waves test by neural networks using individual receiver spacing approach." *Transportation Research Record: Journal of the Transportation Research Board*, No. 1526: 6-13.
- Houston, W.N., Mirza, M.W, Zapata, C.E., Raghavendra, S., (2005) NCHRP WEB ONLY DOCUMENT 113: "Environmental Effects in Pavement Mix and Structural Design Systems"
- Huang, C., Najjar, Y.M. and Romanoschi, S.A. (2007). "Predicting asphalt concrete fatigue life using artificial neural network approach." *Transportation Research Board Annual Meeting*, Washington, DC.

- Kim, H., Rauch, A.F. and Haas, C.T. (2004). "Automated quality assessment of stone aggregates based on laser imaging and a neural network." *Journal of Computing In Civil Engineering*, Vol. 18 (1): 58-64.
- Kim, Y. and Kim, R. (1998). "Prediction of layer moduli from falling weight deflectometer and surface wave measurements using artificial neural network." *Transportation Research Record: Journal of the Transportation Research Board*, No. 1639: 53-61.
- Kim, Y. R., B.Underwood, M.Sakhaei Far, N.Jackson, and J.Puccinelli (2010), LTPP Computer Parameter: Dynamic Modulus, Federal Highway Administration Technical Report No FHWA-HRT-10-035, 260p.
- Kim, Y. R., and LaCroix, A., (2008) "Evaluation of methods for determining the dynamic modulus of hot-mix asphalt concrete."
- Kim, Y. R., Modeling of Asphalt Concrete, 1st ed., McGraw Hill, ASCE press, 2009.
- Kim, Y.R., King, M., and Momen, M. "Typical Dynamic Moduli Values of Hot Mix Asphalt in North Carolina and Their Prediction", CD-ROM. 84th Annual Meeting, TRB, 2005.
- Marasteanu, M., Falchetto, A.C., Turos, M., and Le, J., (2012) NCHRP IDEA 151, IDEA Program Final Report: "Development of a Simple Test to Determine the Low Temperature Strength of Asphalt Mixtures and Binders"
- M-E PDG Version 1.0, NCHRP 1-40 D (2007) Guide for Mechanistic-Empirical Design of New and Rehabilitated Pavement Structures, Final Report. NCHRP, National Research Council, Washington, D. C., March 2004, updated 2007.
- Mirza, M.W. and Witczak, M.W. (1995). "Development of a Global Aging System for Short and Long Term Aging of Asphalt Cements," *Journal of the Association of Asphalt Paving Technologists*, 64, 393-418.
- Mohammad, L. (2010) Characterization of Louisiana Asphalt Mixtures for using Simple Performance Tests and M-E PDG, Recent research from Louisiana Department of Transportation and Development, URL: <http://rip.trb.org/browse/dproject.asp?n=12267>
- Mohammad, L., Saadeh, S., Obularedd, S., and Cooper, S. (2007) Characterization Of Louisiana Asphalt Mixtures Using Simple Performance Tests. Transportation Research Board 86th Annual Meeting, CD-ROM.
- Romero, P., and Masad, E., (2001). "Relationship between the Representative Volume Element and Mechanical Properties of Asphalt Concrete". *Journal of Materials in Civil Engineering*

- Park, S. W. and R. A. Schapery. Methods of Interconversion between Linear Viscoelastic Material Functions. Part I – a Numerical Method Based on Prony Series. *International Journal of Solids and Structures*, Vol. 36, 1999, pp. 1653-1675.
- Propp, M. and Samal, A. (1992) “Artificial neural network architecture for human face detection”. *Intell. Eng. Systems Artificial Neural Networks 2*, pages 535–540.
- Robbins, M. M. and Timm, D. (2011) “Evaluation of Dynamic Modulus Predictive Equations for NCAT Test Track Asphalt Mixtures”, Proceedings of the Transportation Research Board 90th Annual Conference, January 23-27, 2011.
- Rowley, H., Baluja, S. and Kanade, T.(1998). “Neural network-based face detection” In *IEEE Patt. Anal. Mach. Intell.*, volume 20, pages 22–38.
- Sakhaeifar, M.S., Underwood, S., Ranjithan, R., and Kim, Y.R. (2009) “The Application Of Artificial Neural Networks For Estimating The Dynamic Modulus Of Asphalt Concrete”, *Transportation Research Record: Journal of the Transportation Research Board*, Vol. 2127, pp 173-186.
- Singh, D., Zaman, M., and Commuri, S. "Evaluation of Predictive Models for Estimating Dynamic Modulus of HMA Mixtures Used in Oklahoma", 2010.
- Sung, K. and Poggio, T. (1998) “Example-based learning for view-based face detection”, In *IEEE Patt. Anal. Mach. Intell.*, volume 20, pages 39–51.
- Tarefder, R.A, White, L. and Zaman, M. (2005b). “Neural network model for asphalt concrete permeability.” *Journal of Materials in Civil Engineering*, Vol. 17 (1) 19-27.
- Tarefder, R.A, White, L. and Zaman, M. (2005b). “Neural network model for asphalt concrete permeability.” *Journal of Materials in Civil Engineering*, Vol. 17 (1) 19-27.
- Tutumluer, E. and Seyhan, U. (1998). “Neural network modeling of anisotropic aggregate behavior from repeated load triaxial tests.” *Transportation Research Record: Journal of the Transportation Research Board*, No. 1615: 86-93.
- Velasquez, R.A, (2009). On the Representative Volume Element of Asphalt Concrete with Applications to Low Temperature. PhD Dissertation. University of Minnesota.
- Witczak, M.W. and Fonseca, O.A., (1996). “Revised predicted model for dynamic (complex) modulus of asphalt mixtures”, *Transportation Research Record*, 1540. Washington DC: Transportation Research Board-National Research Council, 15–23.
- Witczak, M.W., T.K. Pellinen, and M.M. El-Basyouny. (2002), “Pursuit of the simple performance test for asphalt concrete fracture/cracking”, *Journal of the Association of Asphalt Paving Technologists*. Vol. 71, pp.767-778.

Witczak, M.W. (2005) NCHRP Project 9-19 “Superpave Support and Performance Models Management”

Witczak, M.W., Kaloush, K., Pellinen, T., El-Basyouny, M., and Quintus, H.V., (2002) NCHRP Project 9-29 “Simple Performance Tester for Superpave Mix Design”

Zofka, A., Marasteanu, M., and Turos M., (2007) “Determination of asphalt mixture creep compliance at low temperatures using thin beam specimens” Transportation Research Board: TRB 2008 Annual Meeting CD-ROM.